Preface to ‘Surface movement and shallow processes: Stage 2 Report’

The Centre for Natural Gas at The University of Queensland has undertaken research related to natural and anthropogenic drivers of surface movement, including coal seam gas (CSG) production, since early 2017. This activity has primarily had the following aims:

1. Identify the processes, along with their model and input parameters, which contribute to the baseline of net surface movement in the Surat Cumulative Management Area (CMA);
2. Develop an integrated, evidence-based workflow to quantify the magnitude of these contributions.

This Stage 2 report was originally issued in May 2019 for the “Surface movement and shallow processes” project. It is not a final report, rather it documents progress towards the project aims, made during the period from late 2017 to early 2019, via two primary themes:

1. Analysis of surface movement observations acquired using InSAR and interpretation of these data in the context of other geospatial information (e.g. rainfall, land use, soil type)
2. Geomechanical analysis of the subsurface processes (e.g. groundwater extraction from aquifers, gas and water production from coal seams) that can manifest as subsidence.

The target audience of this report was the technical experts within industry who had requested the research. As it was not a final report, it was not intended for publication, and as such it includes extensive technical detail. In addition to the report, two publicly available conference papers were published using results from the report, as referenced in the chapter summaries below.

In Chapter 2, InSAR data sourced from non-CSG producing regions were interrogated to try and identify baseline surface movement at locations throughout the Surat Cumulative Management Area (CMA). Note that ‘baseline’ in this context refers to analysis of areas away from CSG development to understand features, processes and environmental factors that cause fluctuations in surface elevation. This showed a background trend of subsidence in most locations during the period 2012 to 2016 as well as correlation between surface movement fluctuations and rainfall. Extension of this analysis resulted in the independently peer reviewed publication of Masoudian et al. (2019)[1].

Chapter 3 presented research that attempted to estimate the compressibility of subsurface rock and coal layers from high-frequency water bore pressure signals. Compressibility is a key parameter in calculating the possible compaction of the subsurface when pore pressure is reduced via the extraction of water or gas. This work leveraged techniques that have been successfully applied to thick, extensive, sandstone aquifers. However, due to the complexity of the target zones in the Surat Basin (many thin layers of different materials), the precision of, and uncertainty associated with, the resultant compressibility estimates did not represent a significant improvement in contemporary practice. From a research perspective, the application of the techniques existing in 2017-18 to the Surat Basin sediments were unsuccessful and were therefore discontinued.

Finally, Chapter 4 explored the use of computational geomechanical analysis to predict compaction and subsidence in simplified test geometries as a result of water and gas extraction from the subsurface. After validating the approach, the concept of coal shrinkage (due to liberation and production of methane from the matrix) was explored in the modelling. These simplified analyses were conservative (i.e. likely to overpredict rather than underpredict). They showed a maximum potential subsidence on the order of 100 mm but the

[1] Masoudian, Mohsen S., Leonardi, C., Chen, Z., Underschultz, J., Masoudian, M.S., Leonardi, C., Chen, Z., Underschultz, J., 2019. Towards the development of a baseline for surface movement in the Surat Cumulative Management Area. The APPEA Journal 59, 95–114. https://doi.org/10.1071/AJ18181

distance over which this subsidence might occur was not evaluated in this study. This work resulted in the independently peer reviewed publication of Masoudian et al. (2019)[2]

It is important to highlight that the InSAR analysis and geomechanical modelling presented in the Stage 2 report are now being superseded due to ongoing research in both of these areas. Significantly, this includes the generation of an InSAR dataset that is independent of that acquired by the major CSG producers. These latest works will become available via a total of at least four independently peer reviewed journal and conference papers, which are currently at different stages of scientific peer review.

This 'Surface movement and shallow processes: Stage 2 Report' report, has been made publicly available by the UQ Centre for Natural Gas after several requests received in late 2022. Other than the addition of this preface, the body of the report is provided 'as-is', without updating of results and interpretation with more recent data and knowledge. As this is an interim deliverable, and not a final report, and with some analyses now being superseded, readers are cautioned to not to draw any final conclusions directly from this report alone.

Associate Professor Christopher Leonardi
School of Mechanical and Mining Engineering
The University of Queensland

Associate Professor Phil Hayes
Centre for Natural Gas
The University of Queensland

February 2023

[2] Masoudian, M. S., Leonardi, C., Chen, Z., Underschultz, J., 2019. The Effect of Sorption-Induced Shrinkage on the Ground Surface Movement Above Gas-Producing Coalbeds. Presented at the 53rd U.S. Rock Mechanics/Geomechanics Symposium, OnePetro.

THE UNIVERSITY OF QUEENSLAND
AUSTRALIA

Surface movement and shallow processes

Stage 2 Report

Celoxis System ID: 149345
Report release date: 28/05/19

Research Team

Dr. Christopher Leonardi[1], Dr. Mohsen Masoudian[1], Dr. Katarina David[2], Prof. Suzanne Hurter[3], Dr. Zhongwei Chen[1], Prof. Wendy Timms[4], and A/Prof Phil Hayes[3]

[1] School of Mechanical and Mining Engineering, The University of Queensland

[2] School of Mineral and Energy Resources Engineering, University of New South Wales

[3] Energi Simulation Industrial Chair in Onshore Gas Reservoir Modelling, Centre for Coal Seam Gas, The University of Queensland

[4] Faculty of Science, Engineering and Built Environment, Deakin University

Acknowledgements

The project team would like to acknowledge the contribution of the members of the technical working group, who have been of great assistance in the completion of this report: Patrick McKelvey, Tracey Gill, Fabian Brandimarte, Stephen Denner, St.John Herbert, Emma Tavener, David Gornall, David Lavery, Thomas Flottmann, Ryan Morris, Michele Lochhead, and Andrew Moser. Access to the surface movement observations generated by the Altamira-CSG Industry Consortium is particularly appreciated. We would also like to thank the CCSG and UQ staff that have contributed in various ways, including Andrew Garnett, Jim Underschultz, Alexandra Wolhuter, and Helen Schultz.

Disclosure

This project is funded by the UQ, Centre of Coal Seam Gas and the foundation Industry members (Arrow Energy, APLNG, Santos, and Shell/QGC). The Centre conducts research across Water, Geoscience, Petroleum Engineering and Social Performance themes.

For more information about the Centre's activities and governance see
http://www.ccsg.centre.uq.edu.au/

Disclaimer

The information, opinions and views expressed in this report do not necessarily represent those of The University of Queensland, the Centre for Coal Seam Gas or its constituent members or associated companies. Researchers within or working with the Centre for Coal Seam Gas are bound by the same policies and procedures as other researchers within The University of Queensland, which are designed to ensure the integrity of research. You can view these policies at: http://ppl.app.uq.edu.au/content/4.-research-and-research-training

The Australian Code for the Responsible Conduct of Research outlines expectations and responsibilities of researchers to further ensure independent and rigorous investigations.

This report has not yet been independently peer reviewed.

Document Control Sheet

Version #	Reviewed by	Revision Date	Brief description of changes
1.0	Reviewed by CL, PH and WT.	28/05/19	Issued as draft to TWG
1.1	H Schultz	27/06/2019	Final review

Executive Summary

The aims of this project are to (i) identify the processes, along with their model and input parameters, which contribute to the baseline of net surface movement in the Surat Cumulative Management Area (CMA) and, subsequently, (ii) develop an integrated, evidence-based workflow to quantify the magnitude of these contributions. This report communicates the findings of Stage 2, which partially covers both aims.

The visualisation and analysis of the InSAR data for the non-producing areas revealed four regions of interest (either because of large magnitude of the surface movement or its fluctuation), mainly with downward surface movement (subsidence). The surface movement within these regions referred to as focus areas were interrogated alongside the other publicly available data. For the four focus areas (coded FA1 – 4) this included soil type and composition, data of groundwater bores from The Water Atlas, the rainfall and soil moisture data from Bureau of Meteorology (BOM).

FA2 showed smallest overall subsidence among the FAs (~6 mm), and FA4 showed the largest (~23 mm). The mean surface movements within all areas showed a fluctuating pattern whose magnitude was significant compared to the overall surface movement in FA1, FA2, and FA3. For FA4, the fluctuation was negligible with respect to the overall surface movement, and instead a continuous subsidence was observed that amounts to nearly 23 mm over the period of observation. Analysis of groundwater data revealed no significant change in the groundwater level in any of the focus areas and it was concluded that the surface movement observations in these areas could not be related to the groundwater drainage-induced compaction of aquifers.

Analysis of the available precipitation data, soil types, and soil moisture suggested that the fluctuation in the observed surface movement in FA1, FA2, and FA3 correlates with rainfall events. This suggests that the surface movement observations may be due to rainfall infiltration into shallow layers, which can cause consolidation of soil and the swelling of high-clay soil down the profile. The overall downward movement in FA4, however, cannot yet be explained by the mechanisms suggested for the other focus areas, and hence, exploring other possible phenomena is underway. Direct modelling of these natural phenomena does not seem feasible. Thus, it is recommended that other techniques for automating quantification of surface movement should be explored, including but not limited to machine learning techniques.

In alluvial sediments, the change in groundwater level is important, in particular where the strata are heterogeneous and of varying thickness. A workflow to estimate settlement from high frequency pore pressure is developed where downhole geophysical data to estimate porosity and historic groundwater drawdown data from head measurements and literature are processed alongside the high frequency groundwater level data. Then, the compressibility of the formation is estimated using the earth tides and barometric loading methods. This workflow was applied for calculation of surface subsidence in Condamine alluviums, showing small predictions of movement ranging from 1 to 50 mm (depending on the method used) due to groundwater level declines.

In order to simulate the subsurface poroelastic processes and estimate their contribution to the surface subsidence, a coupled hydro-mechanical model has been developed using advanced numerical codes. An example from the recent Independent Expert Scientific Committee report (IESC 2014) is solved with these models for both steady-state and transient flow conditions. Preliminary results indicated the magnitude of production-induced subsidence to be of the same order of magnitude as the natural

background movement observed in a number of locations (i.e. between 50 and 100 mm). The numerical models developed demonstrate capabilities available for advanced analysis of subsurface processes. These models could be extended for more complex subsurface processes associated with coal seam gas (CSG) production (e.g. swelling/shrinkage, two phase flow). These further developments could lead to development of practical tools for surface subsidence prediction and also reservoir management and simulation of reservoir geomechanics.

Table of Contents

1 Introduction

The coal seam gas (CSG) industry in Queensland has been investigating surface movement in CSG development and adjacent areas through its Ground Motion Consortium. This group has engaged remote sensing company, TRE-Altamira, to provide processed historical (where available) and current ongoing observations from interferometric synthetic aperture radar (InSAR). The primary output of TRE-Altamira's data collection and processing is a spatial and temporal distribution of measured net (i.e. positive and negative) surface movement.

The industry partners that comprise The University of Queensland's Centre for Coal Seam Gas (UQ CCSG) agree that they need to be able to distinguish surface movement related to CSG production from that influenced by other, baseline factors. These include, but are not limited to, tectonics, changes in soil moisture and the associated shrinkage and swelling, groundwater abstraction and recharge and the resultant poroelastic effects, and land use, each of which contributes a component to the net surface movement that InSAR detects. It is therefore important to be able to separate and quantify the different components of net surface movement so that:

1. The distribution and significance of CSG-related surface movement can be understood within the context of key geomechanical characteristics and processes of the shallow geological framework;
2. Future surface movement associated with CSG development, as a proportion of net surface movement, can be more accurately forecast, and;
3. The industry has a sound technical basis to respond to any future amendments to changes in legislation, which may assume that any surface subsidence is the result of CSG development with "the burden to prove otherwise".

1.1 Aims and objectives

The activities of this project are directed towards two, closely-related aims. The first is to identify the processes, along with their model and input parameters, which contribute to the baseline of net surface movement in non-CSG development areas. Subsequently, the second is to develop an integrated, evidence-based workflow to quantify the magnitude of the baseline contribution to net surface movement in these areas.

The objectives that support these aims are summarised as follows.

1. Review all processes (e.g. active tectonics, aquifer depressurisation and recharge, changes in soil moisture, geomorphology) which have the potential to contribute to net surface movement in the regions of interest;
2. Interpret and interrogate InSAR measurements of surface movement in non-CSG development areas to define spatially-dependent reference data for model validation;
3. Develop model(s) of net surface movement for the processes (e.g. shrinkage and swelling of soils, poroelasticity) identified to be most significant in the regions of interest;
4. Assemble the available data that facilitate characterisation of the key processes, and identify if there is sufficient data available, both in terms of soil composition and rock properties, to undertake the proposed modelling;
5. Select a number of study locations from non-production areas, analyse them using the methodology developed in the project, and then use the predictions to validate and or history-match the modelling workflow;

6. Determine the additional work required to extend the developed workflow for application in CSG development areas.

This project requires activities in a range of disciplines, including but not limited to geology, hydrogeology, soil science, geomechanics, remote sensing, geostatistics, and geospatial data analysis. A multidisciplinary team comprised of researchers from within and outside UQ has been assembled to address most of the facets of the project. However, it may be possible to collaborate with other research providers, and potentially government organisations such as Geoscience Australia, to fill any capability gaps. This is particularly relevant in the area of remote sensing and InSAR data processing.

1.2 Project schedule

The activities of this project have included reviews, interpretation, and analysis of data and literature, and model development, validation, and application. The project team is comprised of specialists from a range of backgrounds, and some tasks will be and have been performed concurrently. Three stages and associated checkpoints have been defined as a means of periodically reviewing the future directions and resources for the project, and the tasks for each of these are defined as follows. Stage 1 was delivered in October 2017.

1.2.1 Stage 1: Literature and data review and interpretation

- Review and geostatistical interpretation of the TRE-Altamira InSAR data from non-CSG development regions, including an assessment of the associated uncertainty and noise, along with the potential need to transform the measurements to a reference frame aligned with the surface normal;
- Review of regional data availability and spatial resolution, mapping, and compilations including land use and vegetation, soil types, alluvial lithology, groundwater hydrographs for alluvial sediments, rainfall data, and groundwater extraction and recharge information;
- Review and interpretation of borehole drilling data and associated geophysical logs for the determination of soil and rock properties, including comment on whether or not the available data is sufficient for input in subsequent modelling;
- Literature review of the shallow processes that contribute to surface movement with a focus on contributions from soil shrinkage and swelling, depressurisation and recharge of porous strata, and active tectonics. This review will aim to answer the questions:
    - How and where has this phenomenon been documented in the literature?
    - What is the propensity or past evidence for this occurring in the regions of interest?
    - What techniques are best suited to predicting this phenomenon?
    - What data are available or required for such predictive techniques (e.g. high frequency water levels, hydraulic and geotechnical properties of soils and rocks etc.)?
- Review of options for modelling poroelastic effects in the areas of interest (i.e. simplified compaction models, three-dimensional geomechanical models, groundwater flow simulators);
- Selection of pertinent case study areas from areas of non-CSG development;
- Compilation of report and hosting of workshop to communicate Stage 1 findings;
- ***Stage Gate 1: Proceed with Case Study Analysis and Clarify the Forward Work Program (Timing and Budget).***

1.2.2 Stage 2: Model development and validation

- Continue to collate information on the techniques used by TRE-Altamira to process and interpolate InSAR measurements of net surface movement, including how Geoscience Australia

infrastructure is used (if at all) in the process;

- Develop computational scripts that facilitate large-scale, semi-automated interrogation and visualisation of the InSAR data that has been provided to the project, and apply these scripts to continue the search for locations with a discernible subsidence profile;
- Refine the final list of study areas that encapsulates the hydrogeological diversity (e.g. both alluvial sediments and consolidated strata, presence and absence of clays, geological boundaries, groundwater abstraction and recharge) in the Surat Cumulative Management Area (CMA);
- Acquire and process high-frequency water level and barometric data to calculate compressibility *in situ* at the point of observation. The compressibility can be calculated for alluvium or rock matrix and then used to estimate specific storage of groundwater. The compressibility values can be calculated from water level response to both barometric and earth tide stresses. The compressibility and specific storage will then be used it to estimate compaction and subsidence. This parameter can also be adapted for use in finite element modelling;
- Develop 1D consolidation models for comparison with InSAR measurements, based on unit thickness obtained from bore lithology logs, void ratio, in situ compressibility values, and history of groundwater level changes;
- ***Stage II Progress meeting on 30/06/18 (held 04/09/18)***
- Develop two-dimensional and three-dimensional finite element models of compaction (expansion) and subsidence (uplift) based on the geological models of the study areas, and use these to make forward predictions of non-production sources to net surface movement. These models will:
    - Predict compaction in both unconsolidated and consolidated strata;
    - Allow for the addition of complexity in circumstances where supporting input data (e.g. stratigraphy, material properties) exists, including material inelasticity, non-planar strata, distinct bedding planes, major subsurface faulting, and surface topography;
    - Capture a steady state or transient solution, with the former achieved by the prescription of pore pressure and saturation distributions throughout the model, and the latter performed using in-built seepage modelling (as is available in the Elfen code, or by coupling fluid flow from a reservoir or groundwater simulator).
- In collaboration with TNO Netherlands, determine a workflow to validate and or history match the developed models using the data available at the study areas;
- ***Stage II Progress Meeting on 15/12/18 (Progress Report Issued 19/12/18)***
- Interrogate the models to determine their key features and input parameters, and answer the following questions:
    - What level of model complexity (e.g. constitutive material model, discrete modelling of strata etc.) is required to capture the characteristic surface movement observed throughout the Surat CMA?
    - Which parameters exert the most influence on subsidence predictions, and is this consistent across the hydrogeological diversity of the Surat CMA?
    - Does the compressibility of fluid due to the presence of gas effect subsidence predictions?
    - What additional data, if any, would improve the accuracy model predictions?
    - What software/modelling options (i.e. are there open-source packages available?) could be used to best integrate the findings of this research into the workflow of the

industry partners?

- Compilation of report and hosting of workshop to communicate Stage II findings;
- ***Stage Gate 2: Proceed with Expanded Case Study Analysis and Clarify the Forward Work Program***

1.2.3 Stage 3: Expanded model testing

- Validation and or history matching of the developed models against an expanded number of case study locations;
- Secondary assessment of the relative magnitude of the various contributors to net surface movement, and their key model and input parameters;
- Compilation of report and hosting of workshop to communicate Stage 3 findings;
- ***Stage Gate 3: Proceed with Workflow for Describing Baseline Surface Movement.***

1.2.4 Stage 4: Definition of workflow for describing baseline surface movement

- Determine the work required to extend and apply the developed models to make predictions of net surface movement in CSG development areas or where no InSAR data is available;
- Identify and infer the major contributors to net surface movement in CSG development areas;
- Compilation of report and hosting of workshop to communicate Stage 4 findings;
- Reporting and publication of findings in international, peer-reviewed journals.

1.3 Report Structure

This report communicates the findings of Stage 2 of this project. Section 2 covers the visualisation and interrogation of the InSAR data and summarises other data available to correlate the observed surface movement with the soil moisture and rainfall events. In Section 3, a workflow for evaluation of the relative magnitude of contributors to surface movement is presented. The workflow is designed such that it includes steps required for estimating the surface movement from high frequency pore pressure data. Section 4 presents field-scale numerical modelling techniques and their application for prediction of surface subsidence due to groundwater drawdown. Finally, Section 5 summarises this report and provides some concluding remarks.

2 The InSAR data analysis

Remote-sensing techniques such as InSAR (interferometric synthetic aperture radar) have been widely used to study the spatio-temporal characteristics of land displacement at a regional scale (Li et al., 2017). The total interferometric phase that is calculated from SAR data is the sum of components due to flat-earth differences in range distance, topography changes, ground movement, atmospheric effects, and noise. Atmospheric phase effects are a function of water vapour, air temperature and pressure along the observation path, while water bodies and vegetation create dispersion in the reflected SAR signal (Tomás et al., 2014). Different precisions have been reported for the use of InSAR in land displacements, with Reeves et al. (2014) reporting a value of 10 mm/year. Garthwaite et al. (2015) studied the surface movement in the Surat CMA and showed that the uncertainty of InSAR data could be as low as 1 mm/year. It is worth noting that InSAR technology is a low-cost technique suitable for large study areas such as that discussed in this report (Tomás et al., 2014).

In order to monitor ground surface movement in the Surat CMA, a consortium of CSG companies operating in Queensland engaged a third party to provide processed, historical InSAR observations. The primary output of this data collection and processing is a spatial and temporal distribution of measured net (i.e. positive and negative) surface movement. A subset of this data has been made available for use in this project, and includes only the areas in which CSG is not currently being produced. The areas included in the InSAR dataset are illustrated in Figure 1.

2.1 InSAR data at basin scale

The InSAR time-series data from each of the industry proponents were received in different formats, requiring that they were all converted into common comma separated values (i.e. CSV) files for further processing and visualisation. The data were compiled and processed with MATLAB, to provide images of ground surface movements for specific times. It is worth noting that dealing with such a large number of data points typically requires significant computational resources and hence a multicore Windows server (two 8-core Intel Xeon E5 processors with 2.5 GHz frequency and 125 GB of memory) was used.

The scatter plots contain data “points” with colours representing the values of surface movement. The common practice when creating contour plots is the use of a gridded interpolation technique over the scattered data points (based on triangulation), but the interpolated surfaces usually fail when there are replicates, or when the data has many collinear points. They may also be unsuitable for extrapolating beyond the convex hull of data unless specific forms of interpolation techniques are used (e.g. biharmonic spline interpolation), which can be impractical due to their computation time (Deng and Tang, 2011). Regardless of the interpolation type chosen, the physical memory required for computations is the square of the number of data points. Thus, an efficient code (Gridfit), which creates a “smooth” surface based on a global approximation through local “bilinear interpolation” was used. Discussion of this technique is beyond the scope of this report but details of the code can be found in (D’Errico, 2006).

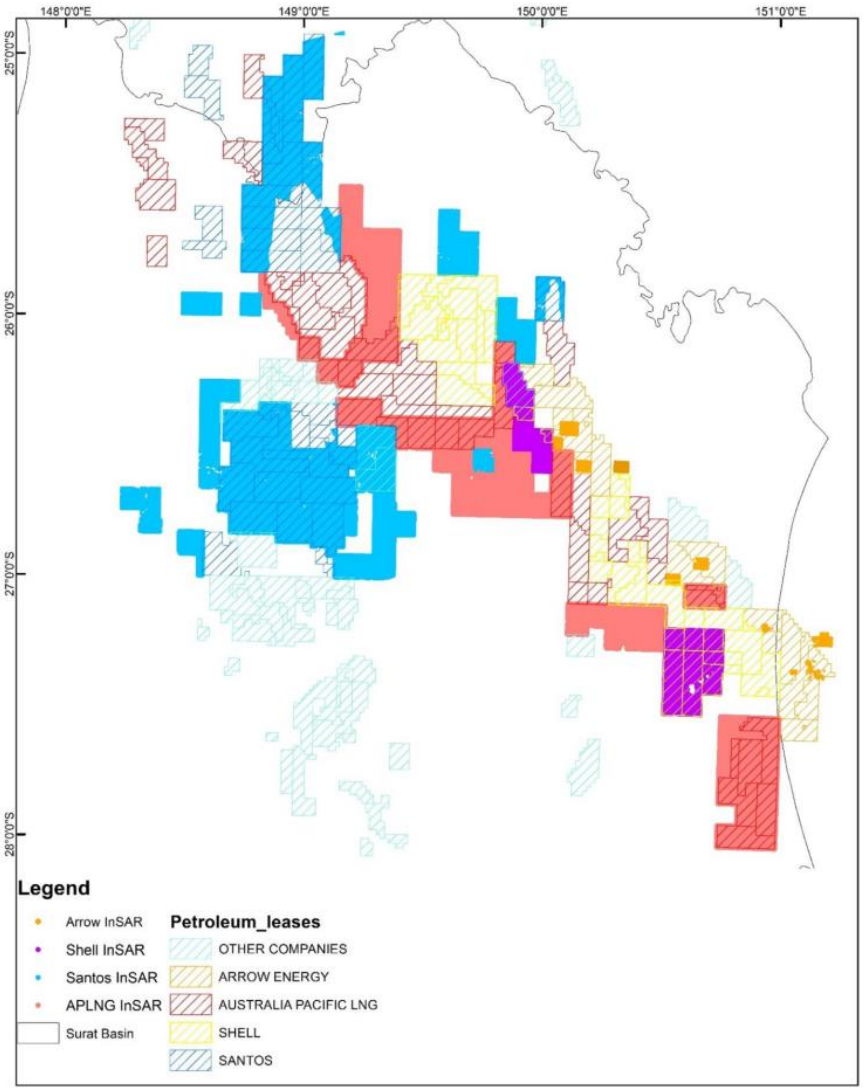

Figure 1: The map of the InSAR data provided by each industry partner, along with associated petroleum leases. The outline of the Surat Basin is included for reference.

The data generally cover the period between July 2012 and December 2016 with a sample interval of 14 days. For each time interval, two types of plots (scatter and contour) were created. Snapshots of data at different times are provided in Figure 2 and Figure 3. The movement of the ground surface with time is evident in these figures. It should be noted that because of the spatial discontinuity of the data points in many areas, the contour plots are not precisely representative of the data. As such, it is proposed that when dealing with discontinuous data, a scatter plot is much more useful/reliable and contour plots need to be examined cautiously. A more detailed analysis and interrogation of the data is presented in the next section.

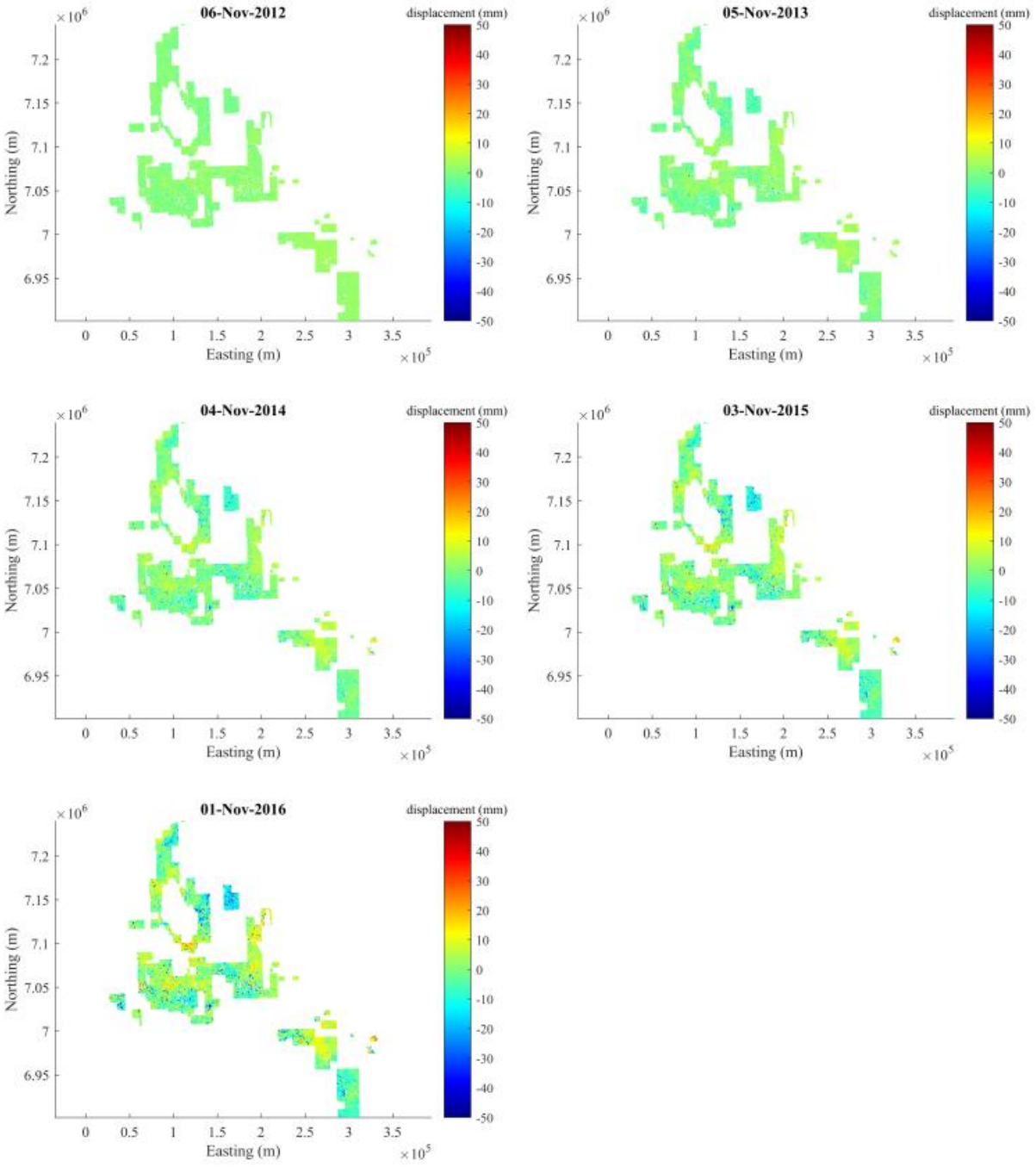

Figure 2: Scatter plots of the total surface movement observed by InSAR at yearly intervals.

As stated earlier in this report, the InSAR data possess inherent error and uncertainty. To quantify the absolute error in the data, reference values of surface displacement are needed, which unfortunately are not available for this area. However, significant noise in the data arising from the weather conditions, surface vegetation, surface water etc. is expected to be present, which makes it more difficult to identify and quantify the source of noise in the SAR signal. Some models are documented in the literature to mathematically model the noise in InSAR observations, however their description is beyond the scope of this report (e.g. Agram and Simons, 2015). In this report, only some statistical analysis of the InSAR dataset is presented to describe the spatio-temporal variability without discussing or quantifying the noise and its sources.

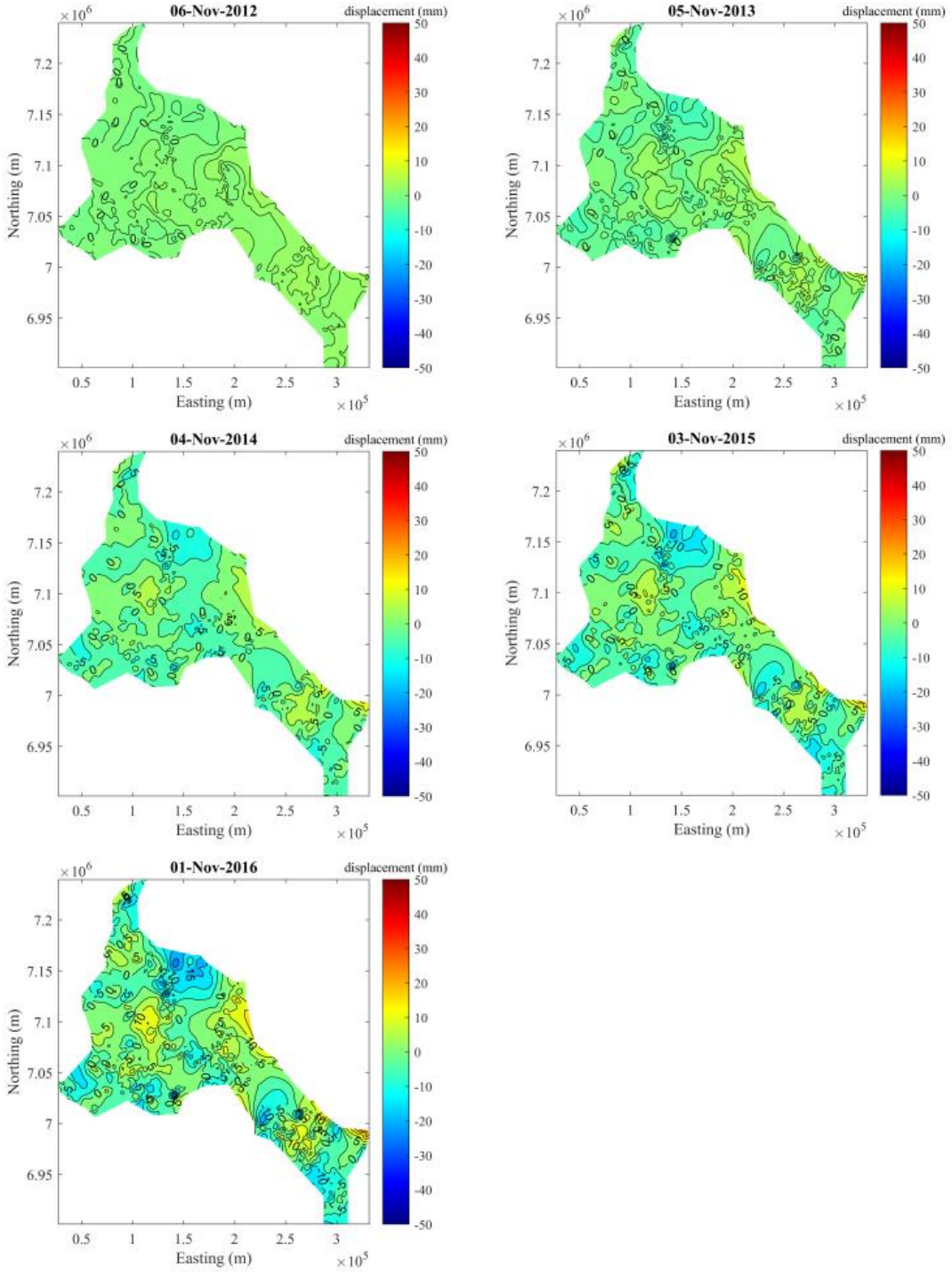

Figure 3: Contour plots of the total surface movement observed by InSAR at yearly time intervals.

2.2 Analysis of InSAR data in the focus areas

The plots presented in Figure 2 and Figure 3 cover a very large area and interpreting the movement of ground surface for the whole area is neither reasonable nor valid. Instead, a number of focus areas were selected for closer study. Four focus areas were chosen following the visual inspection of the scatter plots in a sequence (stack of scatter plots converted into an animation), which exhibit the most noticeable displacements. These four focus areas are shown in Figure 4, with squares approximately illustrating the borders of the focus area and the code names of FA1, FA2, FA3, and FA4. This section covers the detailed analysis of the InSAR data in these four focus areas.

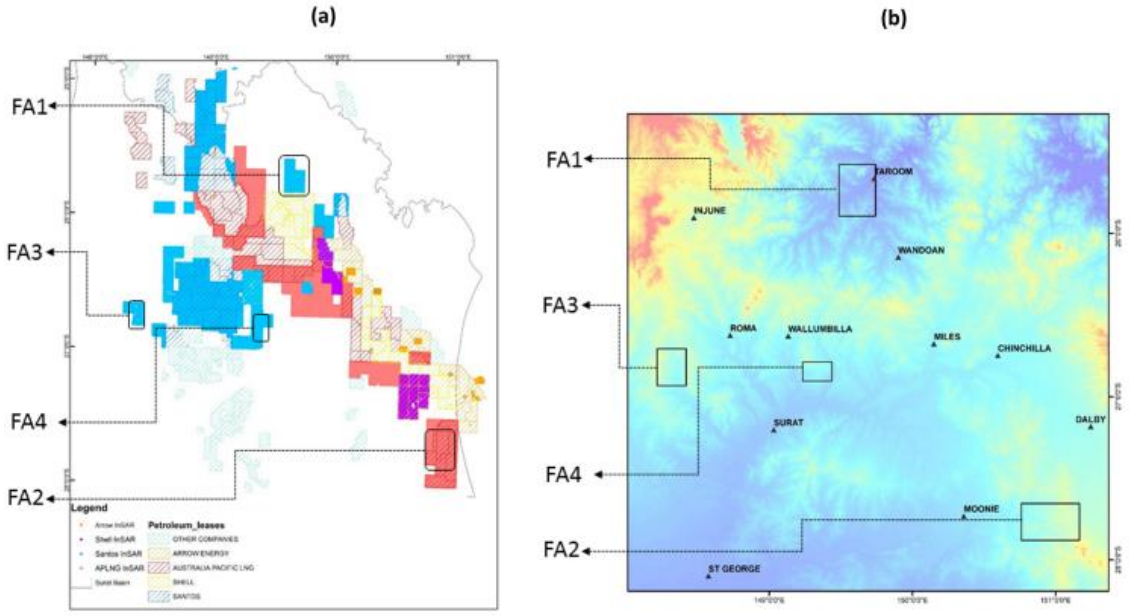

Figure 4: The focus areas for detailed investigation shown on (a) the map of InSAR data, and (b) a digital elevation map (DEM).

2.2.1 FA1

Area FA1 covers nearly 875 km^2 and is near Taroom, a small town in western Queensland. The land in the area is mainly covered with grazing native vegetation and some cropping (DSITI, 2016). The scatter plots of the InSAR data points within FA1 are demonstrated in Figure 5 at different times, along with the temporal evolution of the mean and standard deviation of the data. The scatter plots clearly show a downward displacement of the ground surface with time in FA1. The temporal evolution of the mean value of surface displacements also shows a general downward displacement with significant fluctuations. Also, note that the standard deviation increases with time and its value is almost the same as the absolute value of mean, which shows a relatively large spatial variability in the data.

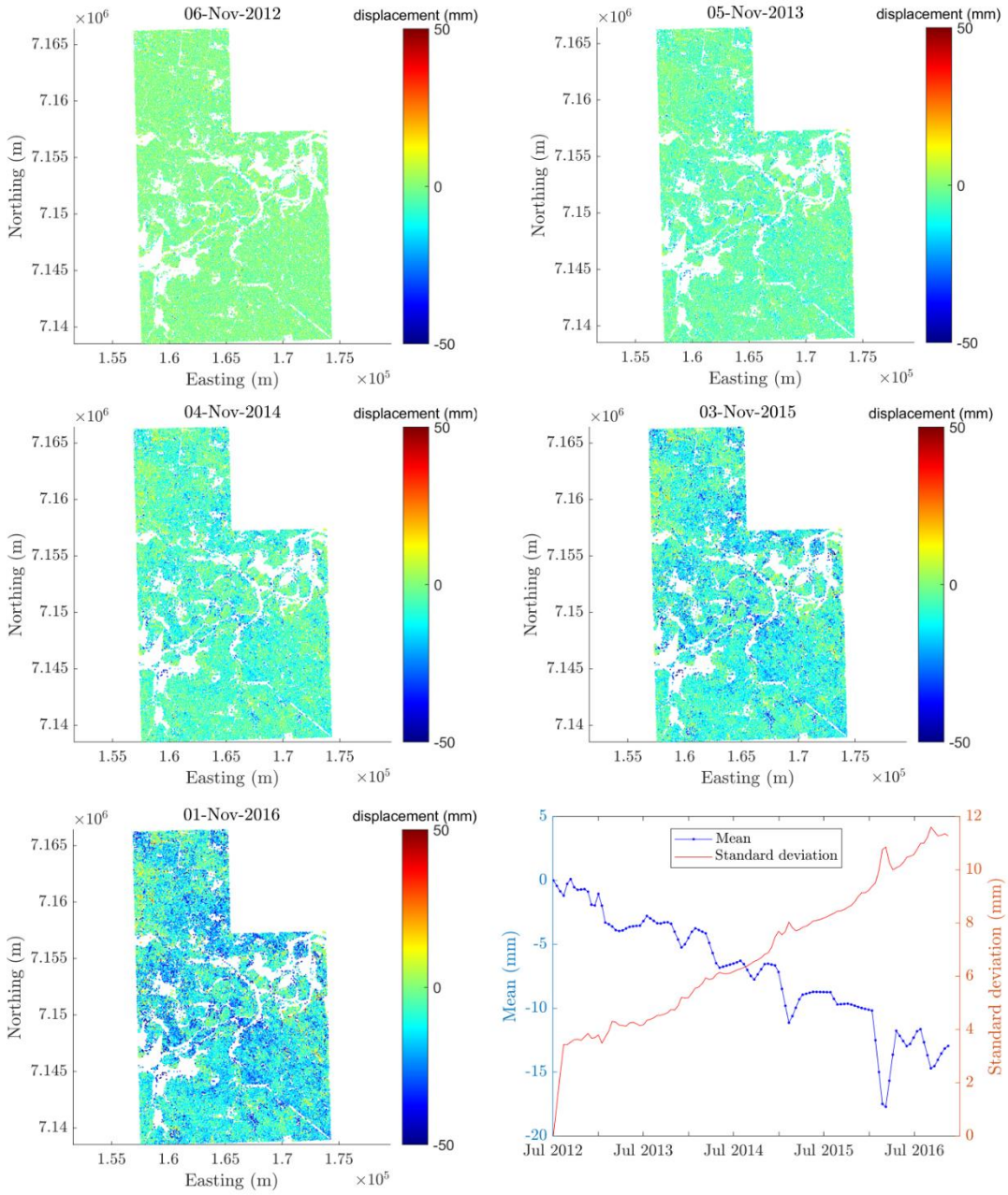

Figure 5: Scatter plots, mean and standard deviation of the total surface movement observed by InSAR in FA1.

2.2.2 FA2

Area FA2 (nearly 324 km^2), is near Cecil Plains, a small rural centre in western Queensland. The land in the area is mainly covered by production native forests, grazing native vegetation, some cropping and limited irrigated land (DSITI, 2016). The scatter plots of the InSAR data points within FA2 depicted in Figure 6 clearly show a downward displacement of the ground surface with time in FA2, but it is smaller than that observed for FA1. The temporal evolution of the mean value of surface displacements also shows a general downward displacement with some fluctuations. Also, note that the standard deviation increases with time and its value is almost the same as the absolute value of the mean, which shows the significant spatial variability of the data. It should also be noted that the final displacement of the ground surface is smaller than that of FA1.

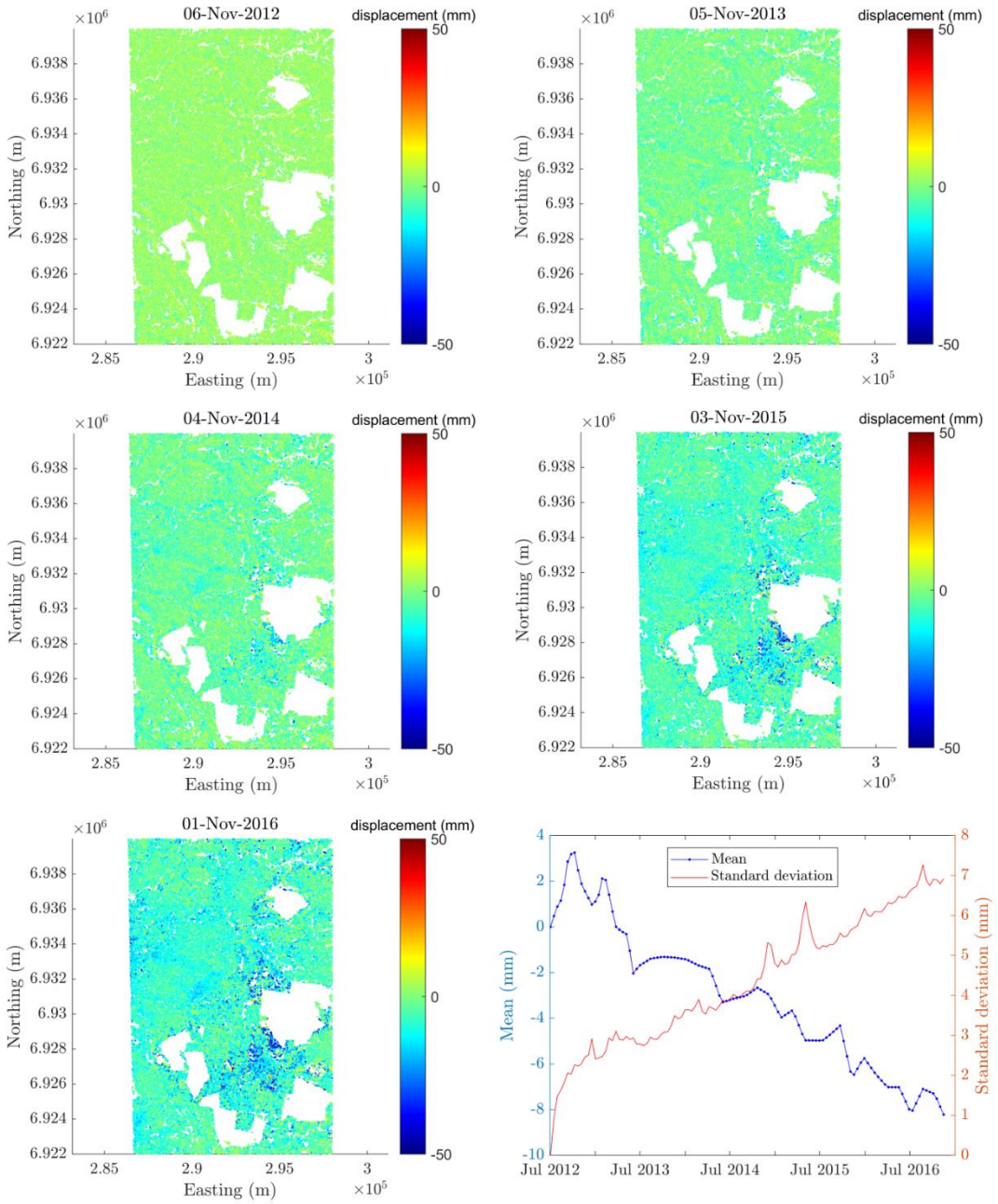

Figure 6: Scatter plots, mean and standard deviation of the total surface movement observed by InSAR in FA2.

2.2.3 FA3

Area FA3 (nearly 425 km^2), is located southwest of Roma, a town in western Queensland. The land in the area is mainly covered by grazing native vegetation and some cropping (DSITI, 2016). While the scatter plots of the InSAR data points within FA3 (Figure 7) show changes, the spatial variability does not allow much useful interpretation of the general trend of the surface movement. However, the temporal evolution of the mean value of surface displacements shows a general downward displacement with some fluctuations, but it is much smaller than those of FA1 and FA2. On the other hand, the standard deviation is larger than those of FA1 and FA2, being almost twice the absolute value of the mean. This shows that the spatial variability of the data in FA3 is much larger than those of other areas, as can be seen in the scatter plots.

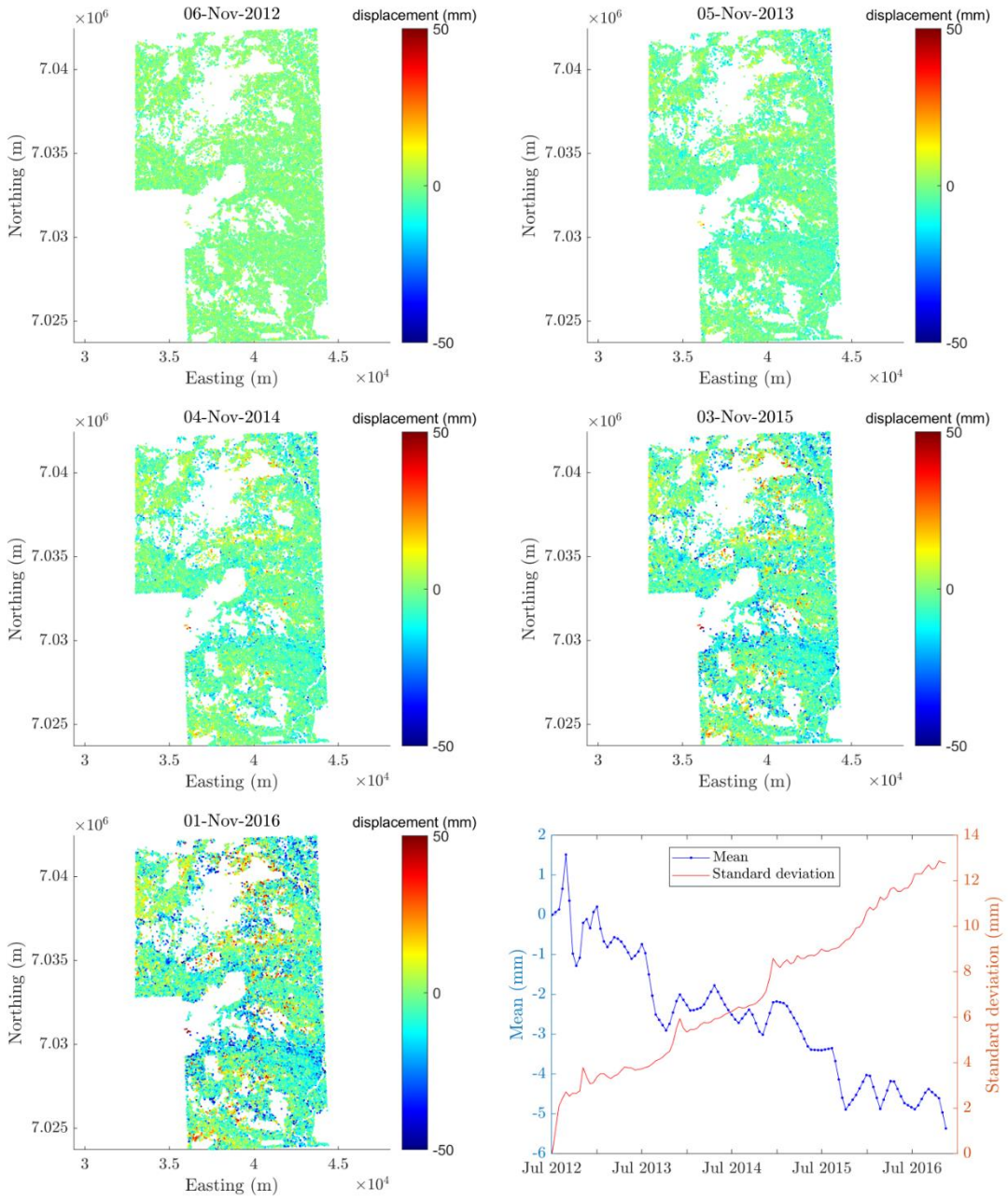

Figure 7: Scatter plots, mean and standard deviation of the total surface movement observed by InSAR in FA3.

2.2.4 FA4

Area FA4 (nearly 27.5 km^2), is located near Yuleba State Forest, east of Roma and west of Miles, and is nearly an order of magnitude smaller than the other focus areas. The land in the area is mainly covered by grazing native vegetation and some production native forests and some cropping (DSITI, 2016). The scatter plots of the InSAR data points within FA4 (Figure 8) show a relatively large downward movement in parts of FA4 with sharp boundaries. The temporal evolution of the mean value of surface displacements shows a large downward movement with the final displacement of nearly 20 mm, which is the largest among all focus areas. The standard deviation of the InSAR data point is near the absolute value of the mean, showing that the spatial variability is similar to those in FA1 and FA2, and smaller than that in FA3.

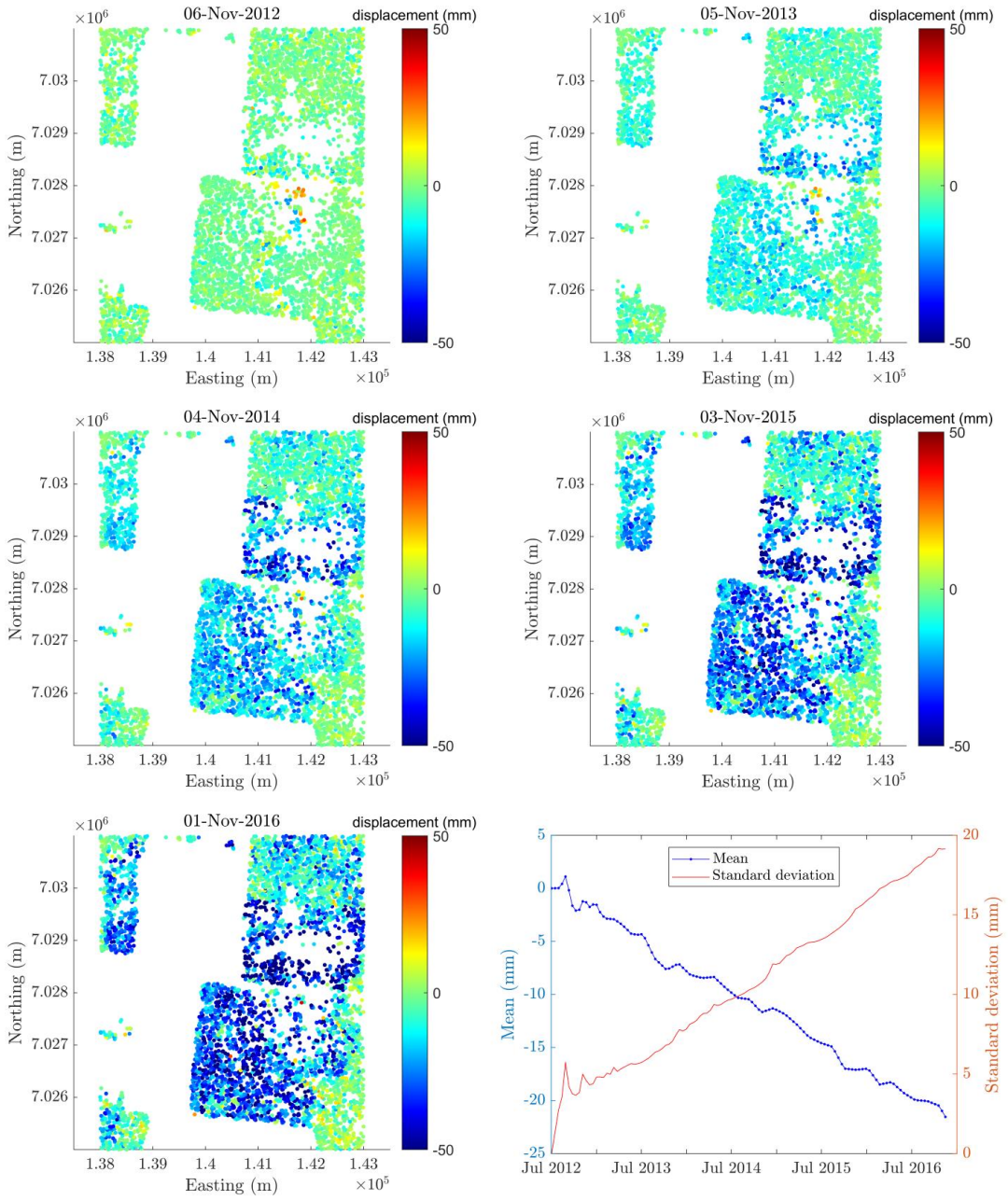

Figure 8: Scatter plots, mean and standard deviation of the total surface movement observed by InSAR in FA4.

2.3 Possible sources of surface movement

The objective here, is to qualitatively investigate existing data to understand the possible mechanisms that affect surface movement data observations. The precise correlation of the surface movement data with complex surface and subsurface processes will be the subject of future development of sophisticated models and this is briefly discussed in the next section of this report. In this section, a range of available data from different sources are presented to identify the underlying mechanisms of surface movement in the focus areas. Such qualitative analysis is a necessary step in any workflow for assessment of the processes contributing to the surface movement.

As discussed, the withdrawal of subsurface fluid is considered an important contributing cause of ground surface movement. While the areas of study in this report are non-CSG producing areas, groundwater may be extracted for agricultural, town water supply and industrial uses as previously

detailed in this report. Thus, investigating the transient groundwater levels is imperative in determining whether this can be a contributing process in the surface movement observations within the focus areas. Groundwater data for the four focus areas were extracted from the 3D CSG Water Atlas (The University of Queensland, 2017), a dataset integrating the data from The Office of Groundwater Impact Assessment (OGIA) and Queensland Government Groundwater Database. However, no useful data were found for FA3 and FA4, due to either lack of monitored wellbores or lack of groundwater data synchronous with the InSAR data. The available groundwater data are shown in Figure 9. The formations (and their depths) at which the water level measurements are reported are given in Table 1. Two wellbores were found within FA1 with presentable data while four wellbores are found within FA2. It can be seen that the water level change within FA1 is small (nearly ±1 m). The simplest way to calculate the groundwater drawdown effect on surface movement is to consider the one-dimensional consolidation of the aquifer. Assuming that groundwater is incompressible, the specific storage (S) can be defined as (Burbey, 2005),

$$S = \frac{\Delta b}{b \Delta h}, \qquad \textbf{Equation 1}$$

where b is the thickness of the aquifer, Δh is the change in the hydraulic head, and Δb is the associated compaction of the aquifer. Given that the specific storage of formations in Table 1 were all reported to be around 5×10-6 m^{-1} (IESC, 2014), the compaction for a metre of change in the hydraulic head is estimated to be 0.5 mm for a 100 m thick aquifer, which is believed to only have a negligible effect on the surface movement. In FA2, three of the wellbores show negligible changes in water level (less than one metre) while wellbore number 36 (northeast of FA2) shows a drop of approximately four metres during the period of interest. Given the large depth of the Springbok sandstone formation (from 247 m to 283 m), and relatively small compressibility of sandstone, it is believed that four metres of hydraulic head change will make an insignificant contribution to the ground surface movement. According to (OGIA, 2016), large water level drops (tens of metres) due to non-CSG activities, have only been observed within the Condamine Alluvium formation, which is outside all of the focus areas. On this basis, while no data are available for FA3 and FA4, the same conclusions can be drawn.

Table 1: The depths and formations at which the water levels are monitored at each wellbore

Area	Wellbore number	From depth (m)	To depth (m)	Formation name
FA1	27	502.9	595.9	Evergreen formation
	95	3	56.4	Birkhead formation
FA2	10	686.04	890.04	Hutton sandstone
	13	68.9	81.1	Gubberamunda sandstone
	27	86.8	88.4	Kumbarilla beds
	36	247	289	Springbok sandstone

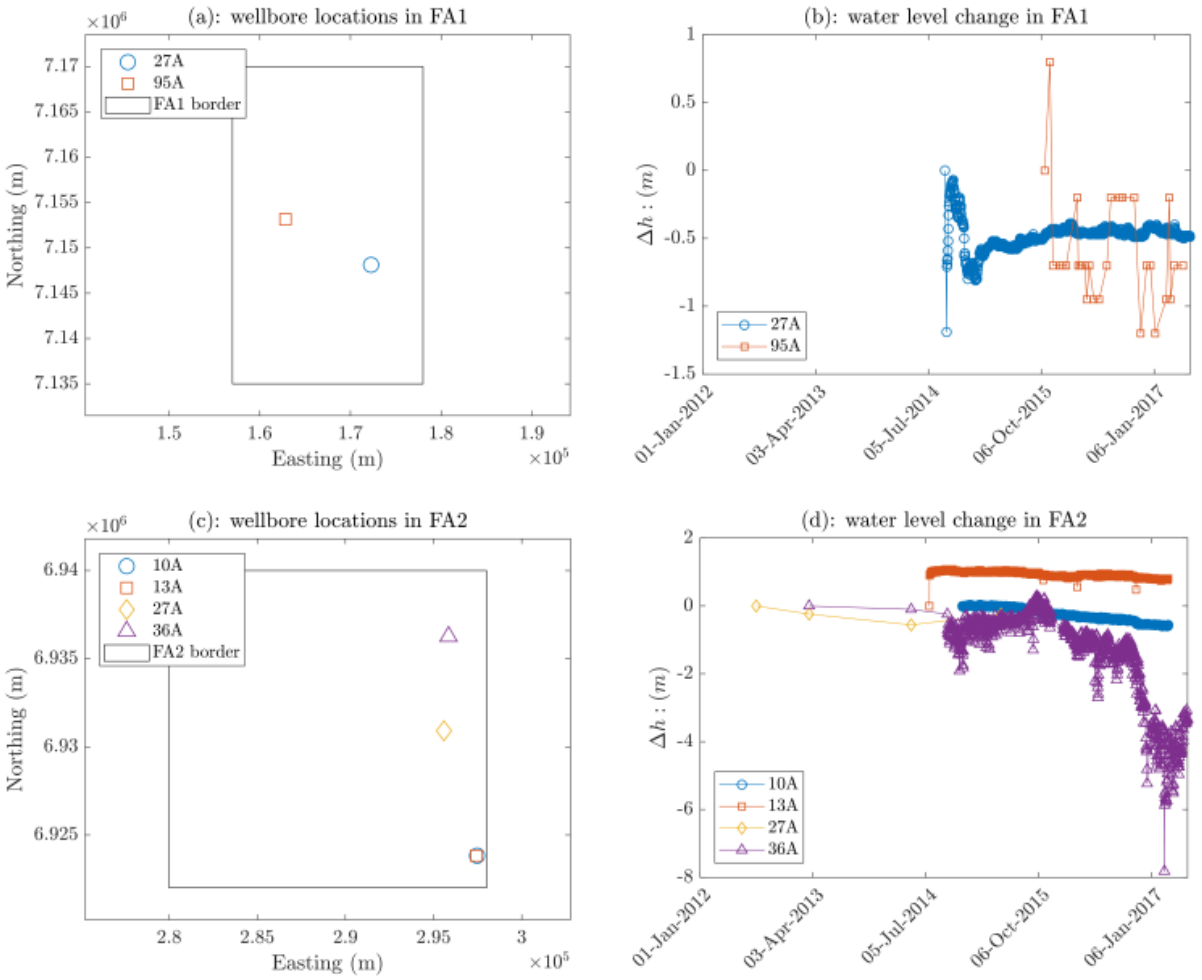

Figure 9: Summary of the available groundwater data in the focus areas, showing (a) the wellbore locations in FA1, (b) water level change in FA1, (c) the wellbore locations in FA2, and (d) water level change in FA2.

Seasonal rainfall events and the infiltration of rainwater into shallow soil layers can potentially lead to ground surface movement. In order to examine this process as a possible source of surface movement, the data collected from weather stations within or around the focus areas (BOM, 2018) were analysed as shown in Figure 10. For FA1, FA2 and FA3, almost all the local minima of ground surface movements coincide with the wet season and heavy rainfall events. It can be seen that the ground surface moves upwards (uplift) following the rainy season and would reach the largest uplift almost immediately after the peak of rainfall, after which the ground surface moves downwards (subsidence) during the dry season. These graphs suggest that the fluctuations observed in the mean surface displacement are due to the effect of rainfall infiltration into shallow soil layers near the surface. Although, this apparent correlation cannot fully explain the overall trend of downward movement of the ground surface, it can be argued that the effect of rainfall infiltration may be associated with some hysteresis so that the downward movement of the ground surface does not fully recover during the wet season. Such conclusions cannot be drawn for FA4, where the ground surface continuously moves downward and the seasonal surface movements appear small compared to the total displacement.

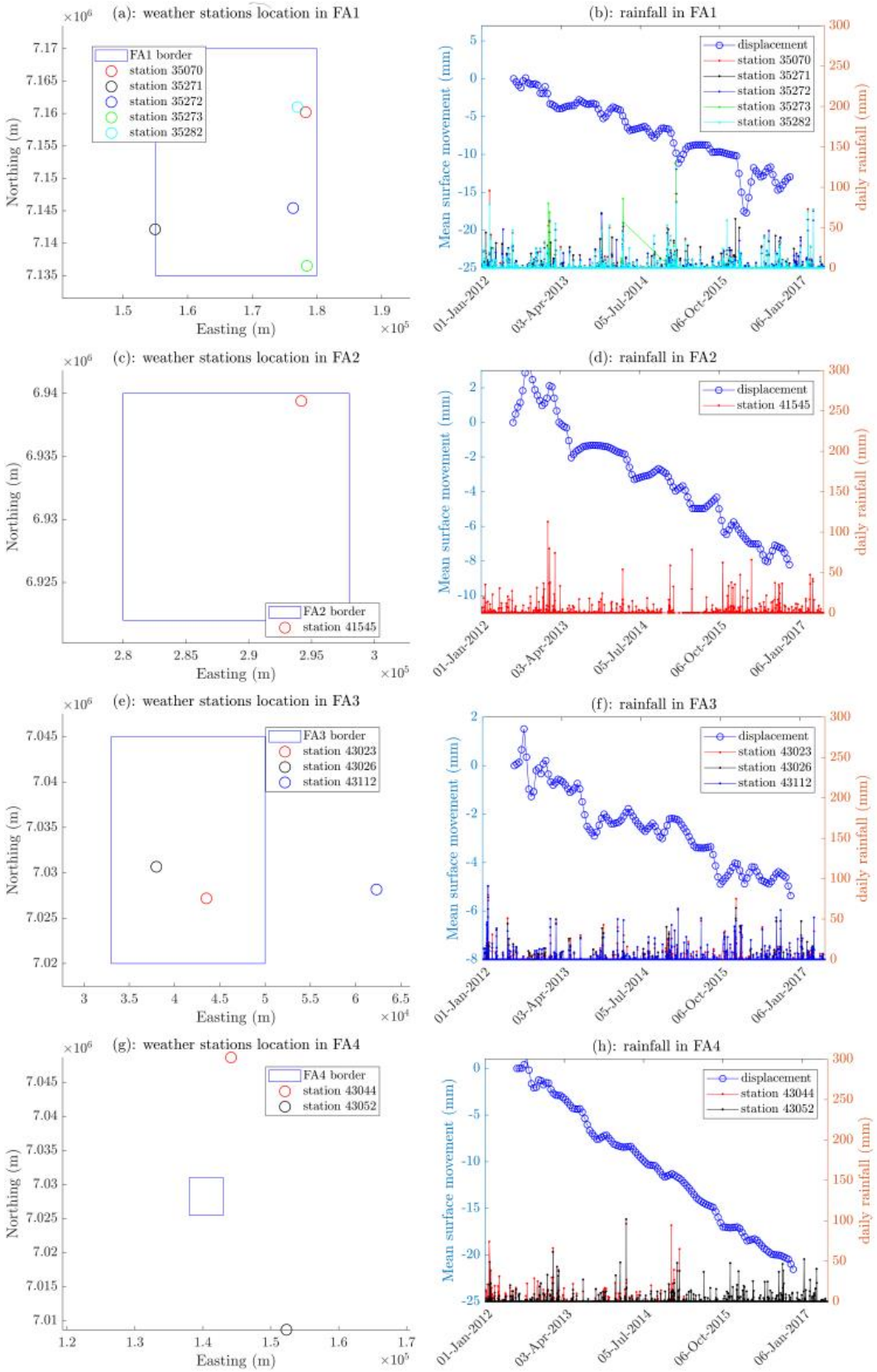

Figure 10: The locations of the weather stations (a, c, e, g) and the associated daily rainfall (b, d, f, h) for the four focus areas. Note that the average surface displacement is plotted alongside the daily rainfall in b, d, f and h.

In order to further test the hypothesis that the rainfall infiltration causes the observed seasonal ground surface movement, more data were reviewed. Figure 11 depicts the shallow soil types (based on

Australian Soil Classification) and the depth of regolith (weathered in situ and transported material overlying unweathered bedrock) in the Surat CMA with marked borders of the four focus areas. The depth of regolith is generally low within FA1 (Figure 11a), and the soil is mostly Vertosols (Figure 11b), a clay-rich soil (clay content >35%) with uniform texture, shrink-swell properties and strong cracking when drying. The high clay content suggests a high sensitivity of surface movement to moisture. On the other hand, the shallow regolith suggests a small contribution to the net surface movement, as well as a small lag between the rainfall infiltration and the volumetric response of the soil because of a shorter seepage path. These are in close agreement with the surface movement observations in Figure 10b, where fluctuations of up to 10 mm are seen following rain events. The depth of regolith is generally low within FA2 (Figure 11a), and the soil is mostly comprised of Sodosols (Figure 11b); that is sandy silt with low permeability, high sodium content and high erodibility, and an abrupt clay content increase down the profile. As can be seen in Figure 10d, the magnitude of surface displacement and its fluctuation within FA2 are both smaller than that in FA1 (nearly half). Also note that the heave of the surface during the dry season is a much longer process (a gentler slope of the curve), which may be explained by the low permeability soil. FA3 also has a generally shallow regolith (Figure 11a) containing Vertosols (clay) in the north and northeast, and Chromosols (silt) in the rest of the area. As mentioned earlier, Vertosols are clay-rich soils with shrink-swell properties, while Chromosols do not contain much expansive clay but clay content abruptly increases down the profile. These suggest a generally small contribution of rainfall-induced surface movement, which follows the rainfall events, as can be seen in in Figure 10f. FA4 is mostly covered with a deep regolith that is mainly made up of Chromosols with little to no expansive clay. This means that the surface movement is not sensitive to the rainfall event and soil moisture. The review of these data shows that the rainfall-induced consolidation and the moisture-induced swelling/shrinkage can be the most likely cause of the surface movements observed in the InSAR data for FA1, FA2, and FA3. For FA4, however, the seasonal precipitation does not seem to have affected the surface movement, and the surface movement observation must be related to another cause.

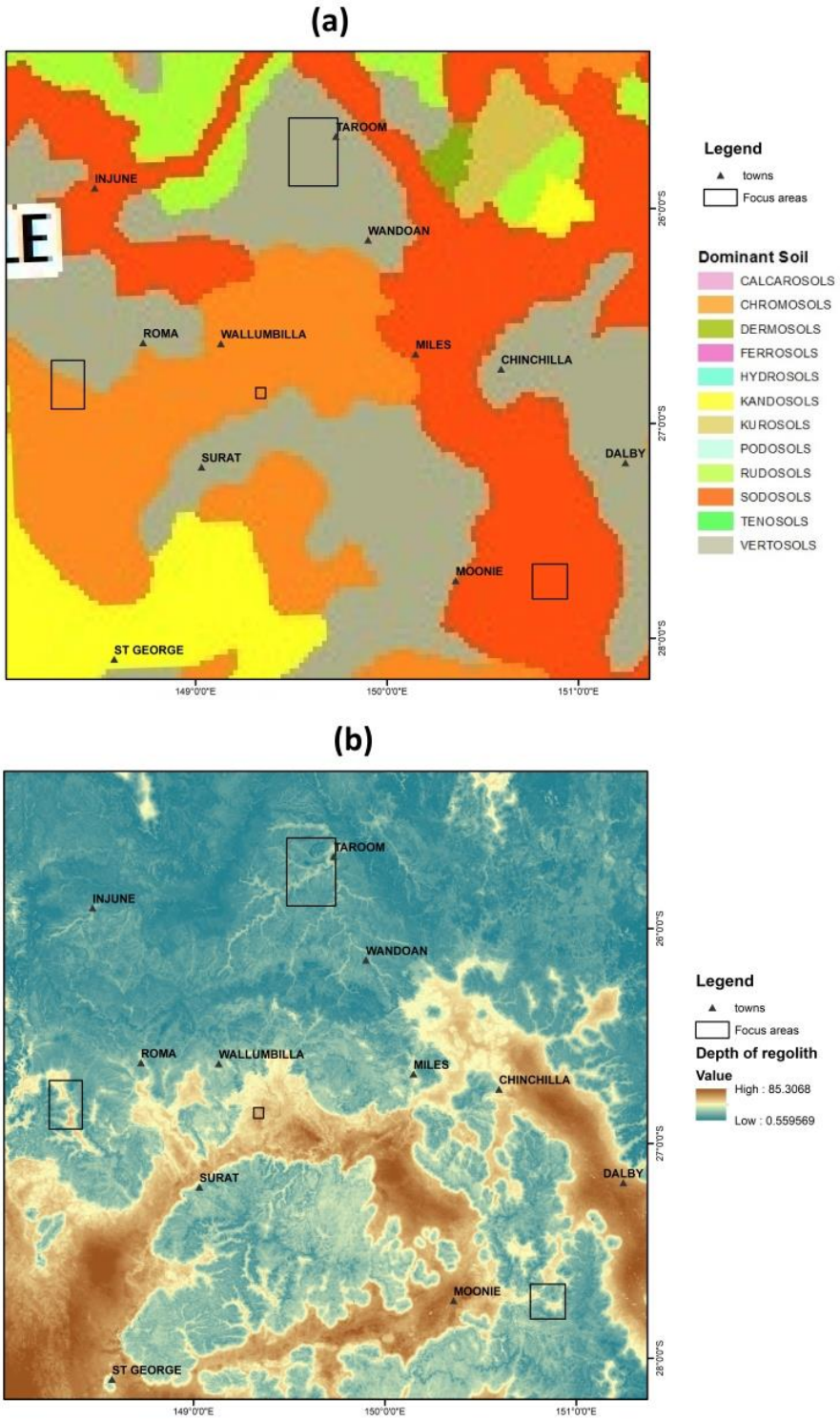

Figure 11: Information on the shallow soil within the study area, including (a) dominant soil types based on Australian soil classification (CSIRO 2013), and (b) the depth of regolith (Wilford et al. 2015).

To better explain the mechanisms of surface movement due to rainfall infiltration, one should consider the distribution of the moisture in the superficial soil layers, as well as the composition of the clay content. The behaviour of unsaturated soil is known to be very complex, but generally speaking an increase in the moisture content reduces the matric suction. Matric suction plays an important role in the strength of soil, holding soil particles in place, and the infiltration of rainwater can reduce the matric suction and wash out the cement and or fines between the particles. As a result, soil may lose its cohesion and solid content, which in turn can lead to the collapse of its newly formed structure. This is

known as the pore-volume collapse and its association with the increasing moisture content has been studied extensively in the literature (Houston et al., 2001; Lawton et al., 1992; Li et al., 2016; Or, 1996). On the other hand, the volume of some clay minerals increases upon hydration (swelling), with smectites exhibiting the largest effect (Worden and Morad, 2009). In order to relate the above-mentioned two mechanisms (collapse and swelling) to the InSAR observations, the soil moisture data and the content of smectite within the four focus areas have been presented in Figure 12 and Figure 13, respectively. These will be discussed alongside each other. First note that the deep soil moisture (DSM) remains nearly unchanged during the study period, which means the water-soil interactions at depths greater than 1.0 m do not contribute to the observed surface movement. However, it can be seen that the fluctuations of the surface movement closely follows those of upper soil moisture (USM) and lower soil moisture (LSM). For FA1 and FA3, the fluctuations are much sharper and the lag between rainfall and uplift is clear, while the upward movement in FA2 is comparatively smaller and slower. This can be attributed to the swelling/shrinkage behaviour of smectite, the content of which is much higher in FA1 and FA3 (see Figure 13). The overall downward movement in FA1, FA2, and FA3 may be related to the collapse of the soil during cycles of wetting and drying, which is known to be largely irreversible as opposed to the largely reversible clay swelling. As discussed, the overall downward movement is the largest and the seasonal fluctuations do not seem to affect it by much, despite the relatively high smectite content.

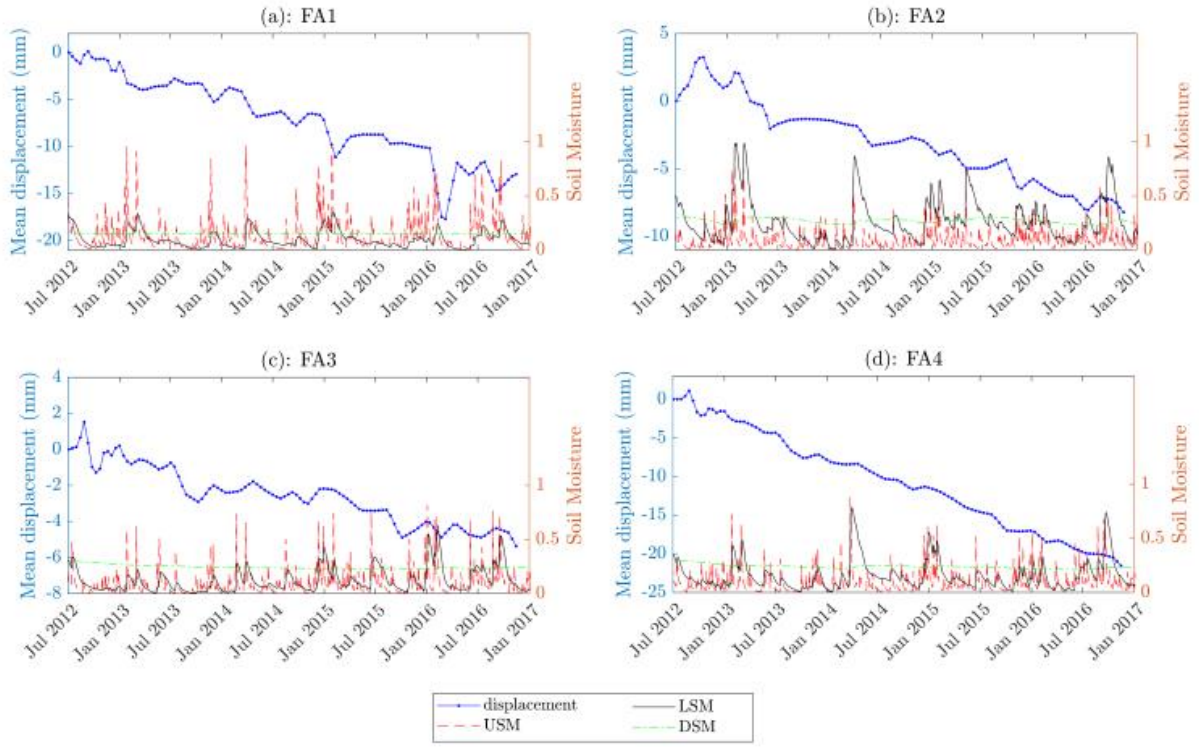

Figure 12: Soil moisture content evolution versus the surface net displacement within (a) FA1, (b) FA2, (c) FA3, and (d) FA4. Note that USM, LSM, and DSM are the Upper Soil Moisture (0-0.1 m depth), Lower Soil Moisture (0.1-1 m depth), and Deep Soil Moisture (1-6 m).

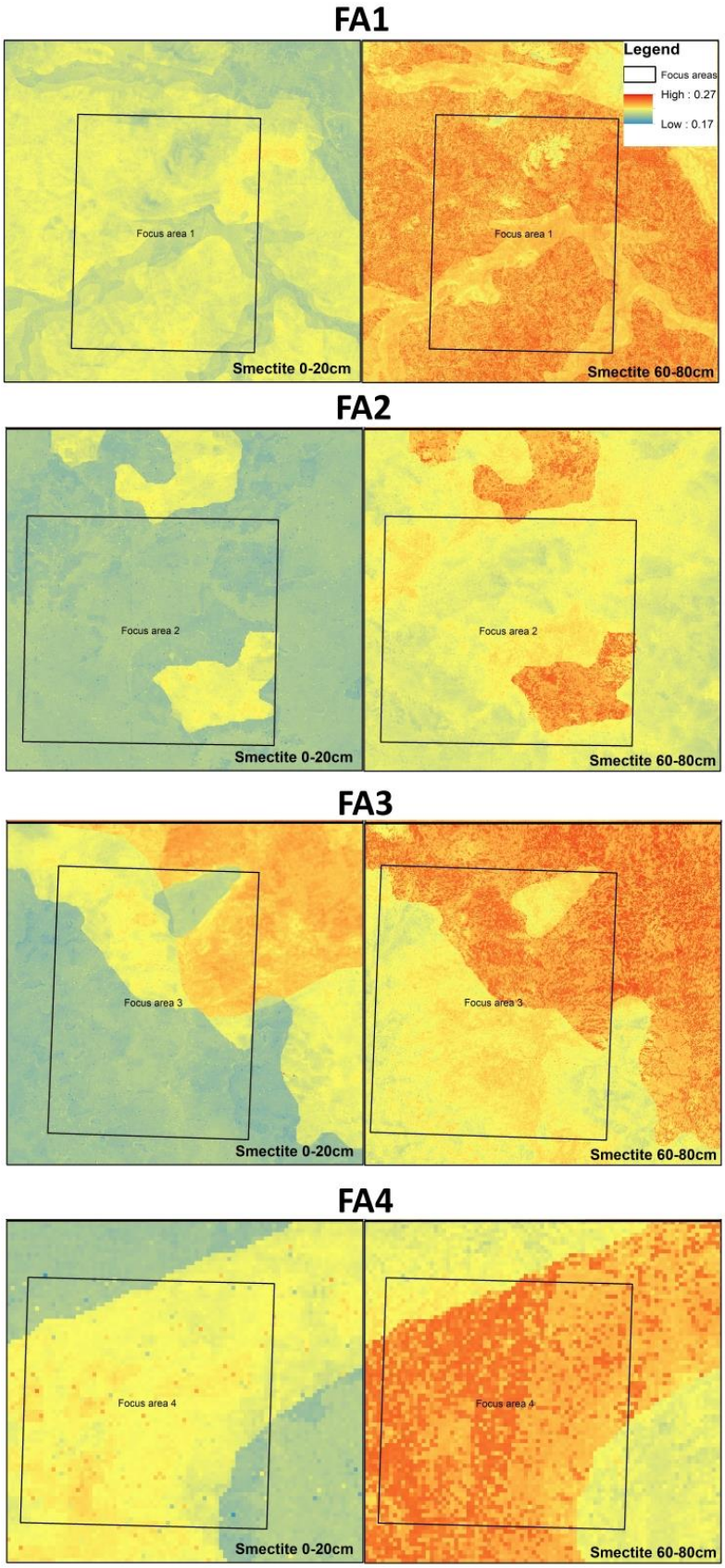

Figure 13: Smectite content in two different horizons within the four focus areas, namely 0-0.2 m and 0.6-0.8 m.

3 Settlement of soils and alluvium related to natural soil conditions and groundwater abstraction

This part of the report aims to provide quantitative estimates of settlement of alluvium and rock strata based on *in situ* compressibility values derived from analysis of high frequency groundwater level data. The focus of this analysis was the shallow (typically <50 m in thickness) unconsolidated soils, alluvium (up to 130 m in thickness), and rock strata where groundwater level data was available. The work targeted selected areas in the Surat CMA where groundwater level data was available at high frequency (several times per day) from groundwater monitoring (Figure 14). Unfortunately, such data were not available in areas where InSAR data had also been provided.

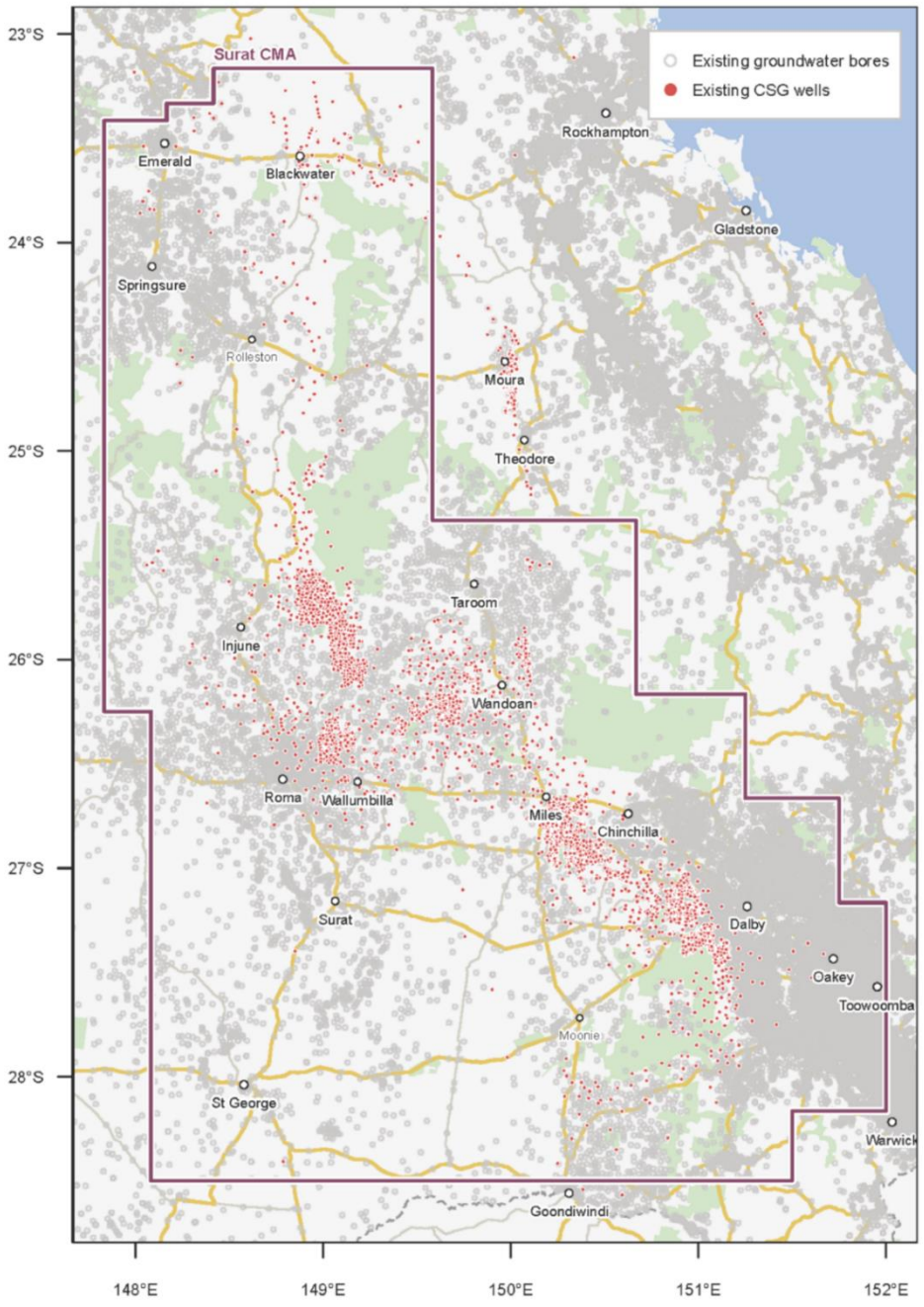

Figure 14: Map showing the investigation area including the coal seam gas tenements and registered groundwater bores (Keir, 2017).

3.1 Objectives and Scope

The objective of this part of the investigation were to estimate the surface settlement in unconsolidated sediments, alluvium and rock strata by a number of methods using high frequency groundwater level data, combined with historical groundwater and downhole geophysical data. The estimation of surface settlement in this study is related to the areas outside of CSG exploration or production activities. The research includes the influence of weather (barometric effects) and groundwater abstraction from the unconsolidated sediments and alluvium on groundwater levels to estimate total surface settlement. The work applied several methods to measure *in situ* compressibility of alluvium and rock strata at the screen depth of monitoring bores where high frequency data was available.

The scope of this analysis was defined as per the Stage 2 agreement between UNSW Australia and UQ, and included the selection of sites suitable for data analysis, the evaluation of selected data available for the assessment of soil compaction, data analysis, and the provision of estimates of surface movement. This scope of works forms the basis for the workflow presented as follows.

3.2 Analysis methodology

3.2.1 Workflow

A schematic illustrating the overall workflow to estimate settlement of the ground surface from high frequency groundwater level data and other hydrogeological information is shown in Figure 15.

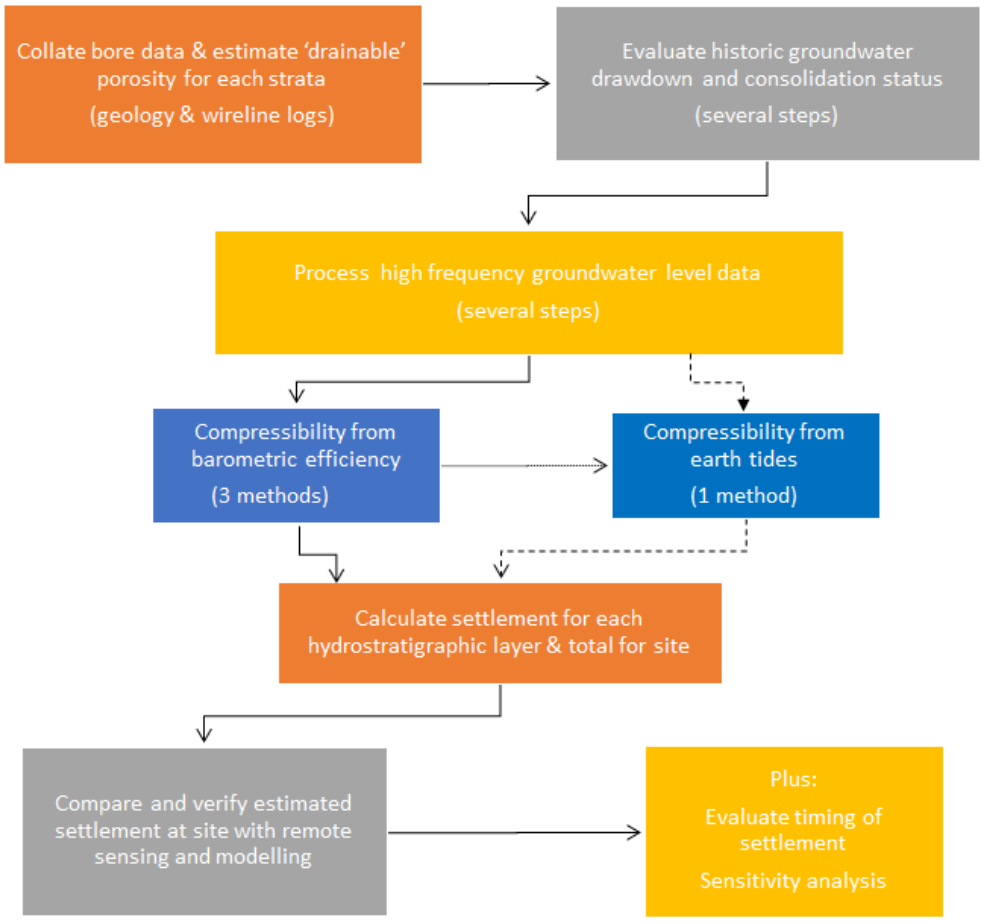

Figure 15: Schematic of the workflow established in this research. Surface movement was estimated for a site with the most complete data, however, data gaps in many areas limited further application.

3.2.2 Data collation

The data considered in this study included the following:

- Construction details for a total of 14 groundwater monitoring bores with the information on the strata where the monitoring bore is screened. Unfortunately, the data required was not simultaneously available in areas where InSAR data were available, particularly focus areas 1 to 4 (see Section 2.2 of this report);
- Groundwater level from piezometers installed in the Condamine River Alluvium (CA) or the transition zone between the CA and Walloon Coal Measures and deeper rock strata. Data was provided by Arrow Energy and was recorded on an hourly basis for the last one to five years;
- Pressure head from vibrating wire piezometers installed at various depths and strata including the Springbok Sandstone. Data was provided by Arrow Energy and is recorded on an hourly basis for the last one to five years;
- Barometric pressure data for each set of monitoring locations recorded at hourly intervals and provided by Arrow Energy;
- Wireline logs for six groundwater monitoring locations;
- Historical groundwater level data obtained from publicly available reports;
- Geological logs for seven of the 14 bore sites referenced in this section.

An estimate of the total settlement of the ground surface, with assumptions on hydraulic connectivity, was demonstrated for a site with the most complete data.

3.2.3 Porosity estimation and evaluation of historical groundwater drawdown

Porosity was estimated for each stratum using different methods based on the data available (Table 1). Porosity (n) is obtained from geophysical downhole logs (wireline) for the relevant drill hole and borehole interval where the pore pressure measurement was taken. Data provided by Arrow Energy had porosity measured using wireline logs in a number of different ways and units, these included limestone density porosity, sandstone density porosity, limestone neutron porosity, sandstone neutron porosity, base density porosity, and base neutron porosity.

Where possible the same approach was used to estimate the porosity from logs to ensure that data could be correlated across different drill holes. Where only limestone neutron porosity and base neutron porosity data was available, these data were used directly, but where neutron and density porosity were available the average was used (Hartmann and Beaumont, 1999),

$$\theta = \sqrt{\frac{\theta_n^2 + \theta_D^2}{2}} \qquad \textbf{Equation 2}$$

where θ_n is neutron porosity and $\theta_D$is density porosity. Density log was also used to calculate the porosity where these data were not directly available,

$$\theta = \frac{\rho_m - \rho_b}{\rho_m - \rho_w} \qquad \textbf{Equation 3}$$

where ρ_m is matrix density, ρ_b is formation bulk density and ρ_w is water density. The formation bulk density was obtained from literature for the lithology based on the gamma log. Where this was not available, a similar reading was estimated based on the nearby drill logs. Where porosity was calculated from density the lithology was assumed based on gamma readings and data for bulk density obtained

from literature.

The porosity obtained from a density log equates to oven-dried total porosity from rock samples, which is the effective porosity. The porosity obtained from neutron log also includes structural hydroxyl chemistry. This means that neutron determined porosity will be somewhat higher than effective porosity (in shales) but lower than the total porosity due to the presence of clay bound water. In order of preference, the following logs should be used to determine the effective porosity: neutron, density neutron, and density.

Typically, porosity logs will be corrected for either limestone or sandstone. For logs recorded in limestone porosity units, if the actual lithology is sandstone, the log porosity is less than the actual porosity. If the actual lithology is dolomite, the log porosity is greater than the actual porosity.

Neutron porosity can be read directly from the neutron porosity graph if the formation has been identified prior to geophysical logging. If lithology was not available prior to logging, then the log needs to be corrected by using charts. It needs to be noted that the neutron porosity readings in shale represent the effective porosity including interstitial water.

Historical drawdown data was obtained from the information available in the report which summarises the data for the Surat Basin and provides the update on the status report and groundwater modelling study.

3.2.4 Pore pressure data analysis

The data provided by Arrow Energy was checked initially to ensure data frequency was sufficient for the analysis. The units of the data were checked and converted as needed from kilopascals to metres of water, assuming a freshwater density of 1.0 g/cm^3.

Pore water pressure records were obtained by absolute pressure transducers that were installed in standard standpipe piezometers. The pore water pressure data were provided as both absolute and gauged (quarterly and hourly increments). Data were also provided for barometric pressure (quarterly increments) for each site. Barometric pressure data were available for Strathenden, Daandine and Lone Pine locations. Both pore pressure and barometric pressure data were resampled at hourly increments such that all data could be uniformly analysed. The gauged data were compensated by Arrow Energy for barometric pressure by subtraction of barometric pressure from pore water pressure (assuming a constant of 1 for barometric efficiency).

A number of methods have been previously developed which use the barometric loading, earth tide loading or a combination of those two methods to determine the elastic properties of strata, and a recent review of those methods is provided in McMillan *et al* (2019). The barometric efficiency is used, as a correction factor, to remove barometric effects on water levels in wells and determine elastic properties (constrained modulus) of the aquifer (Batu, 1998; Domenico, 1984; Rojstaczer and Agnew, 1989). The use of earth tides has similar application, however, it enables the determination of bulk modulus.

Determination of barometric efficiency is challenging because it is difficult to distinguish the component of water level change caused by barometric pressure change from the total water level change (Gonthier, 2007). In this research, four methods were used to analyse pore pressure data to calculate the loading efficiency, namely the visual inspection method (Smith et al., 2013), Clark's method (barometric loading), median of ratios method (Gonthier, 2007), and earth tide analysis (Acworth et al.,

2015). Loading or barometric efficiency should be estimated on data series that are not affected by other processes such as rainfall recharge and groundwater extraction (Clark, 1967) (Davis and Rasmussen, 1993). For all three methods, intervals of time were selected where no processes other than barometric pressure change were observed to influence groundwater levels. Where a spike in water level was observed in the dataset, possibly associated with rain events or sudden decreases in water level resulting from dewatering, the time period was removed prior to estimating barometric efficiency.

3.2.4.1 Visual method

This method was developed by Smith et al. (Smith et al., 2013) and uses the best fit of time series data to loading efficiency by applying visual inspection (Equation 4). This involves two steps and uses barometric loading. First, the absolute pore pressure, p_m, data is converted to gauge pressure by removing the average barometric pressure, B_{ave}, during the period of monitoring. The second step involves multiplying the loading efficiency, γ, (varying from 0 to 1) by the change in barometric pressure (B at the time when measurement was taken minus B_{ave}). The loading efficiency is adjusted by visually finding the best fit to the pore pressure record with least fluctuation. These two steps result in the corrected pore pressure, p_c.

$$p_c = (p_m - B_{ave}) - \gamma(B - B_{ave}) \qquad \textbf{Equation 4}$$

Where the data are received as gauged pore pressure, the first step can be omitted. This method has been found to be relatively objective (Anochikwa et al., 2012) in spite of the fit being observed visually.

3.2.4.2 Clark's method

The method developed by Clark (Clark, 1967) is based on the aperiodic, long-term barometric pressure variation and corresponding measured head changes. This is a standard method which provides comparison with other methods and data processing techniques (Gonthier, 2007; Rasmussen and Crawford, 1997).

The method involves two steps, noting that the barometric and head data need to be collated such that they have the same time increments and the same start and end time. There can also be no missing data in the dataset. In step one, the incremental changes in barometric pressure and head are generated. A positive sign in change in head denotes a rise in head and a positive sign in barometric pressure change represents falling pressure. In the second step, these values are added algebraically. In the second step that data is summarised as given in Equation 5 and Equation 6,

$$\Sigma\Delta W_j = \Sigma\Delta W_{j-1} + \omega_j \qquad \textbf{Equation 5}$$

where $\Sigma\Delta W_j$ is the sum of change in water level after the jth time interval, $\Sigma\Delta W_{j-1}$ is sum of change in water level after (j-1)th time interval and ω_j is absolute value of ΔW_j. The ω_j is the absolute value when the ΔW_j agrees with the ΔB_j (during a specific time interval, water level rises while barometric pressure falls or opposite). The ω_j is negative of the absolute value of ΔW_j if the sign of ΔW_j disagrees with the sign of ΔB_j (both water level and barometric pressure rise or fall). Similarly, $\Sigma\Delta B_j$ is the sum of change in barometric pressure after the jth time interval,

$$\Sigma\Delta B_j = \Sigma\Delta B_{j-1} + \mathrm{I}B_j\mathrm{I} \qquad \textbf{Equation 6}$$

If ΔB_j is zero (there in no change in barometric pressure between intervals), then ΔW_j is ignored so that changes in water level which are not related to barometric pressure are eliminated from further

calculation. With each time interval, the absolute value of ΔB is added to the ongoing sum, $\Sigma\Delta B$.

The time series of head changes are plotted as a function of time series of barometric changes. The slope of regression line drawn through the data represents the barometric efficiency. The loading efficiency is then calculated from barometric efficiency as (Rojstaczer and Agnew, 1989; van der Kamp and Gale, 1983),

$$\gamma = 1 - BE \qquad \textbf{Equation 7}$$

Merritt (2004) found that Clark's method is a good tool for estimating barometric efficiency when head data are of high quality and if influence on water level, not related to barometric pressure, is constant (Gonthier, 2007). However, the method may not be sufficiently robust and can provide values that are too low where datasets are impacted by noise, strong trends, and inaccurate timing.

3.2.4.3 Median of ratios method

This method uses the median of the ratio of water-level change to barometric pressure for consecutive long-term time intervals (over 30 days). It is a simple method and shows the reduction in the effects of barometric pressure and independent water level change. The median is considered to be a more robust estimate compared to the average. This is based on the fact that lack of correlation results corresponds to equal probability that the ratio of change in water level and barometric pressure is greater or less than zero. Therefore, median error in those cases will be equal to zero and median value for the ratio of water level and barometric change is close to barometric efficiency.

3.2.4.4 Earth tide analysis

The use of the frequency domain for pore pressure data analysis has advantages compared to standard time series analysis (McMillan et al. 2019). If groundwater levels are transformed from time series to the frequency domain, the effects of principle earth and atmospheric tide components can be identified and quantified. In this study the conversion from time series to frequency has been undertaken using the software TSOFT (Van Camp and Vauterin, 2005), which can be downloaded with no cost from http://seismologie.oma.be/en/downloads/tsoft. The calculated earth tide components M2 and S2 and the measured spectrum of the response in observed data is used to calculate the barometric efficiency (Acworth et al., 2015),

$$BE = \frac{dh}{dp} = \frac{S_{2h-a}}{S_{2h}} \qquad \textbf{Equation 8}$$

where S_{2h} can be obtained using TSOFT and is the measured spectrum of the S2 component of observed water level, while S_{2h-a} can be calculated from the difference in measured S_{2h} and calculated $S_{2h-earth}$. The $S_{2h-earth}$ is calculated as a product of the M component of the measured spectrum of water level data and the ratio of S2 and M2 components of the earth tide. By using Equation 6 the barometric efficiency can be converted to loading efficiency. The earth tides were generated for one location at Dalby. The TSOFT software converts the time series to frequency domain, with a bandpass filter applied accordingly. An example of earth tide analysis and frequency spectrum for solar and lunar tides are given for Strethenden62 in Figure 16.

3.2.5 Compressibility estimate

Compressibility of a formation can be obtained from the loading efficiency, provided that porosity is known, and given the compressibility of water. Loading efficiency, γ, is related to soil and water compressibility by,

$$\gamma = \frac{\alpha}{n\beta + \alpha}$$ **Equation 9**

where α is the unidirectional drained compressibility of the formation (kPa^{-1}), β is the compressibility of water (4.6 × 10^{-7} kPa^{-1} at 20°C), and n is the porosity of the formation. The value of α depends on the type of the material and its degree of saturation (Black and Lee, 1973; Skempton, 1954; Terzaghi et al., 1996). Thus, the compressibility of the formation (unidirectional drained) can be calculated from porosity and loading efficiency,

$$\alpha = \frac{\gamma\, n\, \beta}{1 - \gamma}$$ **Equation 10**

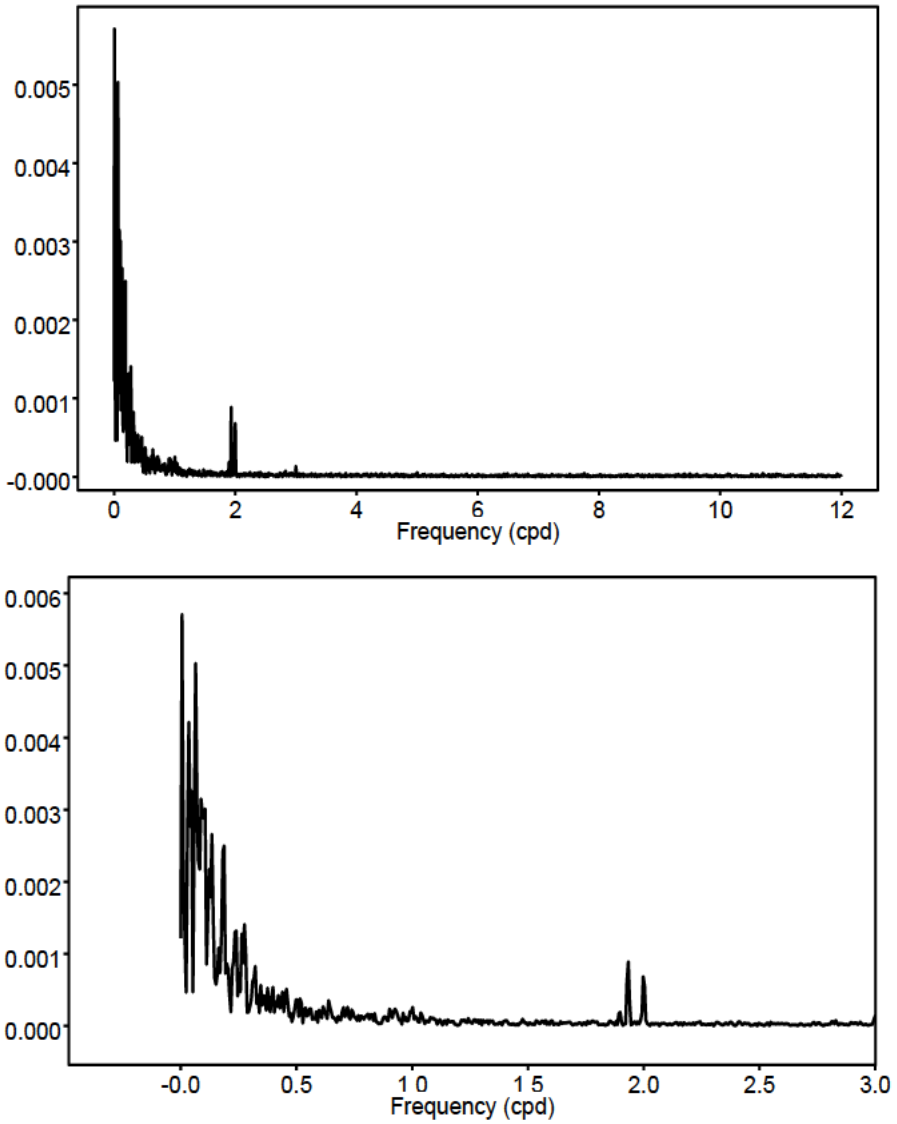

Figure 16: Discrete Fourier transform of time series data for Strethenden62 (frequency of 1 and 2 cpd).

The unidirectional compressibility of the formation is also known as the coefficient of volume change m_v (kPa^{-1}) which is subsequently used in settlement calculations.

It is important to note that several assumptions have been made in this study. Firstly, the response to loading is assumed to be vertical, assuming formations are of large extent, which is an approach that is consistent with the work of van der Kamp and Maathuis (1991) and van der Kamp and Schmidt (2017).

Further, the modulus is considered to be constrained, following the approach of Anochikwa et al. (2012) and Wang (2000). The earth tide data in this case were corrected to represent the constrained compressibility as do those measured by barometric efficiency. Constrained modulus, *M*, was calculated as,

$$M = 3B\frac{1-\nu}{1+\nu} \qquad \textbf{Equation 11}$$

This correction assumed a Poisson's ratio, ν, of 0.3 for all strata, as this parameter was unknown. The loading efficiency, defined for the case of undrained and constrained uniaxial compressibility is assumed equivalent to Skempton's coefficient, *B* (van der Kamp and Schmidt, 2017; Wang, 2000). The Skempton's coefficient represents the undrained pore pressure response to changes in mechanical load based on the assumption that horizontal strain is minor compared to vertical strain. Barometric response can be used to obtain the undrained and constrained uniaxial compressibility which can also then be expressed as a drained constrained modulus (Anochikwa et al., 2012; van der Kamp and Schmidt, 2017).

3.2.6 Calculation and verification of compaction and settlement

The contribution to surface movement from each stratum was calculated at the depth where groundwater level or pore pressure data was available. For normally consolidated soil the settlement, *S*, was calculated as,

$$S = m_v \Delta p H \qquad \textbf{Equation 12}$$

where *H* is the thickness of the target unit, m_v is the coefficient of volume compressibility (kPa^{-1}) and Δp is the change in pore pressure (kPa). The coefficient of volume compressibility, as measured in an oedometer test, is a measure of the reduction of thickness with increased stress. The coefficient of volume compressibility is also the inverse of the modulus that is unidirectional and drained (i.e. excess pore pressure is permitted to dissipate).

The thickness of the unit that was used in settlement calculations was equal to the screen intake length or within 1 m from the sensor depth for vibrating wire piezometers (i.e. the point of pore pressure monitoring) and immediately adjacent strata if similar geology was evident from the gamma log. The settlement in Figures 20 and 21 is based on the depth and length of the intake screen, considered as the point of monitoring.

A second estimate of settlement could be based on the estimated thickness of similar and continuous lithology around the point of monitoring. A downhole gamma log could provide an indication of similar lithology immediately above the screened section as that in the screened part of the bore (Table 2). A more detailed explanation of this procedure is shown in the example in Figure 17.

The change in pore pressure resulting from depressurisation or re-pressurisation is equal to an increase or decrease in vertical effective stress, respectively. Therefore, the difference in hydraulic head is assumed to be equal to the change in Δp if total stress is constant. For a change in head where the change in groundwater level is less than maximum pre-consolidation heads, an elastic response is assumed. In this case study the pre-consolidation stress is assumed to be less than the pre-consolidation stress as long term historical data was not available.

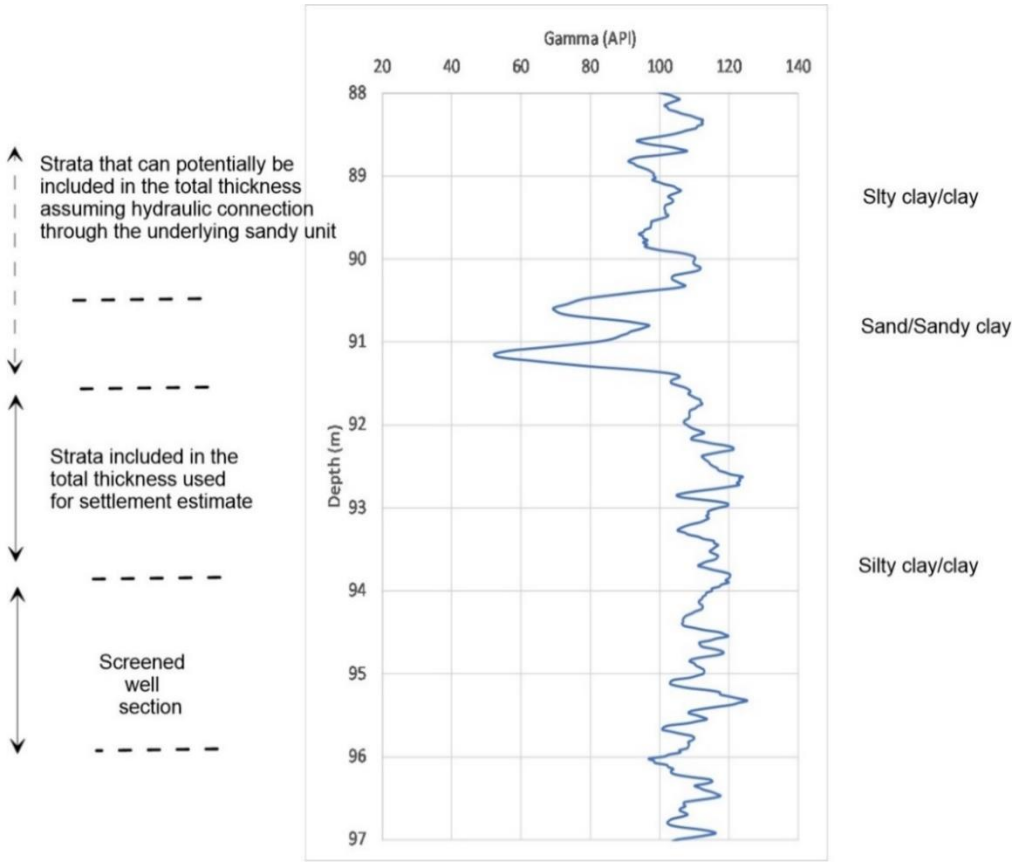

Figure 17: Determination of strata thickness for settlement estimate – example from downhole log of natural gamma activity that indicates clayey content of strata.

Table 2: Summary of monitoring bore data and parameters. Estimated strata thickness near intake screen length included consideration of geophysical data. #denotes bores where geological logs were obtained, however Meenawarra is missing most of the lithology log.

Bore ID	Screen installation depth (m)	Formation	Lithology	Installation type	Estimated strata thickness (m)	Length for settlement (m)	Porosity	Comments
Daandine 161#	45-50.5	Condamine Alluvium	Sand and clayey sands (20-40API)	Standard logger	38	6	0.4	Porosity average for limestone neutron porosity
Daandine 162#	55.6-57.6	Condamine Alluvium	Sand- sandstone (20-30 API)	Standard logger	2	2	0.38	Porosity average for limestone neutron porosity
Daandine 163#	62.5-64	Condamine Alluvium - Walloon Transition Layer	Sand and clay (20-60API)	Standard logger	10	10	0.36	Porosity average for limestone neutron porosity
Lone Pine 15	82.9-84.9	Condamine Alluvium - Walloon Transition Layer	Sand to Clayey sands (20-50API)	Standard logger	7	2	0.38	Calculated porosity from sandstone neutron and sandstone density porosity
Meenawarra-21#	86.3	Springbok Sandstone	n/a	VWP /non-vented	2	2	n/a	n/a
Stratheden-62	28-31.75	Condamine Alluvium	Clayey sands (40-100API)	Standard logger	3.75	3.75	0.52	Porosity average from limestone neutron porosity
Stratheden-63	111-114.8	Springbok Sandstone	Clayey sandstone (50API)	Standard logger	3.8	3.8	0.28	Porosity average from limestone neutron porosity
Stratheden-64	48-53	Westbourne Formation	Clayey sands (40-100API)	Standard logger	10	5	0.6	Porosity average from limestone neutron porosity
Tipton195	58-64	Condamine Alluvium		Standard logger	6	6	0.38	Assumed same as Daandine162
Tipton204#	85	Condamine Alluvium		VWP /non-vented	2	2	0.38	Assumed same as Daandine162
Tipton204#	132.25	Condamine Alluvium - Walloon Transition Layer		VWP /non-vented	2	2	0.28	Assumed same as Strathernden63
Tipton-222#	106-112	Condamine Alluvium - Walloon Transition Layer		Standard logger	6	6	0.38	Assumed same as Daandine162
Tipton206#	162-167	Taroom Coal measures	Shale/siltstone (40 -140API)	VWP /non-vented	20	20	0.6	Processed density average 1.83 g/cm^3 converted to porosity using sandstone density of 2.65g/cm^3 and water density of 1 g/cm^3
Tipton-221#	68.5-82	Condamine Alluvium		Standard logger	13.5	13.5	0.38	Assumed same as Daandine162

3.3 Results

3.3.1 Monitoring bore and geology data

The process of data collation identified several areas and bores where both high frequency data measurement was available in unconsolidated alluvium and in the underlying rock strata. These included Daandine and Tipton 204 bores to the northwest of Dalby, Strathenden bores to the west of Dalby, Tipton 206 and 222 to the east of Dalby, and Tipton 195 and 211, Menawarra21, and Lone Pine 15 to the south of Dalby (Figure 18). Unfortunately, these bores did not lie within the bounds of the InSAR data provided to this project.

The selected bores have sensors installed in the CA and the transition layer between the alluvium and the Walloon Coal Measures. The exceptions are Meenawarra 21 and Stratheden 63, which are monitoring Springbok Sandstone, and Stratheden 64, which is monitoring Westbourne Formation. For most of the bores the geophysical downhole log was available. This enabled classification of lithology within, and adjacent to, the screened intake, which is the point of pore pressure measurement.

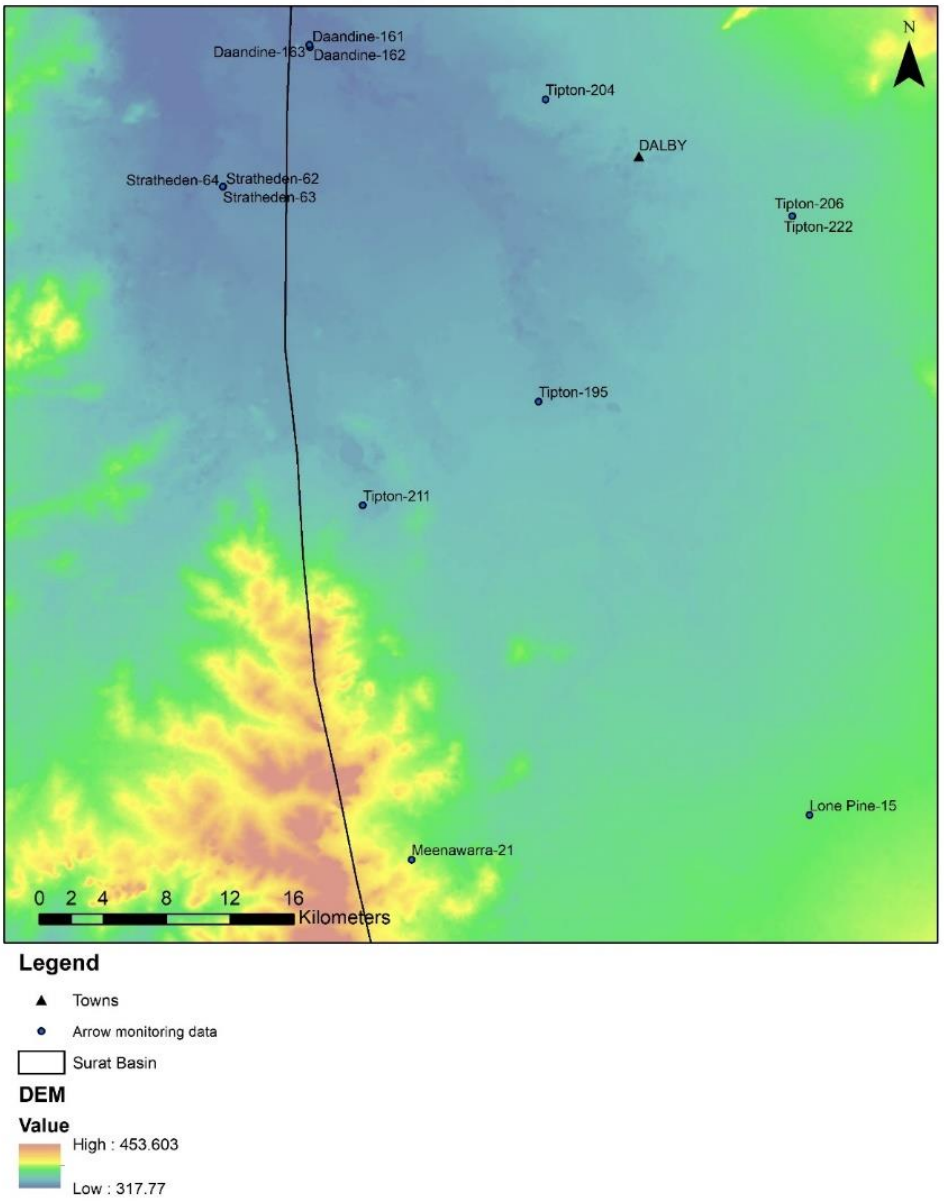

Figure 18: Locations of the bores selected for analysis in the Dalby area.

3.3.1.1 Porosity estimation

The porosity ranges from 0.28 to 0.6 and is calculated or obtained directly from the geophysical downhole log as listed in Table 2. Most of the porosity estimates are at the lower end of this range and are considered to be realistic. However, these results possess a level of uncertainty as discussed in Section 3.2.3.1, given that they are estimated using different methods. However, they provide an indication of the porosity for both alluvium and consolidated formations (Table 2). The porosities at two of the sites are relatively high (Stratheden-64 and Tipton206), warranting further consideration of the limited data.

3.3.2 Geological and stress history of site

The CA uncomformably overlays mostly Jurassic rocks and to a lesser extent Tertiary basalt (Dafny and Silburn, 2014). The Jurassic rocks in the research area (from oldest to youngest) include the Walloon Coal Measures, Springbok Sandstone, and Westbourne Formation. The CA is bounded by the Main Range Volcanics (MRV) of late Paleogene–early Neogene age on the eastern margin of the valley. Since the late Paleogene, terrigenous sediments were accumulated within the alluvial valley. The accumulated sediments in the Condamine valley were derived from various parent materials and deposited in different environments (lacustrine/riverine/fan delta) (Dafny and Silburn, 2014). As a result, the sediments are quite heterogeneous. Faulting associated with Mesosoic and basement structure does not appear to have had an influence on the alluvial sediments (Huxley, 1982). Structural impacts on strata are related to movements associated with the Swan Creek anticline and Swan, Emu and Freestone Creek.

Two schemes now exist which consolidate the alluvial section into prominent units (Huxley, 1982; Sinclair Knight Merz, 1999): one based on depositional environment, transport and sedimentation processes (Huxley, 1982; Queensland Water Commission, 2012), and a second based on borehole lithology and includes three alluvial units (Sinclair Knight Merz, 1999). A transition layer is also part of the CA (identified by both schemes) characterised by a clayey zone between the granular/mixed alluvium and underlying Jurassic formation (Klohn Crippen Berger, 2010; Queensland Water Commission, 2012). In the recent geological history, the Condamine River has been eroding the alluvial Pliocene-Pleistocene terraces and reworking the near-surface sediments (Klohn Crippen Berger, 2010; Lane, 1979; Lumsden, 1966).

The ongoing accumulation of fine alluvial sediments occurs mainly at the eastern rims of the valley with MRV basalts being a primary source of clastic material. Based on the above review of geological conditions, and target research area it can be concluded that the older Jurassic units have been eroded in the past and are likely to be over-consolidated. However, the recent alluvial sediments (Paleogene) have only been subject to limited erosion along the Condamine River. It can also be concluded that although the older Jurassic units have been eroded in the past and are likely to be over-consolidated, the recent alluvial sedimentation (Paleogene) has only been subject to limited erosion along the Condamine River. In addition, the structural geology and faulting that is associated with the basement has had no influence on the CA. We therefore consider the stress regime in the CA sediments which are part of this research to be mainly related to sedimentary deposition. This means that lithostatic conditions prevail and the pore pressures are mainly related to changes in lithology with depth rather than changed stress conditions.

Tectonic stresses, residual from past tectonic activity or active movements are all important in understanding the stress history of the research area. These stresses are mostly horizontal but strongly directional. For example, erosion of valleys causes redistribution of stress resulting in topographically

related stresses (Zhang et al., 2016). As a result, consolidation characteristics will be dependent on geological history of the deposit. The eroded beds are typically over-consolidated, but younger strata is normally consolidated. The younger strata will therefore be influenced by greater extent by settlement, compared to older normally or over-consolidated beds (Atashbari, 2016). The relatively shallow and younger strata are subject to vertical primary stress.

3.3.3 Total load and consolidation state

Short term settlement depends on the elastic properties of the material and occurs immediately upon loading. Reduction in pore pressure causes rearrangement of the particles which impacts the consolidation. In soft material, consolidation may take a long time, but in consolidated material (i.e. rock), consolidation occurs quickly due to their brittle characteristics. Where low permeability material forms the consolidating layer the drainage from that layer will depend on the thickness of such material, and this will become significant if the time aspect is considered.

In soil mechanics, the deposition–consolidation–erosion cycle results in clays becoming over-consolidated. As a result, these clays show a different deformability behaviour. In fractured rocks, when the rock matrix is mostly deformed elastically, the over-consolidation phenomenon may occur in non-planar discontinuities of a rock (Babanouri et al., 2011).

3.3.4 Groundwater extraction

Estimated abstraction (metered and unmetered) varied between 97 and 70 GL/year up until the early 1980's and between 67 and 46 GL/year since then (Dafny and Silburn, 2014). The sustainable yield of the aquifer has been estimated, however, to be only 15 to 30 GL/year (Kelly and Merrick, 2007). Barnett and Muller (2008) reported the metered abstraction of around 31 GL/year. The mandatory reductions in allocations in the 1980's, 1994 and 2010 resulted in metered reduction in abstraction to 46 GL/year (CSIRO, 2008; Klohn Crippen Berger, 2010). Visualisation of the decline in water table elevations during the last 40 years of intensive agriculture are available in the work by Cox et al. (2013). Their work shows the upper Condamine valley as an example where decline in water levels ranges up to 50 m over the past 40 years of dewatering.

3.3.5 Groundwater levels and historical drawdown

A review of groundwater levels was undertaken to understand the seasonal variation and estimate the maximum historical drawdown (Table 3).

For each of the monitoring locations described in this study, the stresses have been calculated (Table 3), where effective stress is total stress minus pore pressure. This calculation assumes fully saturated strata (and fresh water density of 1.0 g/cm^3). The systems based on these results do not appear to be over-pressurised, with pore pressures below the lithostatic pressure. The maximum observed drawdown during the period of monitoring has been used to estimate the change in effective pressure as a result of this withdrawal.

The summary of groundwater level changes over the past 50 to 60 years is presented below (OGIA, 2016):

- In the southern CA area groundwater levels have been stable over the past 40 years with fluctuation of less than 5 m, and with little seasonal variation;
- In the southern central area south of Dalby and east of Cecil Plains in the period from 1965 to 2010, groundwater levels fell by about 25 m with stabilisation after this time period. However, these bores show large seasonal fluctuations;

- In the central area, around Dalby, in the period from 1960 to 2010 the groundwater levels declined by approximately 15 m and have stabilised or recovered since 2007 (OGIA, 2016). In this area there is large groundwater response to seasonal changes. The stabilisation and recovery is attributed to decreased extraction and increased recharge (Dafny and Silburn, 2014);
- In the western part of the CA, the groundwater levels have been stable with fluctuations of less than 5 m, and limited seasonal fluctuation. However, large rises were reported after the floods in 2010 and 2011;
- In the eastern part of the CA the groundwater levels were stable or have risen slightly;
- In the northern area the groundwater levels were relatively stable.

The overview of the groundwater level changes and maximum fluctuations (in particular drawdown) over the past 50 to 60 years provides good basis for setting the maximum expected additional drawdown that could induce surface movement (Table 3).

3.3.6 Compressibility estimate

The results of the analysis of pore pressure data using four methods provided an indication of the likely range of loading efficiency values. These are presented in Table 4 along with their respective compressibility values. Compressibility values derived from the earth tide method are shown in Figure 19 relative to the depth below ground and the strata type. There are no apparent trends in Figure 19, except that sandstone compressibility is relatively low (one value), and compressibility of the Taroom coal measure is relatively high (one value). Additional data points and evaluation of the *in situ* compressibility methods are recommended to confirm these observations.

The compressibility calculated using the *in situ* data was compared to the data presented in IESC (2014). This report presented examples of different modelling approaches to predict compaction due to changes in groundwater pressure. For this purpose, the study assumed a number of layers existed in the sedimentary sequence but did not go into detail in providing the lithology for those layers, with the exception of the CSG bearing formation. The compressibility values (equivalent m_v) provided in that report vary for sedimentary strata from 10^{-4} to 10^{-5} MPa^{-1} (with exception of alluvium and coal seam bearing formation).

In situ compressibility values of 10^{-5} to 10^{-7} kPa^{-1} (10^{-2} to 10^{-4} MPa^{-1}) from our analysis of pore pressure data are consistent with compressibility values reported, although there is a large range that needs to be considered. Our results are consistent with literature values (Baker et al., 2015; Fitts, 2013; Liu et al., 2004; Mbia et al., 2014) of 10^{-4} to 10^{-5} kPa^{-1} for sandstone and 10^{-4} to 10^{-7} kPa^{-1} for shale and clayey strata. The modelling implications of site specific differences between strata, particularly alluvium, rock, and transition zone materials need to be considered. Also, the reasons for a wide range of compressibility values, such as the method and scale of testing (e.g. laboratory core, *in situ* at depth, field monitoring of drawdown and surface movement) are yet to be fully considered.

Table 3: Summary of groundwater levels, maximum drawdown and stresses, as described in Section 3.3.4

Bore ID	Screen installation depth (m)	Pre-development groundwater level (mAHD)	Current maximum groundwater level drawdown (m)	Total stress (kPa)	Pore pressure (kPa)	Effective stress (kPa)	Pore pressure with groundwater withdrawal (kPa)	Change in effective stress due to water withdrawal (kPa)	CA groundwater area	CA groundwater conditions	Max additional drawdown expected (based on historical data)
Daandine 161	45-50.5	315	5.3	1288.1	495.4	792.6	52.0	740.7	Northern	stable	1.06
Daandine 162	55.6-57.6	315	7.2	1469.1	565.1	904.1	70.6	833.5	Northern	stable	1.44
Daandine 163	62.5-64	314.5	5.6	1632.4	627.8	1004.5	54.9	949.6	Northern	stable	1.12
Lone Pine 15	82.9-84.9	320	17.3	2165.5	832.9	1332.6	169.7	1162.9	Western	stable, less than 5 m fluctuat'n, large fluctuation with flood	17.3
Meenawarra-21	86.3	339	34	2201.2	846.6	1354.6	333.5	1021.0	Eastern	stable and rising	8
Stratheden-62	28-31.75	317.7	2.4	808.5	311.5	497.1	23.5	473.5	Central	15 m decline, now stable and recovery, huge seasonal fluct	2.4
Stratheden-63	111-114.8	316.1	0.4	2928.1	1126.2	1801.9	3.9	1798.0	Central	15 m decline, now stable and recovery, huge seasonal fluct	0.4
Stratheden-64	48-53	317.5	0.5	1351.8	510.1	841.7	4.9	836.8	Central	15 m decline, now stable and recovery, huge seasonal fluct	0.5
Tipton195	58-64	324	0.2	1632.4	627.8	1004.5	2.0	1002.6	South	25 m decline, now stable and recovery, huge seasonal fluct	0.2
Tipton204	85	312	0.7	2168.0	833.9	1334.2	6.9	1327.3	Central	15 m decline, now stable and recovery, huge seasonal fluct	0.7
Tipton204	132.25	305	1.6	3373.2	1297.4	2075.8	15.7	2060.1	Central	15 m decline, now stable and recovery, huge seasonal fluct	1.6
Tipton206	162-167	352.2	0.1	4259.5	1638.3	2621.2	1.0	2620.3	Central	15 m decline, now stable and recovery, huge seasonal fluct	0.1
Tipton-221	68.5-82	321.6	0.1	2091.5	804.4	1287.1	1.0	1286.1	South	25 m decline, now stable and recovery, huge seasonal fluct	0.1
Tipton-222	106-112	321.6	0.05	2856.7	1098.7	1758.0	0.49		Central	15 m decline, now stable and recovery, huge seasonal fluct	0.05

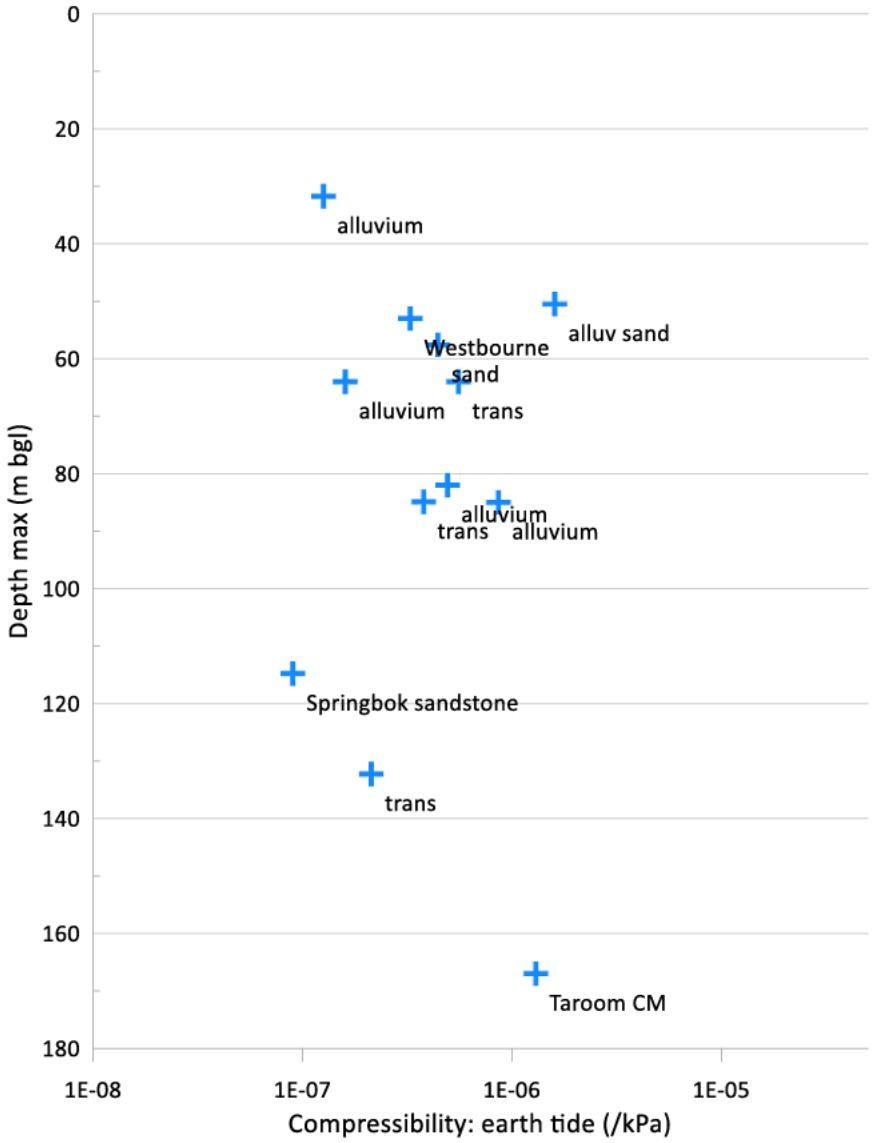

Figure 19: Compressibility of alluvium and rock strata in relation to depth based on the earth tide analysis of pore pressure data. Trans is the transition zone of the Walloon coal measures, Taroom CM is Taroom Coal Measures. Depth of each point is the maximum of the screen depth in metres below ground.

Table 4: Summary of compressibility estimated by four different methods.

		Loading efficiency					Unidirectional compressibility α (kPa^{-1})			
Bore ID	Screen Installation depth (m)	LE (visual method)	LE (Clark's method)	LE (Median of ratios)	LE (earth tide)	Porosity	Visual method	Clark's	Median of ratios	Earth tide
Daandine 161	45-50.5	0.71	0.91	0.94	0.93	0.4	4.50E-07	1.86E-06	2.88E-06	1.60E-06
Daandine 162	55.6-57.6	0.67	0.96	0.99	0.81	0.38	3.55E-07	4.20E-06	1.73E-05	4.43E-07
Daandine 163	62.5-64	0.88	0.98	0.98	0.85	0.36	1.20E-06	8.05E-06	8.05E-06	5.56E-07
Lone Pine 15	82.9-84.9	0.88	0.96	0.98	0.78	0.38	1.28E-06	4.20E-06	8.57E-06	3.79E-07
Meenawarra-21	86.3	0.99	0.978	0.97	0.89					
Stratheden-62	28-31.75	0.81	0.93	0.94	0.46	0.52	1.02E-06	3.18E-06	3.75E-06	1.26E-07
Stratheden-63	111-114.8	0.65	0.72	0.69	0.53	0.28	2.39E-07	3.31E-07	2.87E-07	8.99E-08
Stratheden-64	48-53	0.88	0.97	0.98	0.66	0.6	2.02E-06	8.92E-06	1.35E-05	3.27E-07
Tipton195	58-64	0.81	0.97	1	0.6	0.38	7.45E-07	5.65E-06		1.60E-07
Tipton204	85	0.78	0.48	0.5	0.89	0.38	6.20E-07	1.62E-07	1.75E-07	8.62E-07
Tipton204	132.25	0.8	0.75	0.76	0.73	0.28	5.15E-07	3.86E-07	4.08E-07	2.13E-07
Tipton206	162-167	0.7	0.6	0.55	0.88	0.6	6.44E-07	4.14E-07	3.37E-07	1.30E-06
Tipton-221	68.5-82	0.85	0.89	0.85	0.82	0.38	9.91E-07	1.41E-06	9.91E-07	4.93E-07
Tipton-222	106-112	0.62	0.4	0.38	0.65	0.38	2.85E-07	1.17E-07	1.07E-07	2.01E-07
Geometric mean		0.78	0.79	0.79	0.73		6.68E-07	1.37E-06	1.50E-06	3.84E-07

3.3.7 Compaction and settlement estimate

A workflow has been established and demonstrated for estimating surface settlement based on *in situ* compressibility values (Figure 15). The total settlement of the ground surface was estimated for a site with the most complete data, however, data gaps in most areas limited further application of this workflow (for Stage 2). This study has established and demonstrated this workflow to the extent that is possible with available data. To fully apply the workflow at all sites requires more complete data and information including:

- High frequency groundwater level data (several times a day for a few months) in monitoring bores or vibrating wireline piezometers that are representative of each strata in the profile (including clayey materials);
- Geological drill logs and either measured or assumed degrees of hydraulic connection between different strata;
- Downhole geophysical logs to estimate porosity, and or core measurements of porosity;
- History of groundwater level fluctuations and stresses at the site, including maximum drawdown and possibility of over-consolidated strata.

Verification of total settlement of the ground surface with remote sensing (e.g. InSAR) and modelling with sensitivity tests and further evaluation of timing were proposed as the final steps of the workflow.

Section 3.3.7.1 below estimates settlement of strata at the depth of monitoring for several sites. Section 3.3.7.2 provides an estimate of total settlement of up to **approximately 50 mm at the surface** which was demonstrated for a site where the most information was available. As discussed below, the range of estimated total settlement, from 1.1 to 47 mm, depends on many assumptions. Although it is not possible to verify these estimates at this site, the order of magnitude of surface settlement is consistent with other areas in this study.

3.3.7.1 Estimate of compaction of strata at depth of monitoring

A first pass estimate for settlement is provided for six bore locations in Figure 20 and 21, based on compressibility of the strata at the depth of monitoring only. The maximum potential settlement presented is limited to the strata at the monitoring depth and is based on the maximum incremental drawdown (i.e. any new drawdown beyond previous maximum) during the period of high frequency monitoring data (two to five years of hourly data).

The results for compressibility for all four methods were used to estimate settlement. The additional drawdown range is based on the previously observed drawdown and an example of this new drawdown and associated settlement is shown. The new additional drawdown considers the maximum drawdown as it occurs in the shortest period of time (days to a week). If additional drawdown is occurring over a long period of time (several months), new settlement would not occur unless drawdown exceeds previous maximum drawdown. For example, at the Daandine162 and Lone Pine15 sites, the maximum settlement, if any, had already occurred (based on regular drawdown of similar extent), any additional drawdown (i.e. beyond previous maximum drawdown) could result in additional settlement.

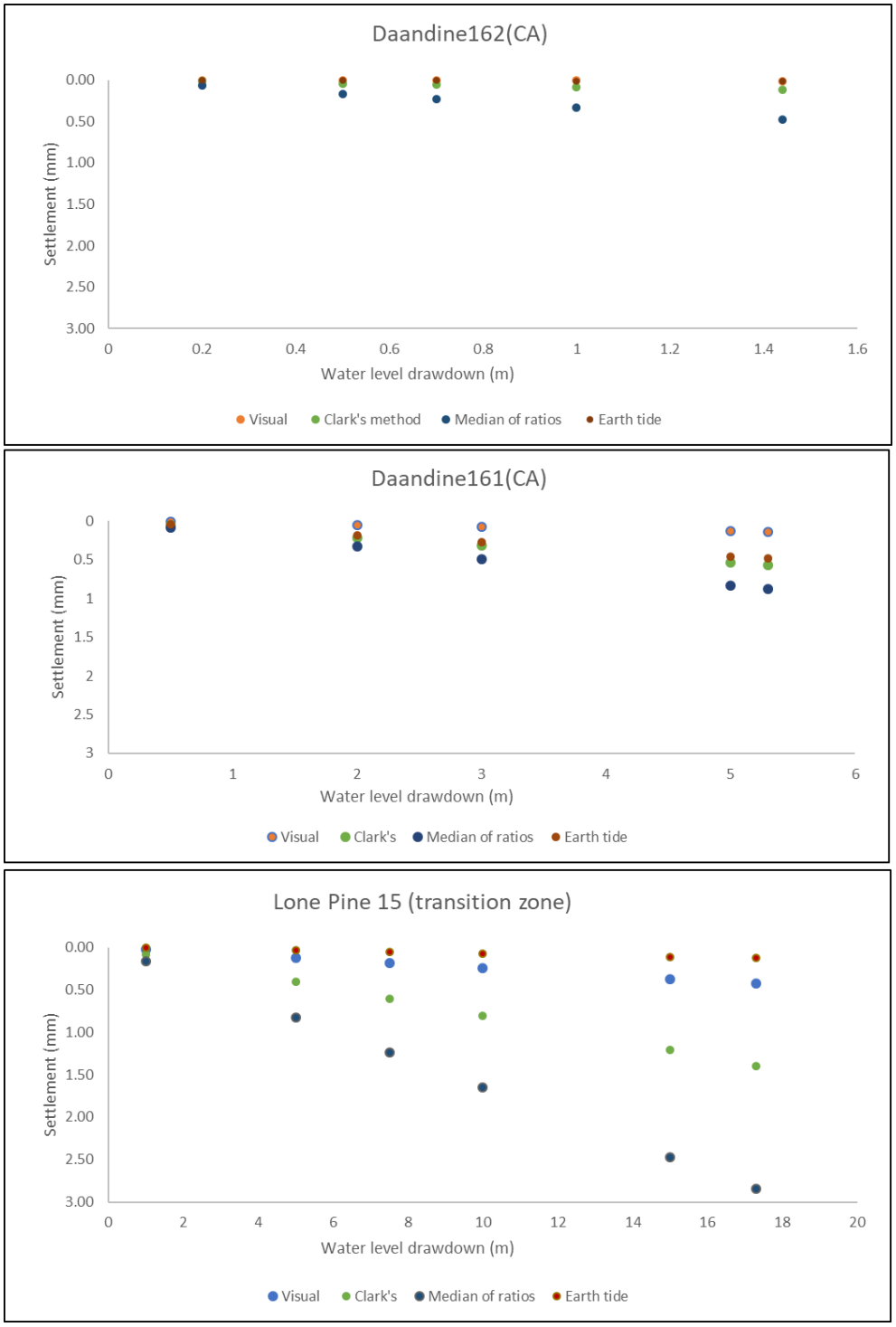

Figure 20: Compaction (considering screened interval as saturated thickness) at (top) Daandine162, (middle) Daandine161 and (bottom) Lone Pine 15 selected bore sites based on the current maximum drawdown and if additional new maximum drawdown increments were to occur. Based on atmospheric and earth tide methods to calculate in situ compressibility of the strata using high frequency pore pressure data.

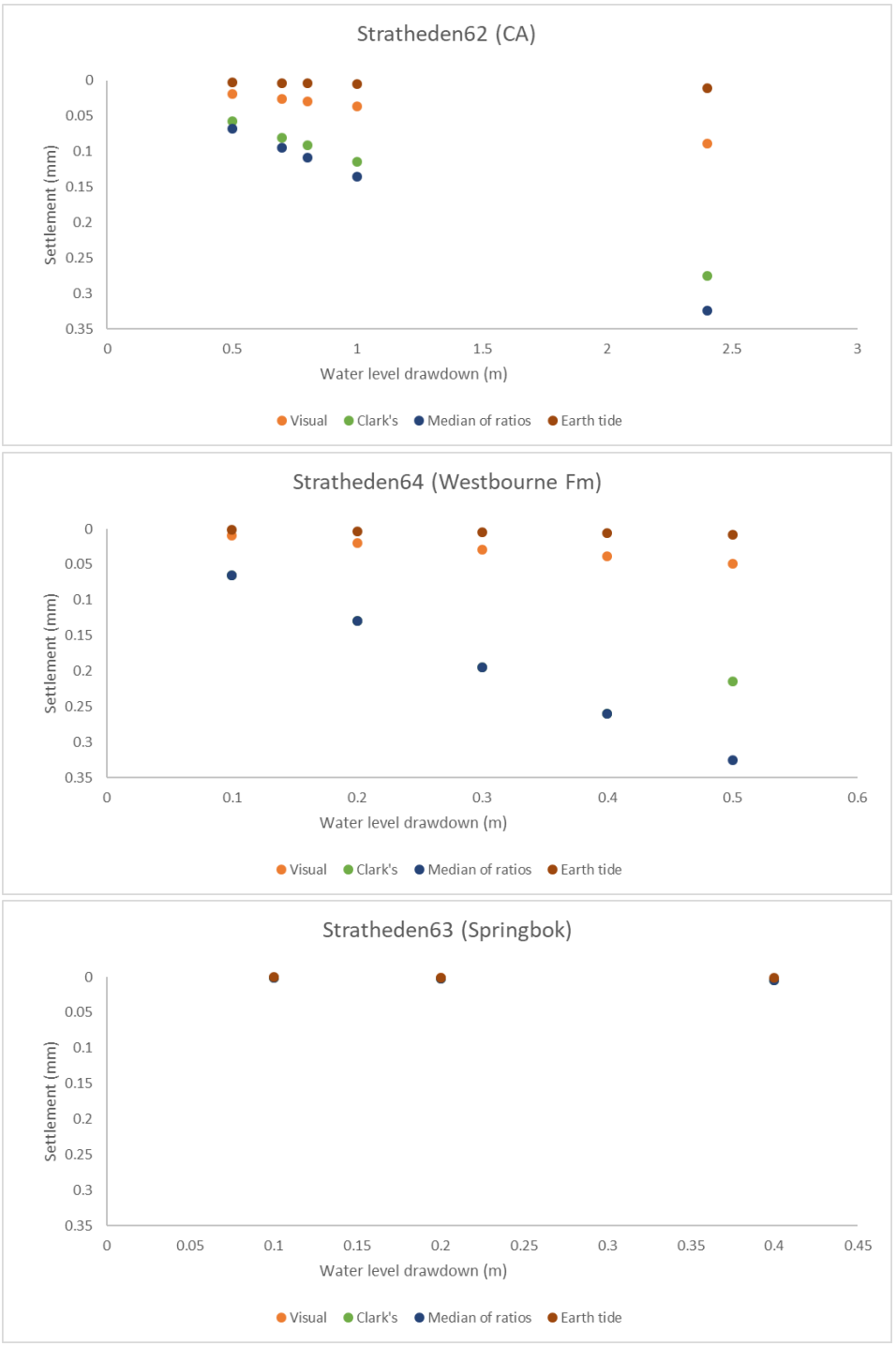

Figure 21: Compaction (considering screened section as saturated thickness) at Stratheden bore sites, (top) Stratheden62, (middle) Stratheden64 and (bottom) Stratheden63 based on the maximum drawdown recorded and if additional new maximum drawdown increments were to occur. Based on atmospheric and earth tide analysis methods to calculate in situ compressibility of the strata using high frequency pore pressure data. Note the vertical axis maximum is different to Figure 20 to better show the variations in these small settlement estimates.

3.3.7.2 Estimate of total surface settlement from ground surface to depth of monitoring

A first pass estimate of total settlement of up to **approximately 50 mm at the surface** was demonstrated for a site where the most information was available. For Daandine161 site with a total of 51 m of clayey and sandy alluvium, the total ground surface settlement was estimated between 1.1 to 47 millimetres

(details in Table 5), for a new maximum of 5.0 m of drawdown beyond the previous maximum drawdown with several assumptions as follows:

- Based on geological logs, simplified as two layers including 32 metres of clayey alluvium overlying 18 metres sand;
- Saturation with fresh water throughout profile;
- Hydraulic connectivity of 10-100% between the clayey material and the underlying sandy alluvium where the groundwater levels are monitored. For example, for 100% connectivity, the drawdown in the clayey material would be 5.0 metres, and for 10% connectivity the drawdown in the clayey material would be 0.5 m;
- Clay compressibility 10 times the sand compressibility;
- Does not account for time lags, or variable states of pre-consolidation of strata.

*Table 5: Range of settlement estimates for a site (Daandine161) with the assumptions described in Section 3.36 and Table 2 including for three methods of in situ compressibility calculation from high frequency groundwater level data at the monitoring screen. *Additional strata adjacent screen as identified in Table 2 and example of downhole geophysics in Figure 17.*

Daandine 161 site	Thickness for settlement estimate (m)	Settlement estimate (mm)			Assumed hydraulic connectivity of clay overlying sand
		Visual method BE	Median method BE	Earth tide method	
Part depth of screen only	6	0.14	0.88	0.49	n/a
Part depth of screen and strata*	38	0.87	5.58	3.09	n/a
Full depth to screen	50	7.3	46.8	25.9	100%
Full depth to screen	50	3.2	20.2	11.2	40%
Full depth to screen	50	1.1	6.9	3.8	10%

Estimates of surface settlement may often assume that the strata above the screened section is of similar compressibility to the depth at which groundwater levels are monitored. However, clayey materials are often relatively compressible but not often monitored for pore pressure changes unless using vibrating wireline piezometers. Further work is warranted on reviewing literature, laboratory and *in situ* values for compressibility that are representative of typical strata, including for clayey materials and for weathered transition zones for rock strata. Finally, additional research is recommended to evaluate each of the methods of estimating compressibility from barometric and earth tide analysis, and to implement ongoing improvements in the methods (McMillan et al., 2019).

The values of compressibility calculated by the 'Median' method is also used to estimate the settlement per metre of the drawdown, as presented in Table 6. These are 'first pass' estimates assuming 100% hydraulic connectivity and constant compressibility with depth, regardless of type of strata. Note that for each monitoring bore, varying thickness of compressible materials are assumed. This is to give a sense of the estimated settlement for each monitoring bore that was studied in this report. The values given in this table should be multiplied by the magnitude of drawdown (in metres) to estimate the absolute value of estimated settlement in millimetres.

Table 6: Calculation of settlement per meter of drawdown (in mm)

Wellbore	Compressibility - 'Median' Method (1/kPa)	Varying thickness of compressible materials (m)				
		1	10	20	50	100
Daandine 161	2.88E-06	0.03	0.3	0.6	1.4	2.8
Daandine 162	1.73E-05	0.2	1.7	3.4	8.5	17.0
Daandine 163	8.05E-06	0.08	0.8	1.6	4.0	7.9
Lone Pine 15	8.57E-06	0.08	0.8	1.7	4.2	8.4
Stratheden-62	3.75E-06	0.04	0.4	0.7	1.8	3.7
Stratheden-63	2.87E-07	0.00	0.03	0.06	0.1	0.3
Stratheden-64	1.35E-05	0.13	1.3	2.7	6.62	13.2
Tipton204	1.75E-07	0.00	0.02	0.03	0.1	0.2
Tipton204	4.08E-07	0.00	0.04	0.08	0.2	0.4
Tipton206	3.37E-07	0.00	0.03	0.07	0.2	0.3
Tipton-221	9.91E-07	0.01	0.1	0.2	0.5	1.0
Tipton-222	1.07E-07	0.00	0.01	0.02	0.05	0.1
* Groundwater density is assumed to be 1000 kg/m3.						
* Values should be multiplied by the magnitude of drawdown [m] to give the settlement.						

3.3.7.3 Summary of data requirements for compaction and settlement estimates

The data requirements for estimating compaction and surface settlement, using in situ compressibility values are summarised here to assist with future work stages and completing the workflow that was developed. Incomplete data available for each monitoring bore site means that there is not the same level of confidence in compressibility estimates across different sites, and the final steps of the workflow that was developed were unable to be completed.

Bore Site Data

- Pore pressure data (essential):
  - Logger data from either open monitoring bores or VWPs, and depth of sensor installation below ground;
  - Loggers should use the most accurate sensors possible (e.g. accuracy at 1% of full scale, so 10 m range logger is more accurate than 50 m range logger, vented loggers if possible);
  - Frequency of 1-4 hourly pore pressure (at least every 6 hours);
  - Duration of approximately three months pore pressure (minimum of one month) when no pumping or major rainfall has occurred;
  - Pore pressure data should, if possible, be provided in raw format without correction for elevation or barometric pressure and indication of units (kPa) and assumptions.
- Bore data (essential and if possible):
  - Bore construction, depth of intake screens, bentonite seals etc., surface elevation;
  - Natural gamma wireline logs and or lithological drilling logs (both if possible).
- Data to improve confidence of calculations (if available):
  - Barometric pressure data from each bore site, at exactly the same timing, frequency and duration as pore pressure data;
  - Neutron wireline logs;
  - Density and natural gamma wireline logs (if no neutron wireline logs).

Regional Data (essential)

- Barometer pressure data – ideally at each of the same as above sites, at the same time.
- Rainfall data, daily from a gauge in the area.
- Historical groundwater level data for regional aquifers.
- Information on hydraulic connectivity of regional aquifers.

4 Numerical modelling of poroelastic processes

The modelling work in this section, represents the example provided in IESC (2014), a report commissioned by the then Department of the Environment on the advice of the Independent Expert Scientific Committee on Coal Seam Gas and Large Coal Mining Development (IESC). However, numerical modelling is used in this document as opposed to analytical models to showcase the computational capabilities that are developing in this project. In this example, a profile of horizontally layered strata is considered (see Figure 22), which includes alluvium and sedimentary geological units underlying and overlying a coal bearing formation (coal measures). The alluvium extends from ground surface to a depth of 60 m (with the water table at 20 m depth), and is underlain by six sedimentary rock units, each of 100 m thickness. One of the rock units is the coal bearing formation, which extends from 360 m to 460 m depth below ground level.

The coal bearing formation is considered to include (potentially numerous) coal seams interbedded with sedimentary units, but the coal seams themselves are not explicitly represented. Instead, the hydraulic and geomechanical properties of the coal seams and sedimentary units in the coal bearing formation have been combined into an amalgamated geological unit. Young's Modulus (E) for the coal bearing formation in Figure 22 (interbedded sedimentary rock and coal seam units) is 14 GPa and is calculated assuming the vertical thickness of this formation consists of five per cent coal (with a drained E of 2 GPa) and 95 per cent sandstone (with E of 20 GPa). The CSG production well is considered to depressurise the coal bearing formation to a groundwater head level equal to 35 m above the top of the gas producing (coal bearing) formation. This is typical of the degree of groundwater depressurisation required for gas production to occur (IESC, 2014).

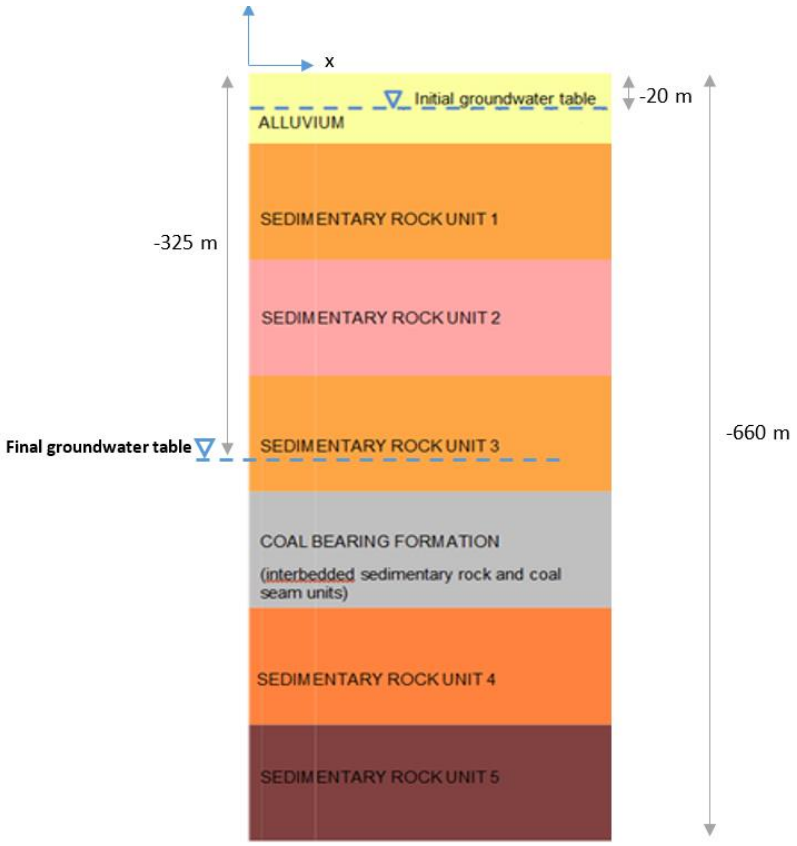

Figure 22: The profile of the horizontally layered strata with coal-bearing formation for the numerical example.

Two sets of models are used in this study to account for the hydro-mechanical characteristics of different geological units: uniform geology and variable geology. Uniform geology models calculate the potential subsidence, as if the geological profile is similar over the whole depth of the model. The simplifications of the uniform geology model may be reduced by accounting for both the variable permeability and the variable elastic properties of the geological units. The hydro-mechanical properties used in the numerical models are equivalent to those used by IESC (2014) as listed in Table 7. Note that k, E, ν, are the permeability, elastic Young's modulus, and Poisson's ratio, respectively. The equivalent m_v is not being used in the numerical models but listed to ensure their values are equal to those reported in IESC (2014).

Table 7. Hydro-mechanical properties of the geological units used in the numerical models.

Geological unit	Uniform geology					Variable geology			
	k (mD)	E (GPa)	ν $(-)$	Equivalent m_v (MPa^{-1})		k (mD)	E (GPa)	ν $(-)$	Equivalent m_v (MPa^{-1})
Unsaturated alluvium	1.064	15.41	0.25	-		1.064	0.20	0.30	-
Saturated alluvium				-		1.064	0.20	0.30	-
Rock unit 1				5.38E-05		1.064	8.00	0.25	1.04×10-4
Rock unit 2						0.319	14.00	0.25	5.95×10-5
Rock unit 3						0.106	20.00	0.25	4.17×10-5
Coal bearing formation						1.064	14.00	0.23	6.16×10-5
Rock unit 4						0.106	28.00	0.25	2.98×10-5
Rock unit 5						0.106	32.00	0.25	2.60×10-5

4.1 Steady state model

The steady-state model is constructed using Elfen (developed by Rockfield), a finite element- discrete element code. It should be noted that under steady-state conditions, the distribution of pore pressure and vertical effective stress is the same for both uniform geology and variable geology cases. The pore pressure before and after groundwater drawdown is depicted in Figure 23a and Figure 23b respectively. As a result of reduction in pore pressure (nearly 3 MPa at the bottom of the model), the vertical effective stress increases as can be seen in Figure 24. Such change in the stress state within the model, leads to vertical displacement of the strata as shown in Figure 25. Note that Figure 25a indicates subsidence of 92.6 mm and 72.8 mm for the uniform and variable geology cases, respectively. These values were estimated to be 72.4 mm and 47.7 mm in IESC (2014), where only the average change in pressure head within each unit is used for calculation of compaction in each unit.

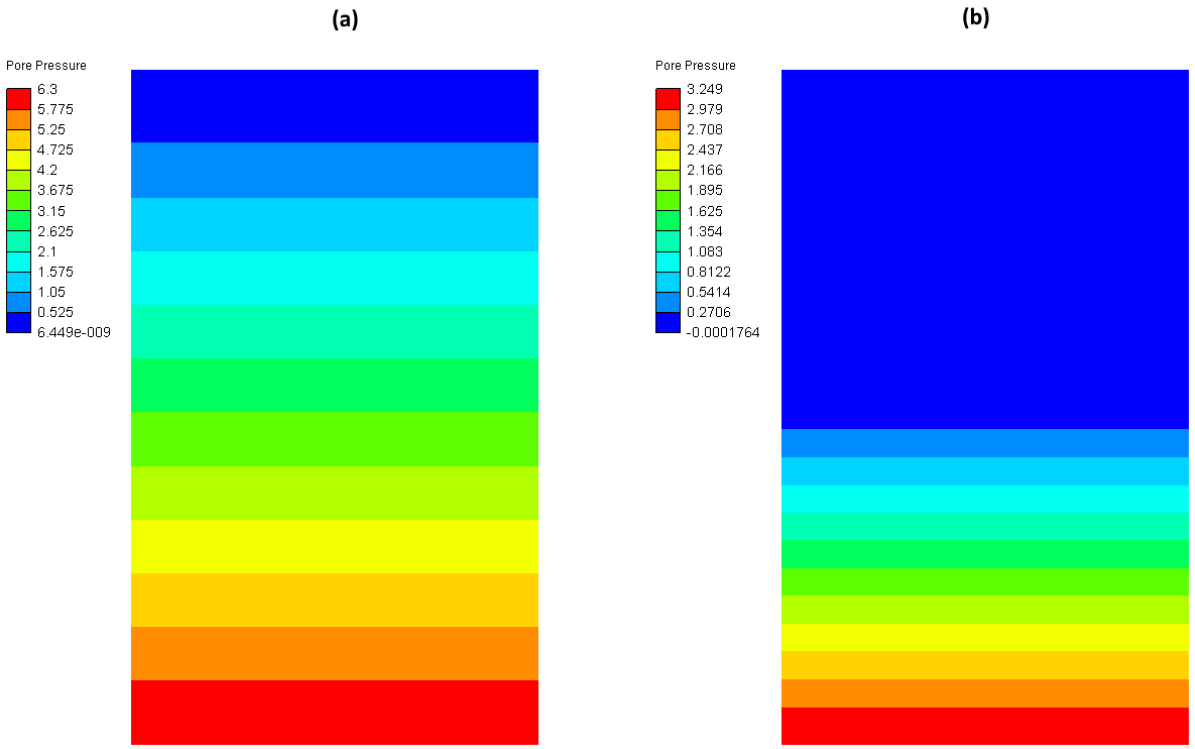

Figure 23: Contours of pore pressure (MPa): (a) before drawdown (b) after drawdown.

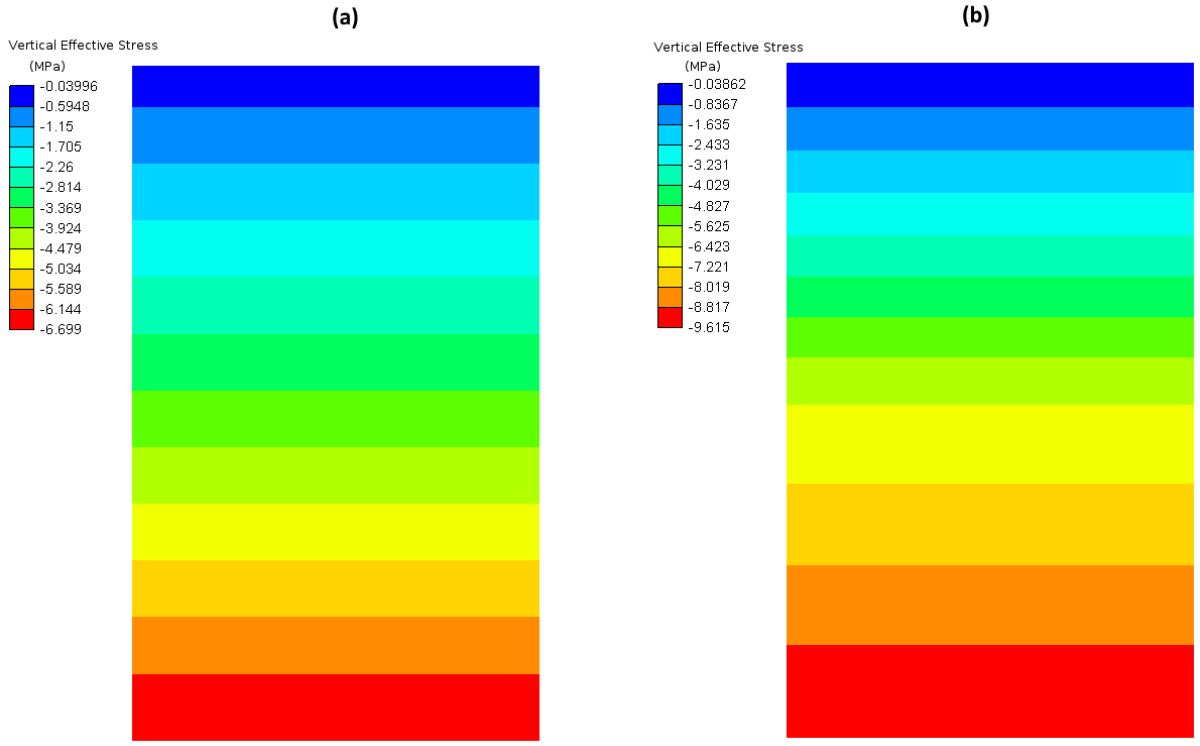

Figure 24: Contours of vertical effective stress: (a) before drawdown (b) after drawdown.

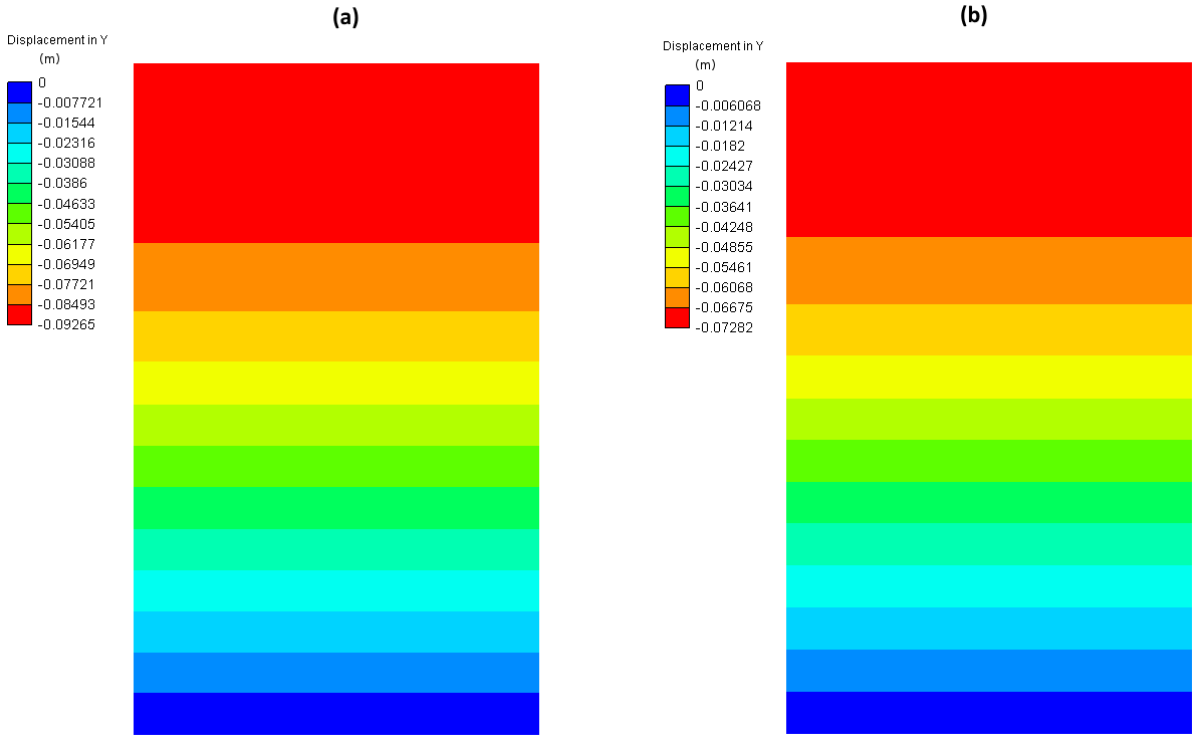

Figure 25: Contours of vertical displacement: (a) uniform geology case (b) variable geology case.

4.2 Transient model

A transient model was constructed using COMSOL Multiphysics, a finite element code, through coupling the Richard's equation and solid mechanics modules. It should be noted that the pore pressure within the alluvium layers is kept constant to keep the model consistent with that in IESC (2014). The hydraulic head in the perforated section of the wellbore (the whole length of the coal-bearing formation on the left side of the model) is kept the same as that in the steady state. The distribution of pore pressure for uniform geology is depicted in Figure 26 at different times (3, 12 and 24 months). As a result of reduction in pore pressure, the vertical effective stress increases as shown in Figure 27. Such change in the stress state within the model, leads to vertical displacement of the strata as shown in Figure 28. Note that Figure 28 indicates that maximum subsidence of 28 mm occurs after 3 months of groundwater extraction and it increases to 43.5 mm after two years for the uniform geology case. The IESC report has not reported the transient model for uniform geology.

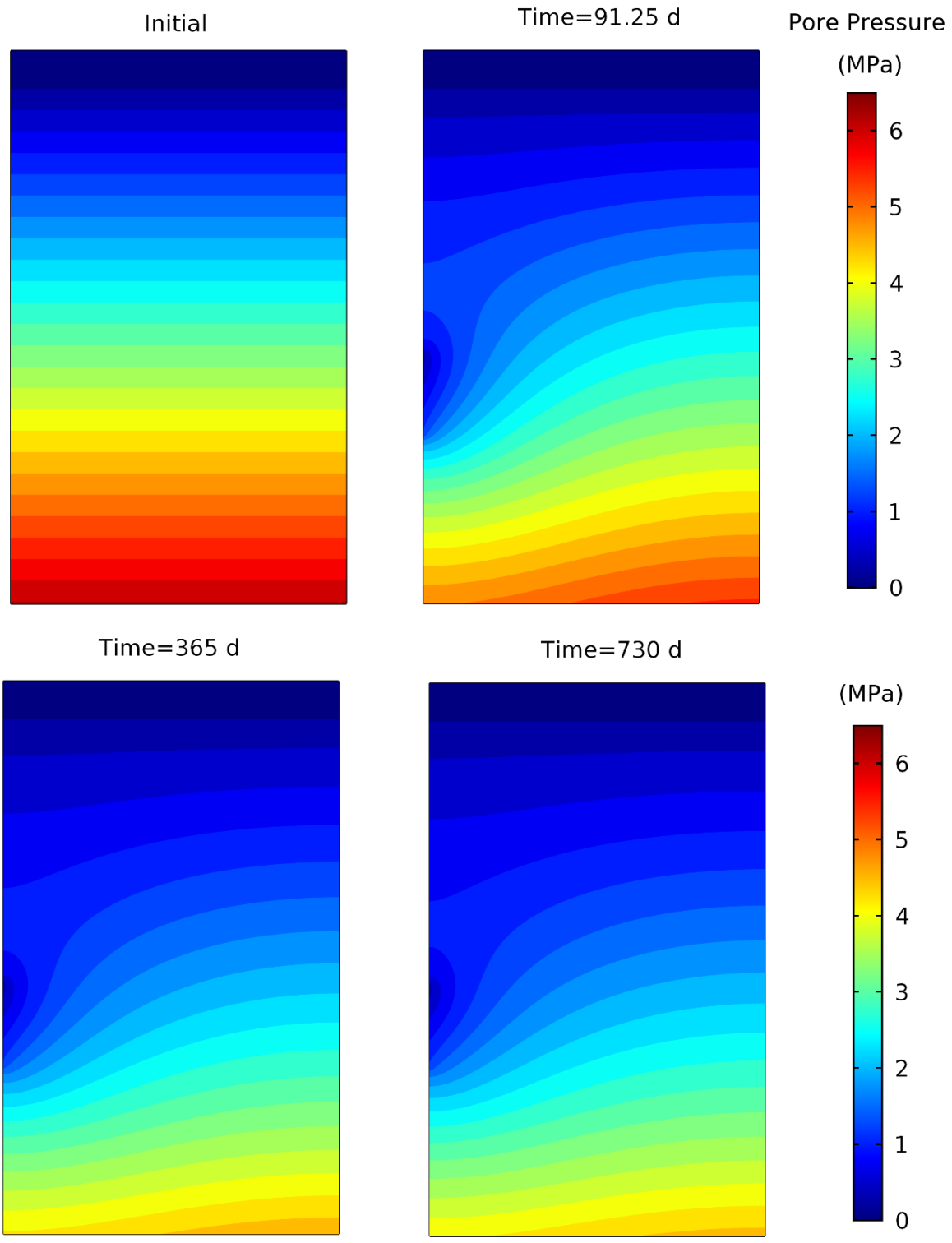

Figure 26: Contours of pore pressure for uniform geology case at different times.

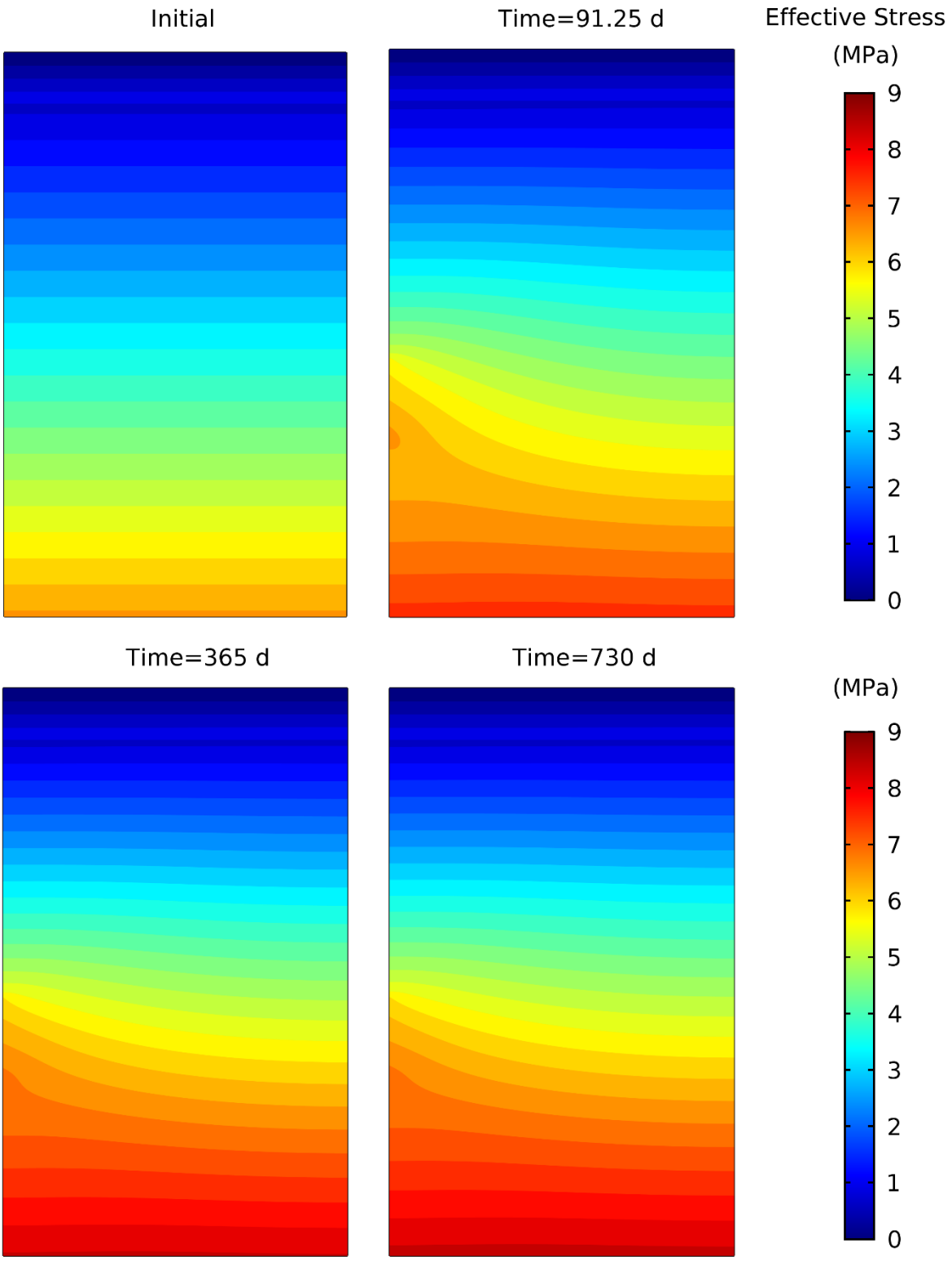

Figure 27: Contours of vertical effective stress for uniform geology case at different times.

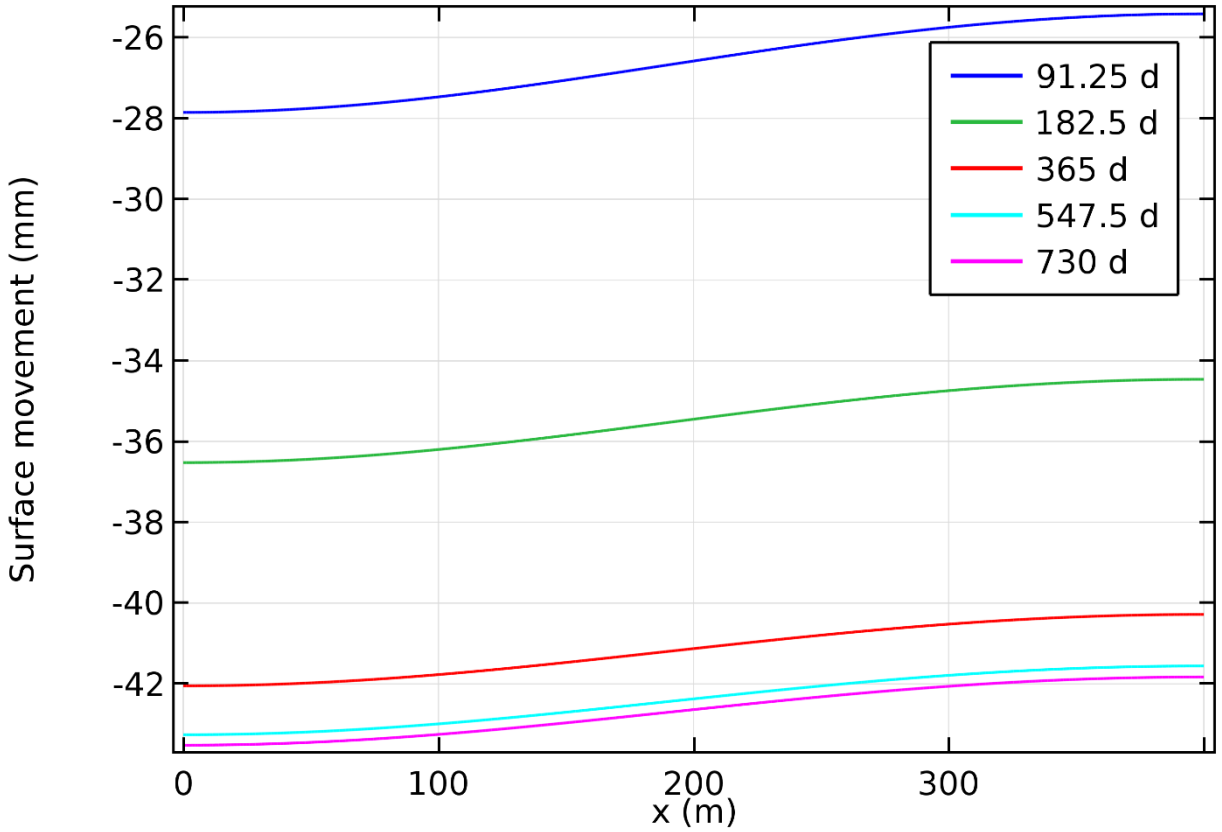

Figure 28: Profiles of ground surface displacement for uniform geology case at different times.

The transient model was then run using material properties of the variable geology, while all other parameters and constraints were kept the same. The distribution of pore pressure for uniform geology is depicted in Figure 29 at different times (3, 12 and 24 months). As a result of reduction in pore pressure, the vertical effective stress increases as shown in Figure 30. Such change in the stress state within the model, leads to vertical displacement of the strata as shown in Figure 31. Note that Figure 31 indicates that maximum subsidence of 17.1 mm occurs after 3 months of groundwater extraction and it increases to 34.8 mm after two years for the variable geology case. The IESC report has not reported the transient model for uniform geology. The difference between the subsidence predicted by the uniform and variable geology cases is due to the lower permeability of the sedimentary rock units in the variable geology that slows down the pressure reduction process.

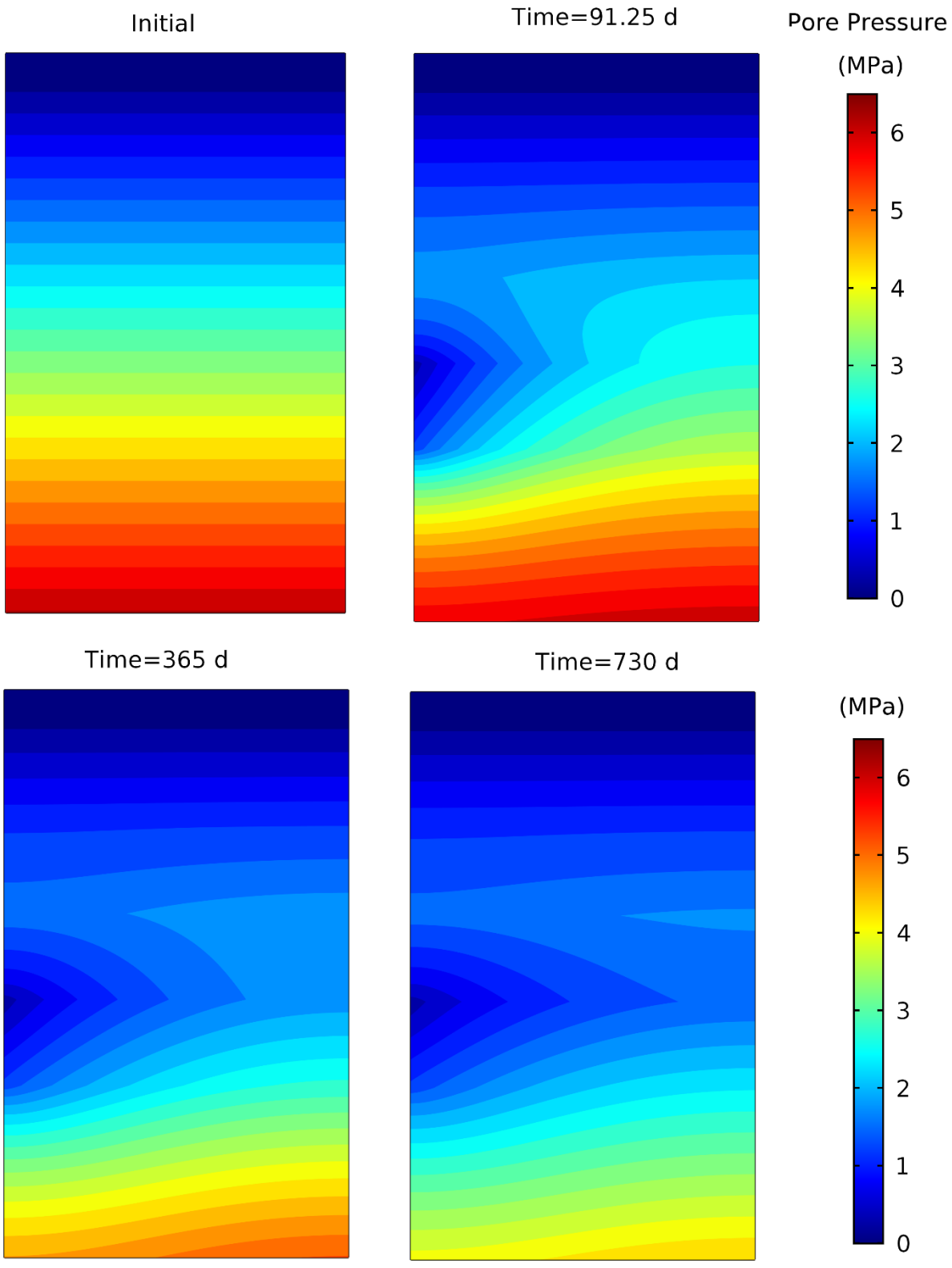

Figure 29: Contours of pore pressure for variable geology case at different times.

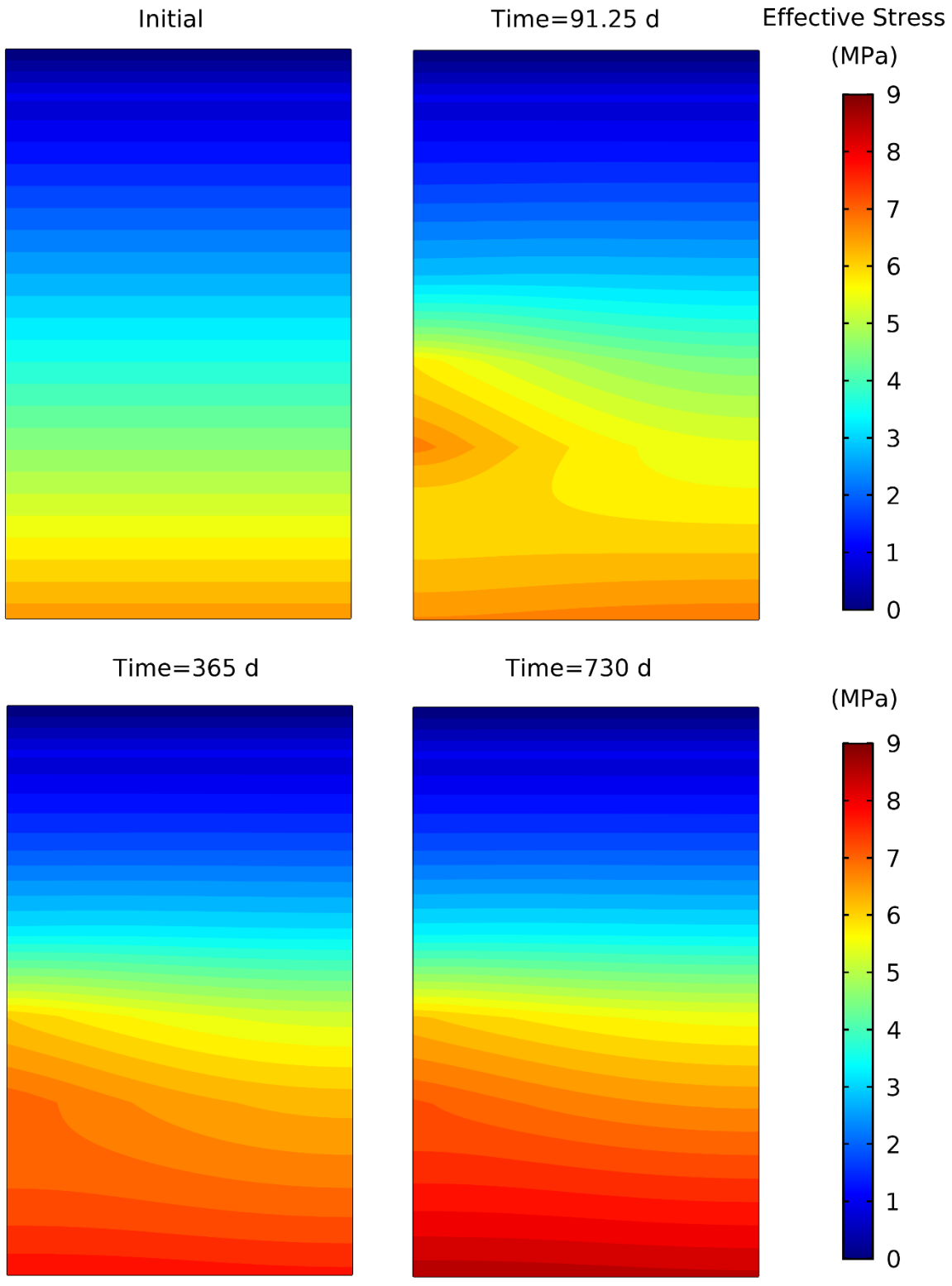

Figure 30: Contours of vertical effective stress for variable geology case at different times.

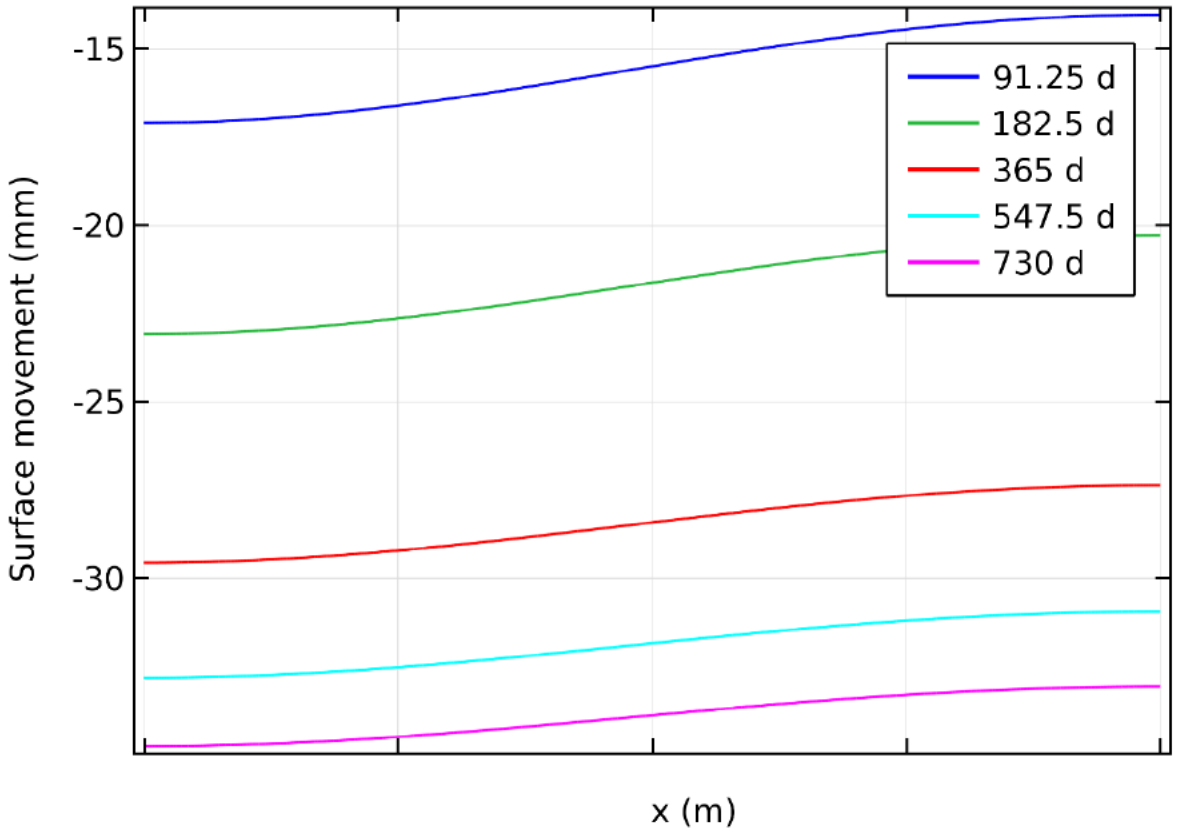

Figure 31: Profiles of ground surface displacement for variable geology case at different times.

Table 8 lists the calculated subsidence estimated using the numerical models in this report and those from the IESC report. As stated earlier in this report, the results of the steady state analysis shows a relatively large difference between the current model and the results of IESC report (IESC, 2014), which can be attributed to the simplified calculation procedure in the IESC report (e.g. only taking the average of the pressure head drop within each geological unit). On the other hand, the results of transient model are very close to values calculated in the IESC report.

Table 8. Comparison of estimated surface movement in the numerical example with the analytical solution the IESC report (IESC, 2014).

Case		Maximum estimated subsidence (mm)	
Flow condition	Geology	Numerical model	IESC report
Steady (long-term)	Uniform	92.6	72.4
	Variable	72.8	47.7
Transient (two years)	Uniform	43.5	N/A
	Variable	34.8	38

4.3 Transient model with more complex phenomena

In order to better understand the effect of more complex phenomena on ground surface movement, the analysis of the IESC example was extended. The IESC example analysed in the previous two sections did not explicitly represent the coal seams. To extend that analysis, the stratigraphical column was assumed to include three coal seams with sand as interlayers instead as depicted in Figure 32. Note that

all initial and boundary conditions remain the same as the analysis in the previous section and the model is constructed using COMSOL Multiphysics.

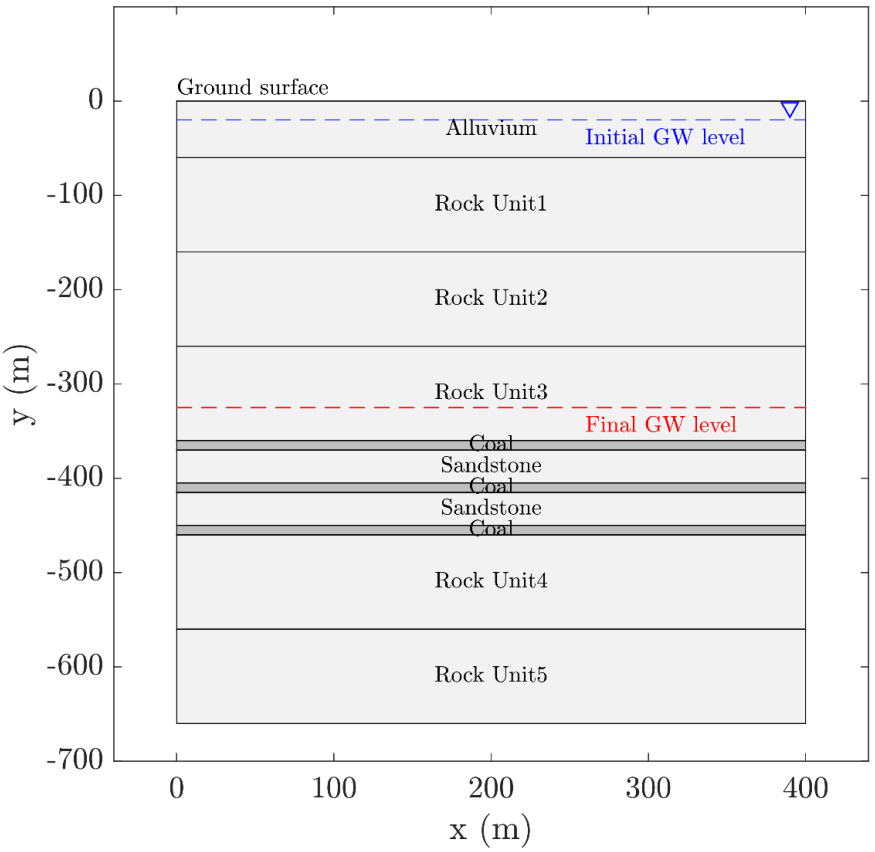

Figure 32: The domain and geometry of the geological profile used in the extended IESC analysis.

As a natural gas reservoir, coal is a naturally fractured medium, usually characterised by a dual porosity system composed of fractures (generally called cleats with apertures ranging from microns to millimetres) and matrix blocks (with side lengths of millimetres to centimetres) (Laubach et al., 1998). It is generally assumed that the flow of gas through cleats is a laminar viscous flow described by Darcy's law, whereas gas transport through the coal matrix (micro-pores) is assumed to be mainly controlled by a diffusive process closely related to the viscous flow and adsorption/desorption of gas molecules (e.g. Chen, 2011; Masoudian et al., 2013a; Masoudian et al., 2016a; Webb and Ho, 2006). Coalbeds are considered low-permeability reservoirs, and gas production involves an initial stage in which groundwater is extracted (depressurisation). The resultant lower pore pressure in the cleats allows the methane molecules to be desorbed and diffuse out of the matrix blocks and flow through the fracture system towards the producing wellbores.

It is well-established that adsorption and desorption of gas leads to relatively large volumetric changes in the coal matrix; i.e. swelling and shrinkage, respectively (Larsen, 2004; Saghafi et al., 2007). Such volumetric changes in the coal matrix can be considered as the key difference in the geomechanical behaviour of coalbeds compared to conventional reservoirs (Masoudian, 2013; Masoudian et al., 2013a; Masoudian et al., 2014). While production from the reservoir is associated with lower pore pressure and hence increased effective stress, the desorption-induced shrinkage of coal matrix can further complicate the geomechanical response of the coalbeds (Masoudian, 2016). While reservoir models consider the shrinkage phenomenon when investigating the variation of the fracture aperture and subsequently the fracture permeability (as reviewed and compiled by Masoudian et al., 2013b; Pan and

Connell, 2012; Peng et al., 2017; Zhu et al., 2018), many geomechanical models neglect or at best oversimplify its influence on the bulk volumetric response of the coalbed and consequently the displacement of the ground surface (Masoudian et al., 2016a; Wu et al., 2018). Nevertheless, the total displacement at the ground surface is the sum of all compaction mechanisms occurring within multiple geological units. It is dependent on the magnitude and direction of compression (which are dictated by pressure changes from groundwater withdrawal and desorption of gas from coal seams), the depth and depth-interval over which compression occurs, and the geomechanical properties of the geological units throughout the entire depth profile.

This work aims to develop a framework for the assessment of ground movement associated with CSG depletion, in which the desorption-induced shrinkage of coalbed will be properly implemented within a coupled geomechanical and reservoir modelling framework. In order to achieve this, a finite element model was constructed, in which a horizontal poro-elastic coal-bearing formation is overlayed by a sequence of overburden formations. The desorption-induced shrinkage in this model is implemented in a way that concurrently impacts both fracture aperture and the bulk volumetric response (and consequently the ground surface movement) of the coal-bearing formation. The results are interrogated to quantify the contribution of two distinct mechanisms to surface movement, namely pore pressure reduction and desorption-induced shrinkage.

4.3.1 Coalbeds and internal swelling

At the microscopic scale, coal is considered as a system of matrix blocks and three orthogonal fracture sets: face cleats, butt cleats and bedding plies (see Figure 33a). Most conceptual models for the microscopic geometry of coal assumes that the matrix blocks are completely isolated by the cleats between them. However, Wang et al. (2014) argues that the matrix blocks are rather connected by bridges, as shown in Figure 33b. The significance of such microscopic geometry becomes more obvious considering the swelling/shrinkage effect in coal. Due to the polymer-like structure of coal matrix blocks, adsorption of gas in micro-porosity of matrix blocks leads to their swelling, and desorption leads to shrinkage (Larsen, 2004). Under confined conditions, the coal bridge and the local matrix block around the cleat begin to swell. Because of the larger area of the matrix block, its swelling force is greater than that of the matrix bridge and as a result the coal bridge and the cleat are compressed by the 'internal swelling' of the matrix block. Gas continues to diffuse into the blocks, the swelling front advances into the blocks and causes an outward expansion of matrix blocks. The 'internal swelling' effect (Liu et al., 2011) leads to smaller fracture aperture and in turn reduced permeability of coalbed. The 'external swelling', however, leads to the expansion of bulk coal (fracture-matrix system). The conceptual representation of this process is depicted in Figure 33c. The laboratory experiment where the sorption-induced swelling (ε^s) is quantified usually involves the use of small coal samples to eliminate the effects of cleats and they are usually fitted to Langmuir isotherm as follows

$$\varepsilon^s = \frac{\varepsilon_L^s \, b_L p}{1 + b_L p} \qquad \textbf{Equation 13}$$

where p is the pressure, b_L is the Langmuir constant, and ε_L^s is a constant representing the maximum volumetric swelling strain of coal. Internal swelling contributes to bulk volumetric changes of the coalbed in the field scale geometry of the model in Figure 32, while the former contributes to the changes in aperture of cleats and consequently the permeability of the coalbed. Therefore, when formulating the permeability model, only a fraction of ε_L^s must be used while the remainder should be included in the bulk deformation of the coalbed. Therefore, F_{in} can be defined as the 'internal swelling ratio' so that

$$\varepsilon_{in}^{s} = F_{in} \times \varepsilon^{s}$$
$$\varepsilon_{ex}^{s} = (1 - F_{in}) \times \varepsilon^{s}$$

Equation 14

where ε_{in}^{s} and ε_{ex}^{s} are the internal swelling and external swelling, respectively. Zang et al. (2015) and Wang et al. (2014) indicated that F_{in} may be a function of coal structure, the cleat aperture (porosity) and the confining stress, but a constant internal swelling ratio has been assumed throughout this paper for simplification.

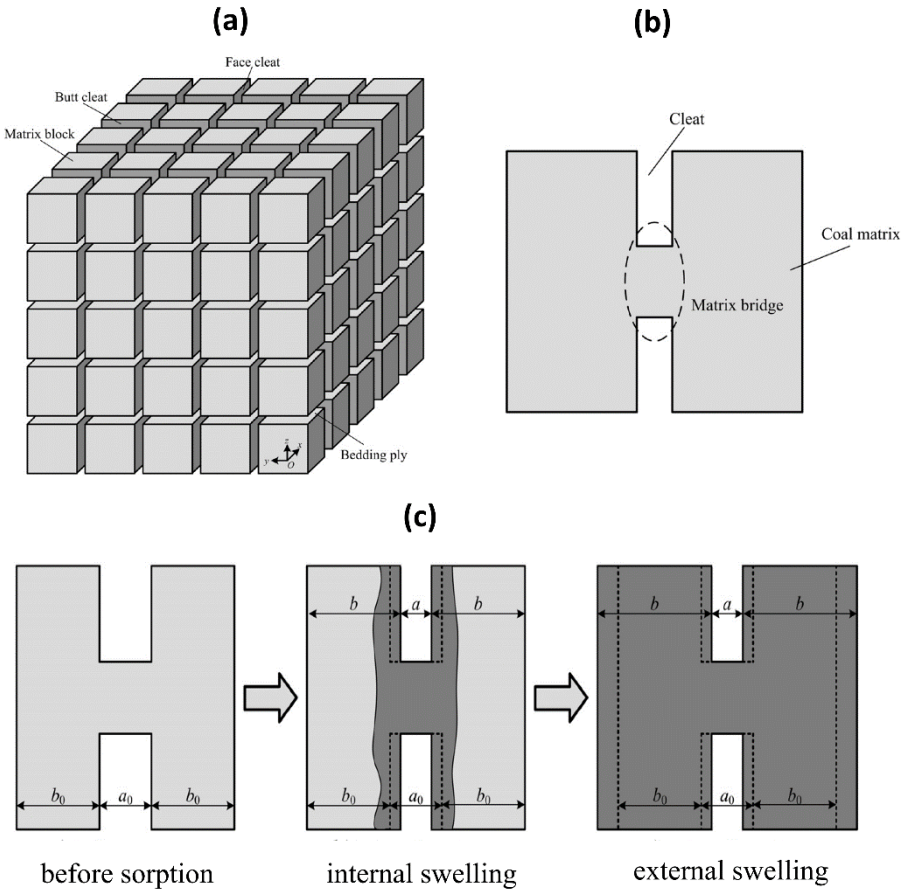

Figure 33: The conceptual representation of (a) microscopic geometry of coal, (b) the bridge structure connecting the matrix blocks, (c) the internal and external swelling (adapted from Liu and Rutqvist, 2010; Wang et al., 2014)

The simultaneous implementation of the internal and external swelling concepts in the model is explained later in this section.

The complete theory and governing equation for Richard's equation model can be found in the relevant literature (COMSOL-Multiphysics, 2012; Richards, 1931; Taigbenu, 1999; Van Genuchten, 1980). The use of Richard's equation here is a simplification of the gas flow in the dual porous structure of coal as desorption of gas from coal matrix is assumed to occur instantaneously upon depressurisation in the fractures. While, this may seem to oversimplify the model, the focus here is on implementation of the sorption-induced shrinkage and its effect of ground surface movement. Thus, such simplification will not significantly impact the comparative results of this study and the main conclusions.

4.3.2 Implementation of the permeability model and poroelastic formulation

As discussed earlier, the fracture porosity and permeability of coalbeds are of great importance for reservoir simulations. Therefore, predictive models are needed to estimate the permeability as a function of pore pressure, which will involve some geomechanical considerations. A relatively large number of permeability models have been proposed previously for different reservoirs (e.g. Palmer and Mansoori, 1996; Pan and Connell, 2012; Peng et al., 2017; Shi and Durucan, 2005; Zhu et al., 2018). The model developed by Cui and Bustin (2005) is one of the most-widely used models, and is employed in this paper. Following their model, the permeability (k_s) can be written as

$$\frac{k_s}{k_{s0}} = \exp\left\{-\frac{3}{K_p}\left[\frac{1+\nu}{3(1-\nu)}\Delta\sigma^e + \frac{2E}{3(1+\nu)}\Delta\varepsilon_{in}^s\right]\right\} \quad \textbf{Equation 15}$$

where K_p is the pore modulus, k_{s0} is the initial in-situ intrinsic permeability of the coalbed, and E and ν are the elastic modulus and Poisson's ratio of coal, respectively. $\Delta\sigma^e$ is the incremental change in the effective stress ($\sigma^e = \sigma - \alpha p$, α being the Biot's coefficient). $\Delta\sigma^e$ is equal to the negative of change in pore pressure ($-\alpha\Delta p$) assuming a constant total stress given $\Delta\sigma^e = \Delta\sigma - \alpha\Delta p$. Note that the swelling term in the original Cui and Bustin (2005) model is replaced by $\Delta\varepsilon_{in}^s$, which is the change in the volumetric internal swelling strain, defined as below

$$\Delta\varepsilon_{in}^s = \varepsilon_{in}^s - \varepsilon_{in0}^s = F_{in} \times (\varepsilon^s - \varepsilon_0^s) = F_{in}\left(\frac{\varepsilon_L^s\, b_L p}{1+b_L p} - \frac{\varepsilon_L^s\, b_L p_0}{1+b_L p_0}\right) \quad \textbf{Equation 16}$$

Substituting this equation into Equation 15 gives

$$\frac{k_s}{k_{s0}} = \exp\left\{-\frac{3}{K_f}\left[-\frac{1+\nu}{3(1-\nu)}(p-p_0) + \frac{2E}{9(1-\nu)}\left(\frac{\varepsilon_L^s\, b_L p}{1+b_L p} - \frac{\varepsilon_L^s\, b_L p_0}{1+b_L p_0}\right)F_{in}\right]\right\} \quad \textbf{Equation 17}$$

Note that a cubic relationship between porosity and permeability is considered as below

$$\frac{k_s}{k_{s0}} = \left(\frac{\phi}{\phi_0}\right)^3 \quad \textbf{Equation 18}$$

While some mechanical considerations were taken into account for the permeability model, the formulations of the mechanical deformation of the geological formation is independent of those stated earlier. For this, the solid mechanics module of COMSOL was employed along with linear elasticity. Following Masoudian et al. (2016b), the elastic stress-strain constitutive relations for plane-strain isotropic condition can be written as below

$$\begin{aligned}
\varepsilon_{xx} &= \frac{1+\nu}{E}\left[(1-\nu)\sigma_{xx} - \nu\sigma_{yy} - (1-2\nu)\alpha p\right] + \frac{\Delta\varepsilon_{ex}^s}{3} \\
\varepsilon_{yy} &= \frac{1+\nu}{E}\left[(1-\nu)\sigma_{yy} - \nu\sigma_{xx} - (1-2\nu)\alpha p\right] + \frac{\Delta\varepsilon_{ex}^s}{3} \\
\varepsilon_{xy} &= \frac{(1+\nu)}{E}\tau_{xy}
\end{aligned} \quad \textbf{Equation 19}$$

where σ and ε are the stress and strain and the subscripts of x and y indicate their directions. Note that the swelling strain term here is different from that of Masoudian et al. (2016b) as $\Delta\varepsilon_{ex}^s$ indicates the change in external swelling strain of the coalbed and is defined as

$$\Delta\varepsilon_{ex}^s = \varepsilon_{ex}^s - \varepsilon_{ex0}^s = (1-F_{in}) \times (\varepsilon^s - \varepsilon_0^s) = (1-F_{in})\left(\frac{\varepsilon_L^s\, b_L p}{1+b_L p} - \frac{\varepsilon_L^s\, b_L p_0}{1+b_L p_0}\right) \quad \textbf{Equation 20}$$

Note that the external swelling strain is modelled using the thermal expansion option in COMSOL and thus it is consistent with the conventional approach that likens coal swelling to thermal expansion. Further description of the geomechanical governing equations can be found in COMSOL-Multiphysics (2012).

4.3.3 Model setup and inputs

In order to simulate a case of CSG extraction and its associated surface movement, an example was solved where the boundary condition on the wellbore is fixed to be a hydraulic head equivalent to the final groundwater level for a period of three years. The elastic modulus and hydraulic properties of layers are listed in Table 9 and are within the range of those in typical Australian CSG development areas (IESC, 2014). Values of other parameters required for the simulation are listed in Table 10 and are within the range of typical Australian black coal. The internal swelling ratio is among those reported by the relevant literature (Wang et al., 2014; Zang et al., 2015).

Table 9. Elastic properties and permeability of different layers the geological profile (IESC, 2014).

Layers	$E\ (GPa)$	$\nu\ (-)$	$k\ (mD)$
Unsaturated Alluvium	0.2	0.3	1.06
Saturated Alluvium	0.2	0.3	1.06
Rock Unit 1	8	0.25	1.06
Rock Unit 2	14	0.25	0.32
Rock Unit 3	20	0.25	0.106
Coal	2	0.23	1.06
Sandstone	20	0.25	0.1
Rock Unit 4	28	0.25	0.1
Rock Unit 5	32	0.25	0.1

Table 10. Other model parameters.

Parameter	Symbol	Value	Unit	Assigned entity
Maximum vol. swelling strain	ε_L^s	0.03	-	Coal
Langmuir's constant	b_L	1/3	$1/MPa$	Coal
Internal swelling ratio	F_{in}	0.5	-	Coal
Pore modulus	K_p	3.3	MPa	Coal
Fluid density	ρ_f	1000	kg/m^3	Fluid
Fluid viscosity	η			Fluid
Dry density	ρ	2000	kg/m^3	All layers
Initial cleat porosity	ϕ_0	0.1	-	All layers
van Genuchten constants	ξ, n, l	1, 2, 0.5	$1/m$, -, -	All layers
Saturated liquid fraction	θ_s	0.25	-	All layers
Residual liquid fraction	θ_r	0	-	All layers
Biot's coefficient	α	1.0	-	All layers

As mentioned earlier, the model is constructed in COMSOL Multiphysics where both internal and external swelling definitions were implemented according to Equation 17 and Equation 20. Equation 17 is coded into the Richard's equation module while Equation 20 is implemented using the thermal expansion option in the solid mechanics module, with ε_{ex}^s as the temperature and ε_{ex0}^s in place of the reference temperature. Such implementation ensures the external swelling is likened to thermal expansion, which is commonplace in coalbed geomechanics. The Richard's equation and solid mechanics modules are coupled through the pore pressure term, where the estimated pressure term is passed onto the solid mechanics module as an external stress defined according to the Biot definition of the effective stress.

The meshing of the numerical model is shown in Figure 34. While experiments showed satisfactory performance with coarser elements (few hundred) without external swelling, its introduction needs much finer meshing (14833 elements) as shown in Figure 34. Running this model requires considerable computational resources and hence a multicore Windows server (two 8-core Intel Xeon E5 processors with 2.5 GHz frequency and 125 GB of memory) was used, and the solution took about 4.5 hours to be completed. A direct solver (MUMPS) is used along a segregated solver for this time-dependent solution (COMSOL-Multiphysics, 2012). The use of a segregated solver ensures a much more efficient numerical scheme as it treats the two physical systems sequentially (rather than simultaneously). Although the segregated approach generally does require more Newton iterations until convergence, each iteration takes significantly less time than one iteration of the fully coupled approach, while it converges to the same answer.

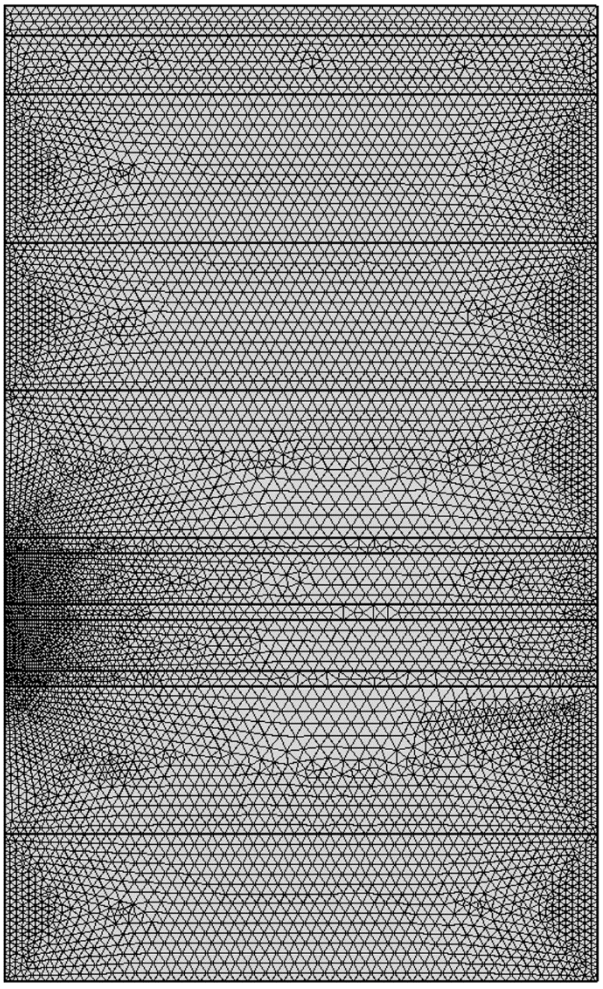

Figure 34: Finite element meshing of the numerical model.

4.3.4 Results and discussion

The pore pressure distribution at different times is shown in Figure 35. It can be seen that the pore pressure drops over time as production continues through the perforated section of the wellbore. The profiles of pore pressure along the horizontal and vertical direction are also illustrated in Figure 36 to complement the pore pressure results. Pore pressure is initially ~6.3 MPa and drops to around 4.9 MPa after a year. The bottom hole pressure of the production well then reduces to 4.2 MPa and 3.9 MPa after two and three years, respectively. It is also evident from Figure 36b that the pressure gradient within the coal-bearing formation is highly variable, which is attributed to the difference between the

permeability of the three coal layers and the interlaid sandstones. It should be noted again that the imposed boundary condition of constant water level within the alluvium layers means that while there is no pressure change within the alluvium, there may still be groundwater seepage loss from the alluvial geological unit into underlying units.

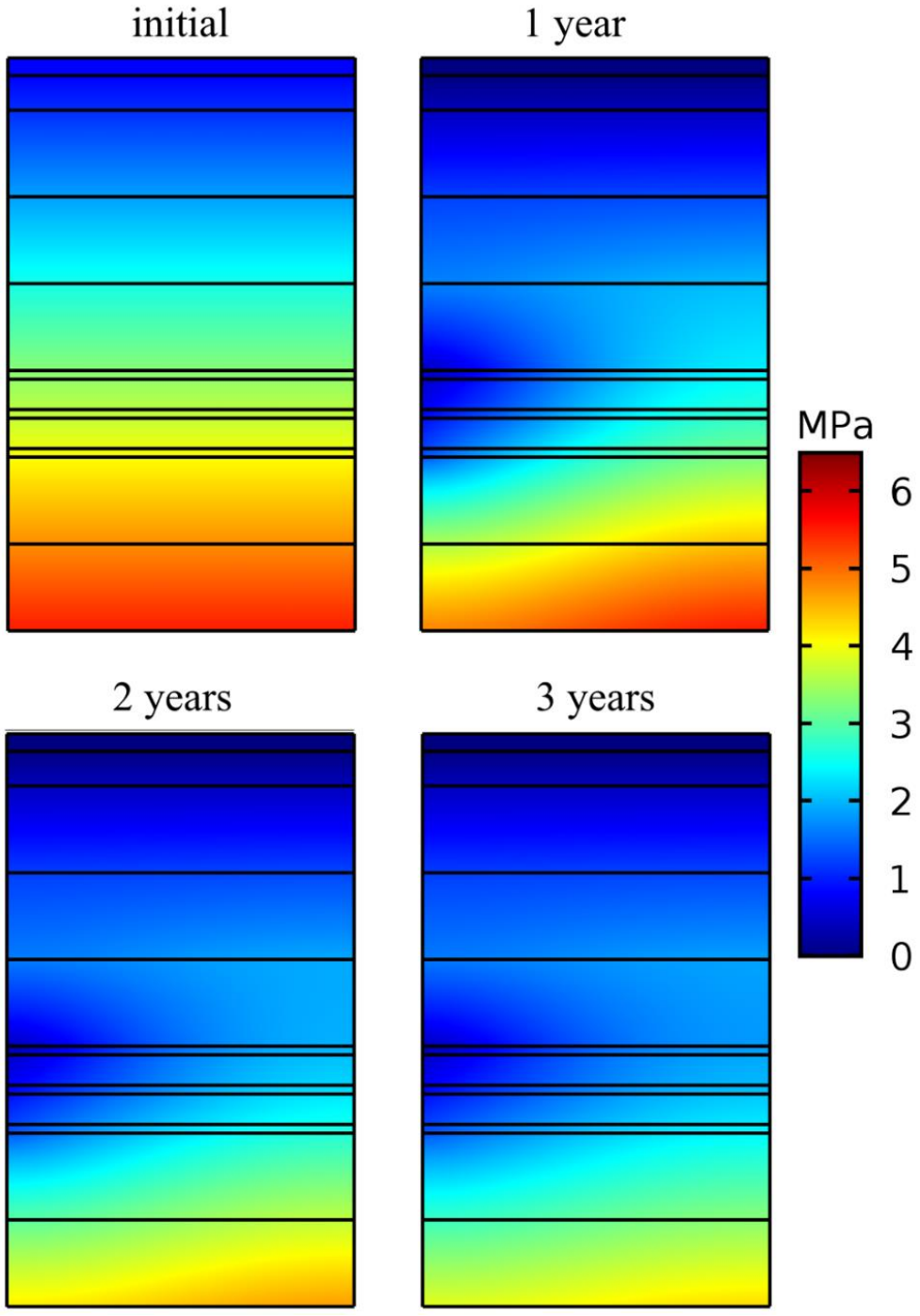

Figure 35: Spatial distribution of pore pressure at different times.

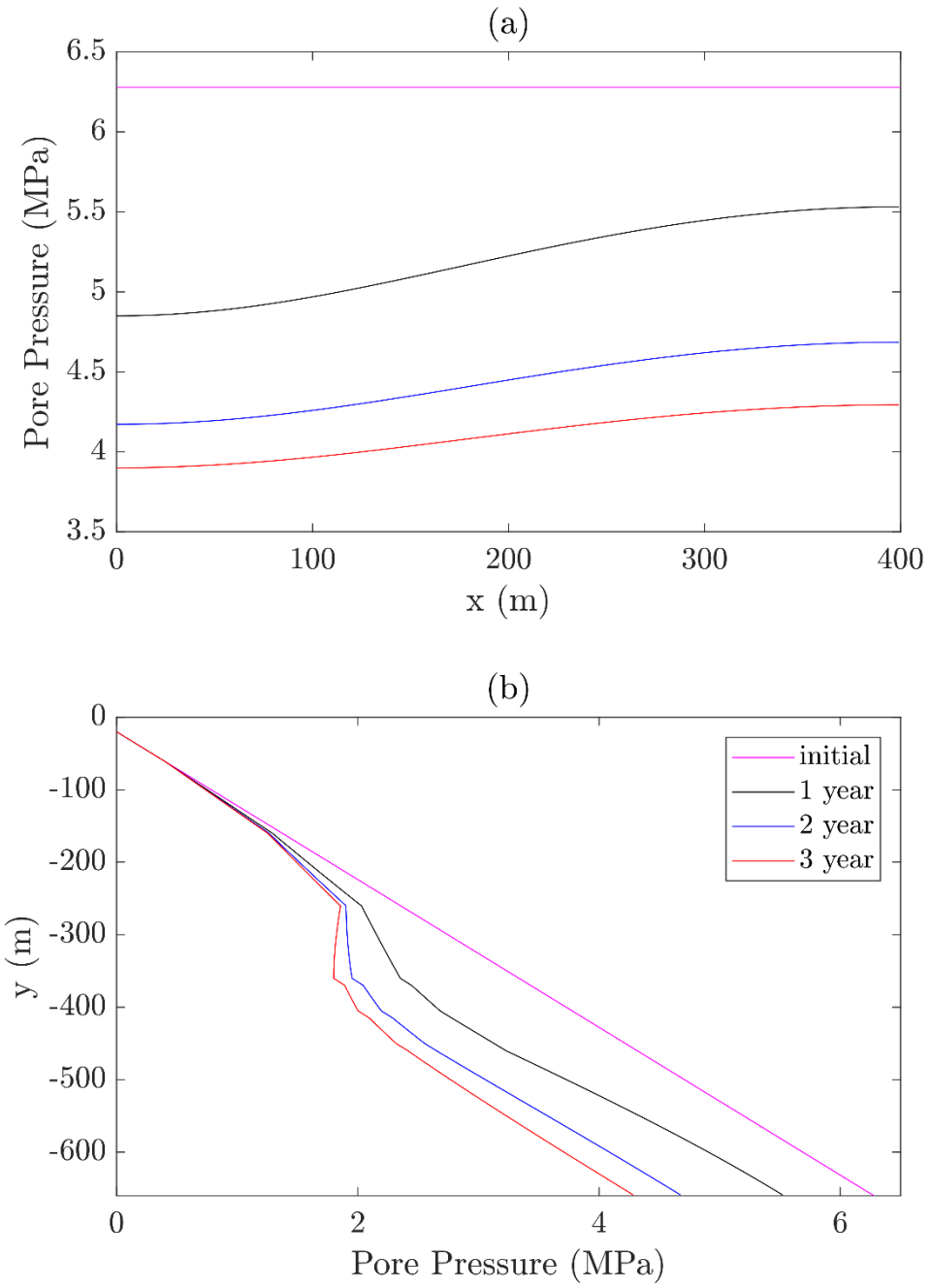

Figure 36: *Profiles of groundwater pressure at different times in (a) horizontal direction at the bottom of the domain and (b) vertical direction along the right side of the domain.*

The contours of change in groundwater pressure head within the model domain are depicted in Figure 37. This clearly shows larger drop in pressure head around the wellbore. The drop within the top two layers remains nearly constant between one and three years, but the depressurisation has a more significant effect over the rest of the domain. This is important because it shows that the mechanical behaviour of the deeper layers may have a more significant impact than that of the shallower layers on the time-dependent deformation of the domain, depending on their mechanical properties.

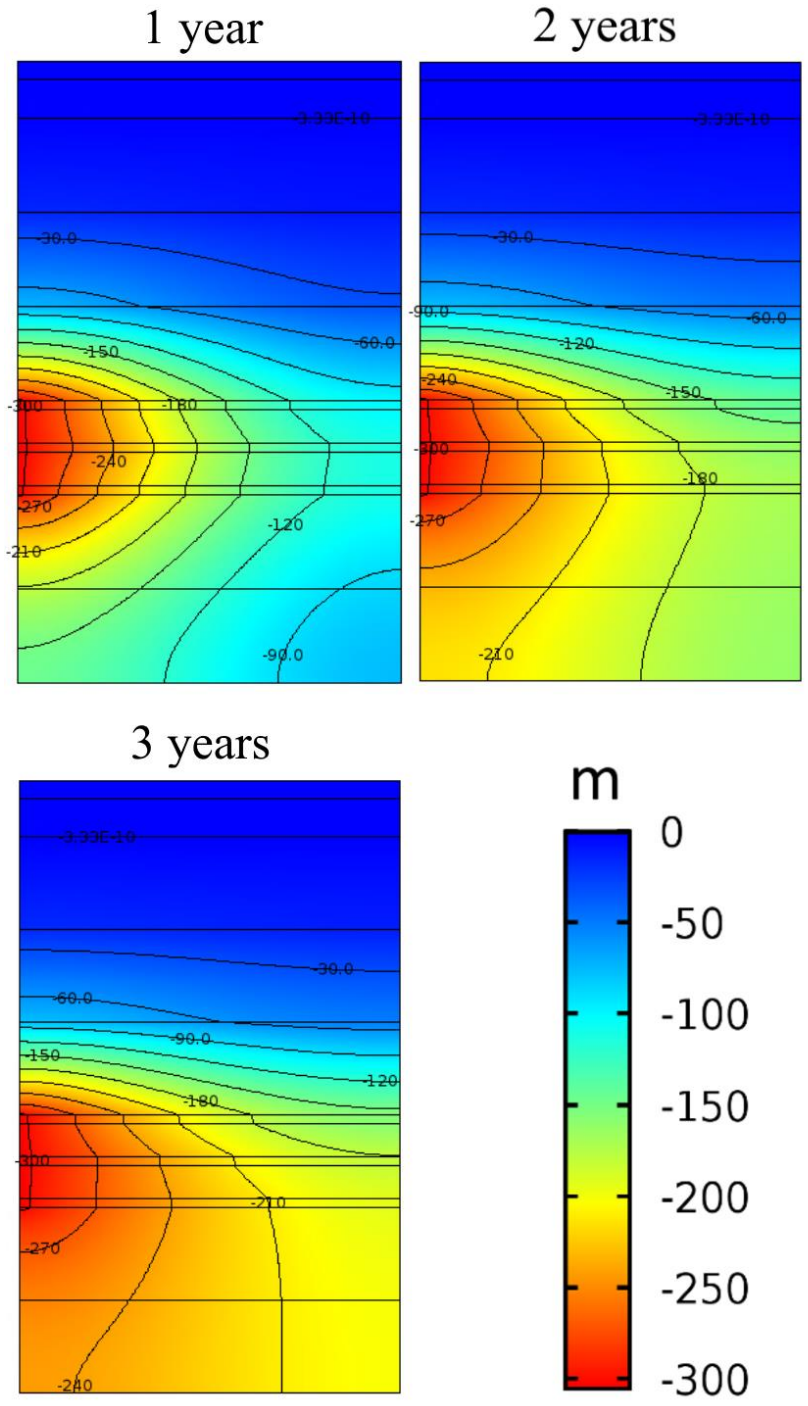

Figure 37: Change in groundwater pressure head at different times.

In order to analyse the stress-dependent permeability variation, the profiles of pore pressure and permeability at the middle of each of the three coalbeds are shown in Figure 38. Figure 38 shows that the coal seam that currently has higher pore pressure exhibit lower permeability ratio. This is because while lower pore pressure leads to higher effective stress and consequently smaller fracture apertures, the internal part of the desorption-induced shrinkage does the opposite and leads to expansion of fractures, as explained in Section 4.3.1 of this paper. This is consistent with the well-known knowledge in primary CSG recovery as reported by the literature (e.g. Liu and Harpalani, 2013). It should be, however, noted that this observation largely depends on the magnitude of the elastic properties and the shrinkage parameters, as the two effects of pore pressure and desorption-induced shrinkage

compete. Given the nonlinear Langmuir relationship for shrinkage effect, the relationship between the reservoir pressure and the fracture permeability is not monotonic and beyond a certain pressure (rebound pressure), increasing reservoir pressure leads to larger permeability during primary production (Shi and Durucan, 2005). The discussion on the effect of internal swelling ratio on rebound pressure is beyond the limits of this report and will be studied in future works.

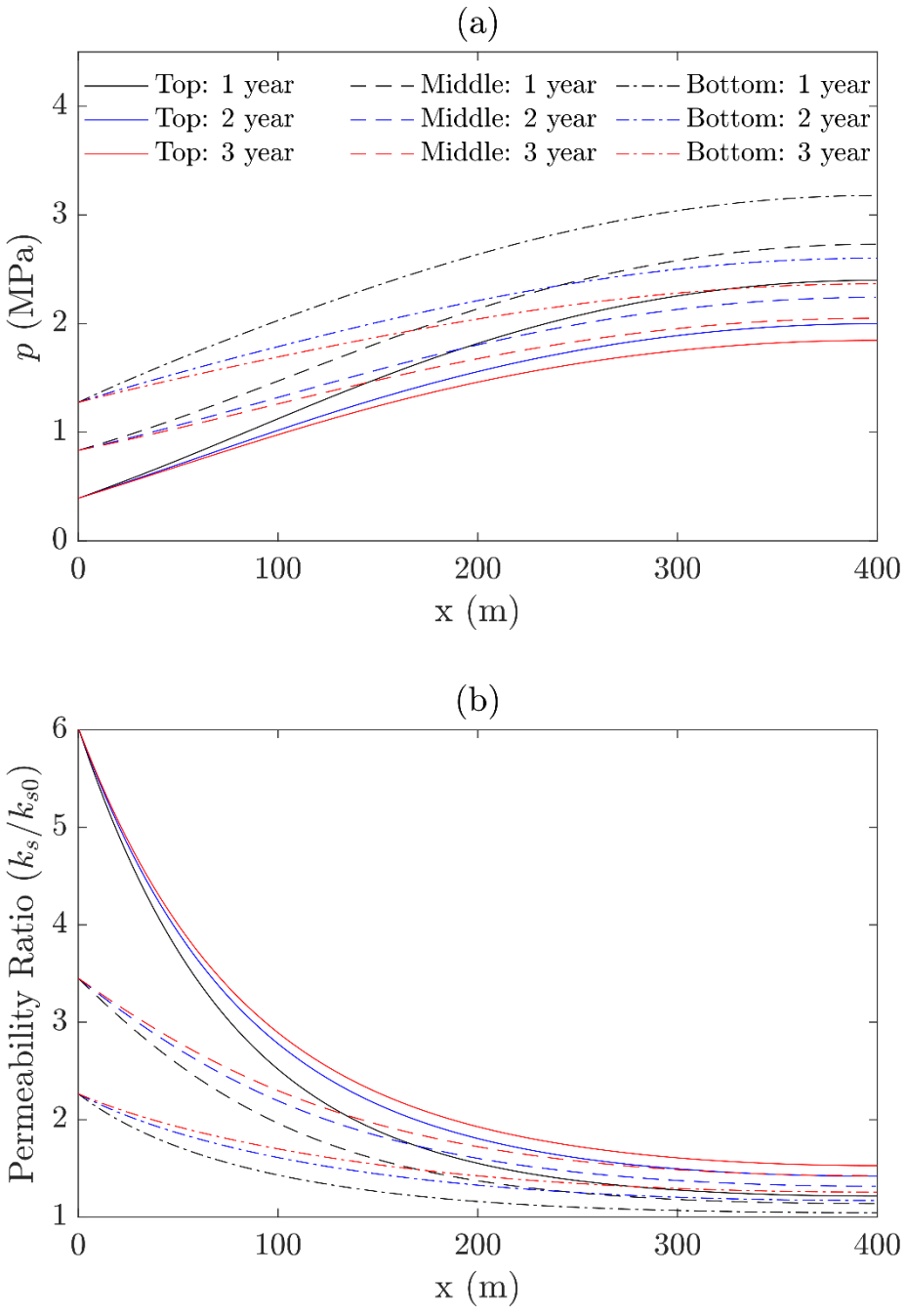

Figure 38: Hydrogeological response in the mid-depth of the three coal layers: (a) Profiles of change in pore pressure, (b) profiles of permeability ratio.

Figure 39 shows the distribution of vertical displacement within the model domain. It can be seen that as depressurisation continues, the geological profiles move downward (negative displacement) and this downward displacement is larger on the left side (towards the wellbore). There is a distinct difference between the displacement within the coal-bearing formation and the underlying rocks, which indicates

the coal-bearing formation is a significant source of the vertical displacement. Figure 40 depicts the profiles of surface movement and it can be seen that after three years, a maximum subsidence of nearly 115 mm occurs, with the maximum surface movement on the left side directly above the wellbore.

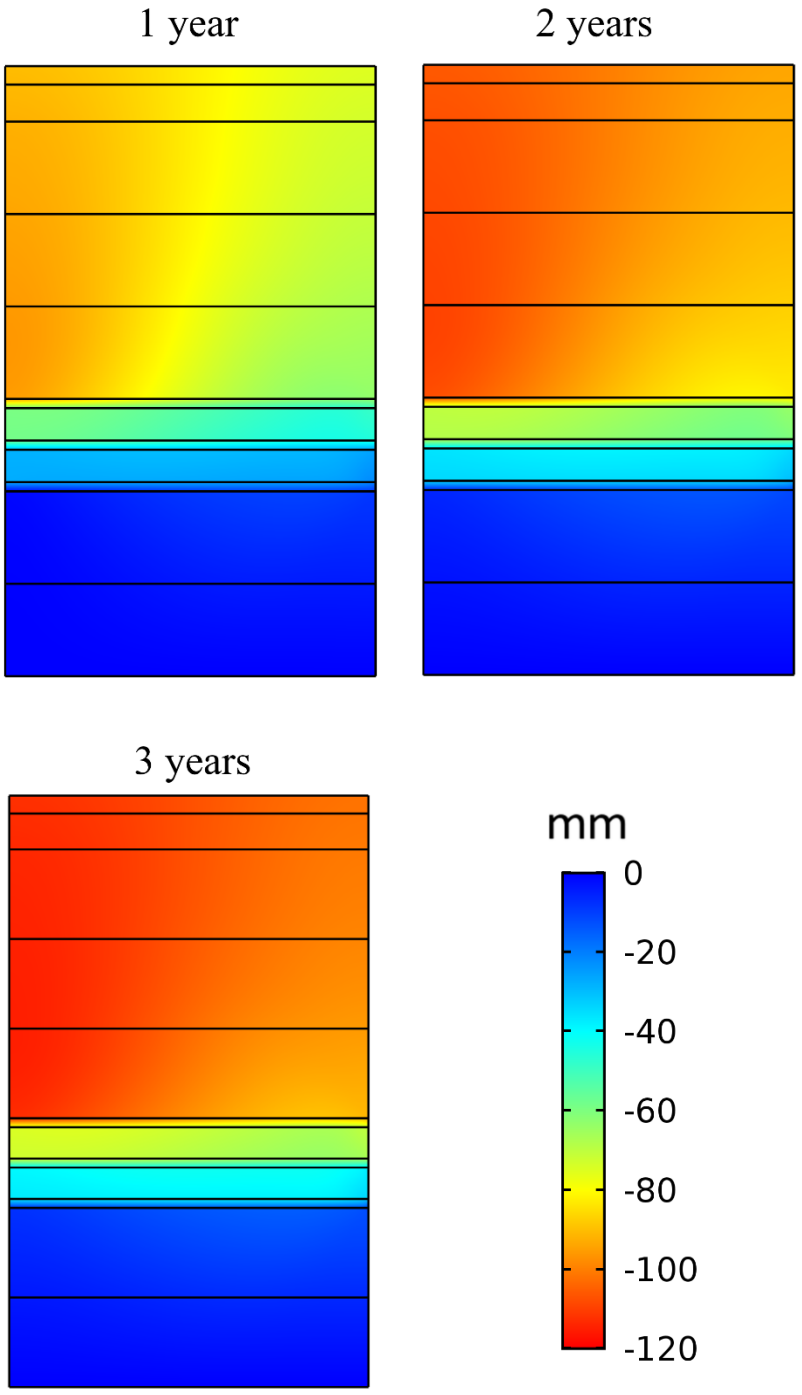

Figure 39: Vertical displacement within the model domain at different times.

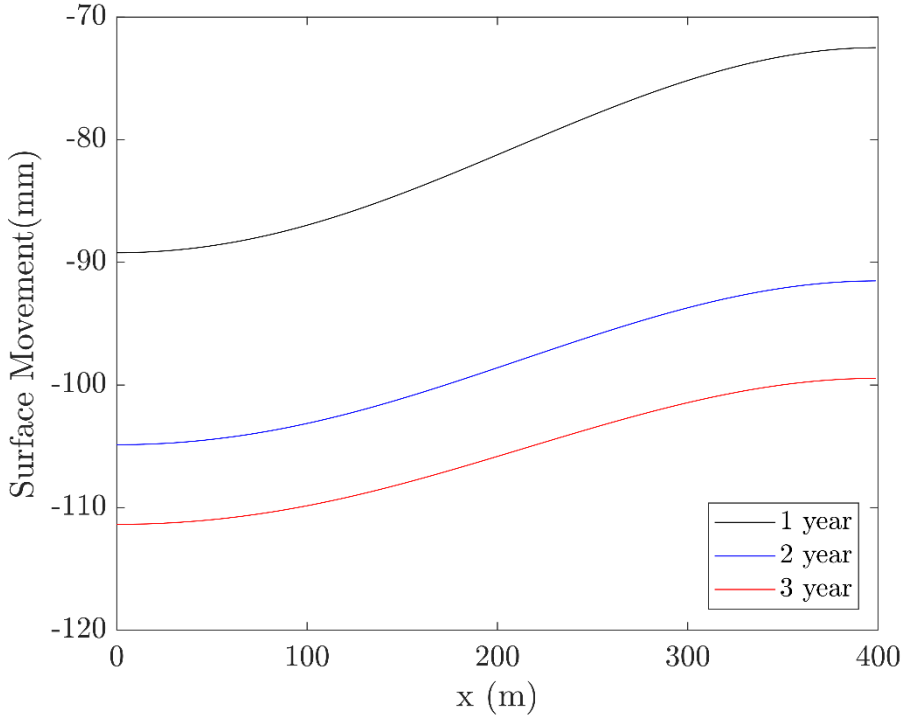

Figure 40: Profiles of ground surface movement at different times.

In order to investigate the effect of internal swelling ratio on time-dependent surface movements, the modelling was conducted using different values for F_{in} and the results are presented in Figure 41. The results of the simulation without considering the effect of desorption-induced shrinkage is also shown where the ground surface movement is evidently much smaller than the cases with shrinkage effect. It can be seen that the effect of F_{in} is not monotonic, with $F_{in} = 0.5$ exhibiting the maximum magnitude of surface subsidence and the more uniform profile of subsidence across the width of the model with $F_{in} = 0.9$. This is because a higher F_{in} leads to a larger permeability increase within coal seams and hence a higher degree of depressurisation and larger subsidence. On the other hand, a larger internal swelling ratio means the shrinkage has a smaller effect on bulk deformation of coalbeds and hence a smaller subsidence. As such, using $F_{in} = 0.9$, 90 per cent of the shrinkage is accounted for the increase in permeability and a rapid depressurisation subsidence (nearly reaching the steady-state condition) leads to a nearly uniform profile but its final magnitude is small. Between $F_{in} = 0.2$ and $F_{in} = 0.5$, on the other hand, the larger internal swelling ratio decreases the contribution of the shrinkage on subsidence, but the larger permeability increase allows a more rapid drawdown and therefore, a larger subsidence is observed for $F_{in} = 0.5$ after the same production duration.

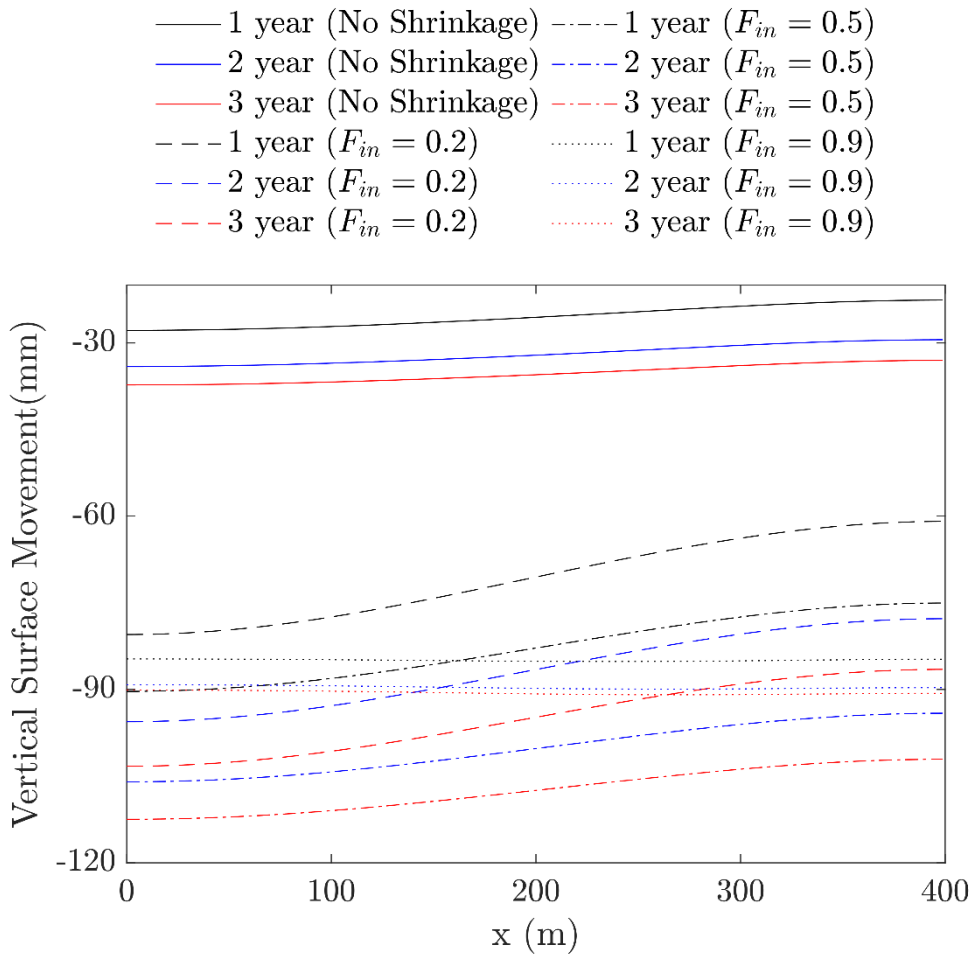

Figure 41: Profiles of ground surface movement at different times with different internal swelling ratio.

5 Conclusions and recommendation for future works

The aim of Stage 2 of this project was to generate preliminary assessment of the relative magnitude of the various contributors to net surface movement, and their key model and input parameters in the Surat CMA. This work is currently focused on drivers of surface movement that are independent of CSG production, such as groundwater pumping for domestic and agricultural use, rainfall, and geomorphology. This report documents the findings of the activities described in Section 1.2.2.

5.1 InSAR data analysis

In this report, remote-sensing data of ground surface movement in the Surat CMA was presented and interrogated. The surface movement data were apparently seasonal with high spatio-temporal variability. Four focus areas were selected for closer inspection of the results, where the changes in surface movement were more pronounced. All of the focus areas exhibited an overall trend of downward movement, with FA4 showing the largest overall subsidence and FA3 showing the smallest. Analysis of groundwater data showed no significant change in the groundwater level in these focus areas and it was concluded that the surface movement observations in these areas could not be related to the groundwater drainage-induced compaction of aquifers. The mean ground surface movement in FA1, FA2, and FA3 seemed to clearly follow the rainfall events. Further data review showed that the soils in these three focus areas are susceptible to consolidation and swelling/shrinkage that can be induced by the rainfall infiltration into shallow layers of soil. It was therefore suggested that the rainfall-related processes in the regolith are the main cause of surface movement in these focus areas. For FA4, however, the cause of surface movement does not seem to have been affected much by the rainfall events and further investigation and data review is needed to explore the cause of surface movement.

Based upon the presented data and results, a number of conclusions could be drawn which will be helpful for future work that deals with understanding the mechanisms of surface movement and their relative contributions. First, it was found that the very large non-producing areas within the Surat CMA exhibit different trends of surface movement, which can be attributed to a number of shallow and deep processes. Thus, focus areas need to be selected based upon their movement magnitude, direction, and fluctuation, in order to explore the possible mechanisms of the observed surface movement. In this process, visualising the data is of great importance to ensure that the magnitude, direction and fluctuation in the surface movement are reasonably estimated and hence focus areas are selected properly.

Four focus areas with the most visible ground surface movements were chosen for investigation in this study. The absolute value of the surface movement data in these areas was as high as 50 mm. The mean of surface movement revealed seasonal changes in the direction superimposed on an overall downward movement. Analysis of the available precipitation data and soil types suggested that the fluctuation in the observed surface movement in FA1, FA2, and FA3 follows rainfall events. This suggests that the observations of surface movements may be due to rainfall infiltration into shallow layers, which can cause consolidation of soil and the swelling of high-clay soil down the profile. The mean of surface movement in FA4, however, showed very little seasonal fluctuation. The overall downward movement in this area cannot yet be explained by the mechanisms suggested for the other focus areas, and hence, exploring other possible phenomena is underway. This is especially important for FA4, as continuous subsidence is observed that amounts to nearly 23 mm over the period of observation.

5.2 Shallow processes

5.2.1 Comparison and limitations of compressibility estimation

Four different methods are presented here to evaluate the settlement resulting from drawdown in groundwater levels. The analysis is based on calculation of in-situ compressibility using the groundwater level response to earth and barometric changes collected by high frequency data loggers.

The results show that all four methods provide results which are not statistically significant. The confidence limits provided for each monitoring site indicate that confidence interval is relatively narrow (0.1) which means that the results are of good accuracy. A limited sensitivity analysis considered change in porosity and thickness of strata for which the compressibility is calculated. This analysis indicates that the settlement estimate is equally sensitive to thickness of strata as it is for porosity. Further full analysis including all monitoring points is needed to fully assess the sensitivity of settlement estimate.

The assumptions made in this study include the following:

- Pre-consolidation change in water levels was not exceeded, all changes are considered to be elastic;
- No time component was included in the estimation of settlement (i.e. the settlement occurs instantaneously.
- Where no lithology data was available the lithology was obtained from similar depth in nearby drill holes;
- The lack of full knowledge of geology and lithology for each of the boreholes is a limitation as the calculations are based on the assumptions that geophysical properties reflect the lithology;
- The estimate of porosity was calculated by different methods from geophysical downhole logs and adoption was made for similar porosity values to other sites based on the depth. Such estimate of porosity may not be entirely accurate as the sedimentary units are heterogeneous;
- Porosity obtained from neutron logs is total porosity, and as such may overestimate the compressibility and settlement;
- Thickness of unit was assumed to be the same as the screened interval or interval where sensor was installed in the drill hole. Calculated strata thickness based on gamma log is presented in Table 1;
- Formation of interest was assumed to extend laterally such that flow was considered negligible and compressibility constrained laterally;
- Horizontal strain is negligible compared to vertical strain in estimation of settlement using barometric loading;
- Stratigraphic unit is porous and homogeneous.

5.2.2 Changes in settlement, compressibility and soil subsidence over time

The settlement in reviewed monitoring bores has already occurred from the point at which groundwater drawdown exceeded the elastic limit. The calculations in this study relate to additional settlement that is predicted to occur based on the additional drawdown which might occur.

To investigate the changes in compressibility over time, a full transient analysis is required. This research work is in progress, with similar studies recently published (Rau et al., 2018).

5.2.3 Concluding remarks on shallow processes

The study of surface subsidence as a result of natural and anthropogenic changes in groundwater level was undertaken by analysing high frequency hydraulic head and barometric pressure data. The anthropogenic changes relate here to withdrawal of groundwater for irrigation and other purposes and exclude gas related exploration or production activities. The maximum drawdown in groundwater levels over the past 5 years (in monitoring bores used in this study) ranged from 0.05 to 17.3 m in the CA. This range depends on the location, production, depth, hydraulic conductivity and other parameters, however, is a good representation of the drawdown range and agrees with data reported in (OGIA, 2016). In some areas such as Stratheden62 and 64 there was minor fluctuation in groundwater levels (<10 cm) from 2013 to mid-2016 with fluctuations of over a metre since then. At most of the Tipton bores, stable or downward trend with minor fluctuations (<1 m) was recorded, however the Daandine and Lone Pine 15 bores showed significant drawdown which is likely related to pumping cycles (8 to 17 m) with good recovery following drawdown periods.

The analysis of compressibility using the hydraulic head response to atmospheric and earth tide loading indicates that several conclusions can be made with respect to behaviour of semi-consolidated CA. The majority of investigated strata are confined with loading efficiency between 0.6 to 0.95 and the average of 0.79. Four different methods used to analyse loading efficiency for the same datasets produced statistically similar results. Data analysed using the visual method typically resulted in the lowest estimated settlement while the median of ratios method resulted in highest estimate of settlement. When the results obtained by earth tide method are compared to the ones using barometric method, the earth tide method results in less settlement.

The primary uncertainty in calculated compressibility and settlement can be attributed to estimated porosity values. These values were either obtained from geophysical logs or were assumed where no information was provided. Compressibility derived from loading efficiency also required an assumed Poisson's ratio. Uncertainty in total settlement at the surface of a site was related to a number of factors including: thickness and geology of each strata, compressibility and degree of hydraulic connectivity of each strata, to the depth where pore pressure was monitored.

The settlement estimate is dependent on the maximum predicted additional drawdown that is expected to occur at a particular location based on the past monitoring data and historically reported trends (OGIA, 2016). As an example, at Lone Pine 15, an additional 3 mm of settlement is predicted as a result of additional decline in hydraulic head, while at Daandine and Strathenden bores where the additional drawdown is not expected to exceed 1 m, a settlement of less than 0.5 mm is predicted.

5.3 Numerical modelling of poroelastic processes

A numerical model was constructed in this report to evaluate the effect of groundwater drawdown in a coal-bearing formation. The example presented was adapted from the IESC report (IESC, 2014) where a geological section of the formation is considered in a two-dimensional hydro-mechanical numerical scheme. The results showed an acceptable level of agreement with simplified analyses of the IESC report. The model provides a very useful tool for a fast and a more reliable analysis of ground surface subsidence and can already be used to estimate the effect of groundwater drawdown on surface movement as one of the key contributors. It is important to note that the geomechanical characteristics of each geological unit plays an important role in the estimated surface movement and hence the results presented in this report may not exactly represent those observed in CSG production areas.

The effect of sorption-induced swelling/shrinkage in coalbeds has attracted a lot of attention in the reservoir simulation community and a large number of models have been developed under different assumptions. However, its significance in geomechanical modelling and the bulk deformation of coalbeds has received little attention. This is important as bulk deformation of a coalbed can have significant impact on ground surface movement. In this report, the definition of 'internal swelling' was used to incorporate the effect of sorption-induced shrinkage on permeability. The 'external swelling' definition is then the remainder of the free swelling that contributes to the bulk volumetric response of the coalbed.

5.4 Future Work

Study of the groundwater data showed that the groundwater level within the focus areas has not changed by more than four metres during the period for which the InSAR data are collected. In fact, within the Surat CMA, only the Condamine Alluvium has shown a large drop in groundwater level (OGIA, 2016) and therefore, obtaining and studying the surface movement data in these areas can be beneficial in future studies for understanding the mechanisms and significance of the surface movement due to groundwater extraction from shallow formations.

Following from the previous point, processing surface movement data from within the CSG producing areas is imperative to acquire a better understanding of the ground surface movement due to CSG development. It should be noted that according to OGIA (2016), the groundwater level within the CSG producing areas has only been affected in the coal formation while the water level in the overlaying formations have been thus far unaffected. Thus, studying the producing areas could be significant for understanding the magnitude and direction of the ground surface movement due to pressure drop and gas desorption. In addition, the use of surface movement data in these areas for characterisation of reservoir deformation would be expected to be relatively straightforward via inverse analysis (Atefi Monfared and Rothenburg, 2011; Dusseault et al., 1993), as the groundwater level remains constant in the overburden.

Since the ultimate goal of this project is to develop a predictive workflow and identify the contributing causes of ground surface movement, and the magnitude and direction of their contribution, developing a baseline for surface movement is necessary. This report documents the progress towards development of such a baseline. In order to complete this baseline, modelling work is currently being undertaken to validate the hypothesis of rainfall-induced seasonal surface movement. In addition, more modelling work is needed to test any explanation for the overall, long-term trend of subsidence observed in focus areas of the Surat CMA, which cannot be fully explained by the seasonal subsidence and uplift cycles described in this paper.

Forward prediction of ground surface movement through deterministic numerical model does not seem to be the best way of dealing with the complex nature of the natural process contributing to the surface movement. Hence, a machine learning scheme is thought to be the gateway to successful forward prediction of surface movement in non-producing areas which will be considered as future work.

Numerical modelling of ground surface movement presented in this report is a simplified two-dimensional case for a horizontally layered formation. In order to develop more realistic model, a detailed dataset of hydro-mechanical properties of a geological unit within the Surat CMA is needed. In addition, an accurate presentation of the geometry of the geological units can lead to more reliable prediction of surface movements due to groundwater extraction. CSG production is also associated with sorption-induced shrinkage of coal. While this has been extensively studied for prediction of coalbed

permeability, its influence on ground subsidence has not been fully investigated. Preliminary results suggest a significant contribution to the net surface movement and therefore implementing shrinkage in the numerical poroelastic model is necessary. The results of the numerical example showed that the estimated surface movement during production is significantly influenced by the sorption-induced shrinkage. However, the interdependence of the internal swelling, permeability, and ground surface subsidence can complicate the interpretation of this effect. Therefore, more comprehensive studies are required to fully explain the relationship between the sorption-induced shrinkage and ground surface movement during coalbed methane recovery. This is also very important if the ground surface movement dataset is to be used for reservoir management purposes.

In addition, full sensitivity analysis is required on all parameters which contribute to surface settlement to improve on the reliability of the prediction. Following this analysis, comparison with InSAR data within the same area as the ones presented in the shallow processes section is required to ensure that the results are comparable.

6 References

Acworth, R. I., Rau, G. C., McCallum, A. M., Andersen, M. S., and Cuthbert, M. O. (2015). Understanding connected surface-water/groundwater systems using Fourier analysis of daily and sub-daily head fluctuations. *Hydrogeology Journal* **23**(1), 143-159. https://doi.org/10.1007/s10040-014-1182-5.

Agram, P. S., and Simons, M. (2015). A noise model for InSAR time series. *Journal of Geophysical Research: Solid Earth* **120**(4), 2752-2771. https://doi.org/10.1002/2014JB011271.

Anochikwa, C. I., van der Kamp, G., and Barbour, S. L. (2012). Interpreting pore-water pressure changes induced by water table fluctuations and mechanical loading due to soil moisture changes. *Canadian Geotechnical Journal* **49**(3), 357-366. https://doi.org/10.1139/t11-106.

Atashbari, V. (2016). Origin of overpressure and pore pressure prediction in carbonate reservoirs of the Abadan Plain Basin. PhD Thesis, The University of Adelaide. Adelaide, Australia.

Atefi Monfared, K., and Rothenburg, L. (2011). Ground surface displacements and tilt monitoring for reconstruction of reservoir deformations. *International Journal of Rock Mechanics and Mining Sciences* **48**(7), 1113-1122. https://doi.org/10.1016/j.ijrmms.2011.07.003.

Babanouri, N., Karimi Nasab, S., Baghbanan, A., and Mohamadi, H. R. (2011). Over-consolidation effect on shear behavior of rock joints. *International Journal of Rock Mechanics and Mining Sciences* **48**(8), 1283-1291. https://doi.org/10.1016/j.ijrmms.2011.09.010.

Baker, R. O., Yarranton, H. W., and Jensen, J. (2015). 'Practical reservoir engineering and characterization'. Gulf Professional Publishing. https://doi.org/10.1016/C2011-0-05566-7.

Barnett, B. G., and Muller, J. (2008). Upper Condamine groundwater model calibration report: A report to the Australian Government from the CSIRO Murray-Darling Basin sustainable yields project. CSIRO. Australia.

Batu, V. (1998). 'Aquifer hydraulics: a comprehensive guide to hydrogeologic data analysis'. John Wiley & Sons.

Black, D. K., and Lee, K. L. (1973). Saturating laboratory samples by back pressure. *Journal of the soil mechanics and foundations division* **99**(1), 75-93.

BOM (2018). Climate Data Online. Bureau of Meteorology. 2018 http://www.bom.gov.au/climate/data/.

Burbey, T. J. (2005). Stress-strain analyses for aquifer-system characterization. *Groundwater* **39**(1), 128-136. https://doi.org/10.1111/j.1745-6584.2001.tb00358.x.

Chen, Z. R. (2011). Poroelastic model for induced stresses and deformations in hydrocarbon and geothermal reservoirs. *Journal of Petroleum Science and Engineering* **80**(1), 41-52. https://doi.org/10.1016/j.petrol.2011.10.004.

Clark, W. E. (1967). Computing the barometric efficiency of a well. *Journal of the Hydraulics Division* **93**(4), 93-98.

COMSOL-Multiphysics (2012). Comsol Multiphysics user guide. *COMSOL, AB*, 39-40.

Cox, M. E., James, A., Hawke, A., and Raiber, M. (2013). Groundwater Visualisation System (GVS): A software framework for integrated display and interrogation of conceptual hydrogeological models, data and time-series animation. *Journal of Hydrology* **491**, 56-72. https://doi.org/10.1016/j.jhydrol.2013.03.023.

CSIRO (2008). Water availability in the Condamine-Balonne: A report to the Australian government from the CSIRO Murray Darling basin sustainable yields project. CSIRO. Brisbane, Australia.

Cui, X., and Bustin, R. M. (2005). Volumetric strain associated with methane desorption and its impact on coalbed gas production from deep coal seams. *Aapg Bulletin* **89**(9), 1181-1202. https://doi.org/10.1306/05110504114.

D'Errico, J. R. (2006). Understanding gridfit. 2018 https://au.mathworks.com/matlabcentral/fileexchange/8998-surface-fitting-using-gridfit.

Dafny, E., and Silburn, D. M. (2014). The hydrogeology of the Condamine River Alluvial Aquifer, Australia: a critical assessment. *Hydrogeology Journal* **22**(3), 705-727. https://doi.org/10.1007/s10040-013-1075-z.

Deng, X., and Tang, Z. (2011). Moving surface spline interpolation based on Green's function. *Mathematical Geosciences* **43**(6), 663-680. https://doi.org/10.1007/s11004-011-9346-5.

Domenico, S. N. (1984). Rock lithology and porosity determination from shear and compressional wave velocity. *GEOPHYSICS* **49**(8), 1188-1195. https://doi.org/10.1190/1.1441748.

DSITI (2016). Queensland Land Use Mapping Program (QLUMP) - 1999 to Current. Queensland, Australia. https://www.qld.gov.au/environment/land/vegetation/mapping/qlump.

Dusseault, M. B., Bilak, R. A., and Rothenburg, L. (1993). Inversion of surface displacements to monitor in situ processes. *International Journal of Rock Mechanics and Mining Sciences & Geomechanics Abstracts* **30**(7), 1219-1222. https://doi.org/10.1016/0148-9062(93)90098-X.

Fitts, C. (2013). 'Groundwater Science', 2nd edn. Academic Press: Boston, MA, USA.

Garthwaite, M. C., Hazelwood, M., Nancarrow, S., Hislop, A., and Dawson, J. H. (2015). A regional geodetic network to monitor ground surface response to resource extraction in the northern Surat Basin, Queensland. *Australian Journal of Earth Sciences* **62**(4), 469-477. https://doi.org/10.1080/08120099.2015.1040073.

Gonthier, G. J. (2007). A graphical method for estimation of barometric efficiency from continuous data—concepts and application to a site in the Piedmont, Air Force Plant 6, Marietta, Georgia. Geological Survey Scientific Investigation Report 2007-5111. http://pubs.usgs.gov/sir/2007/5111.

Hartmann, D. J., and Beaumont, E. A. (1999). Predicting Reservoir System Quality and Performance. In 'Exploring for Oil and Gas Traps'. (Eds E. A. Beaumont and N. H. Foster.) Vol. 3, pp. 0. American Association of Petroleum Geologists: Tulsa, Oklahoma. https://doi.org/10.1306/TrHbk624C9.

Houston, S. L., Houston, W. N., Zapata, C. E., and Lawrence, C. (2001). Geotechnical engineering practice for collapsible soils. *Geotechnical & Geological Engineering* **19**(3), 333-355. https://doi.org/10.1023/A:1013178226615.

Huxley, W. J. (1982). The hydrogeology, hydrology and hydrochemistry of the Condamine River Valley alluvium. Masters by Research Thesis, Queensland University of Technology. Brisbane, Australia.

IESC (2014). Monitoring and management of subsidence induced by coal seam gas extraction. Commonwealth of Australia, Prepared by Coffey Geotechics for the Department of the Environment, Commonwealth of Australia. Canberra.

Keir, G., Bulovic, N., McIntyre, N.,Callow,I., Herbert, C.,Reading, L.,Costa, F. and Roux, E. (2017). Characterisaiton of current groundwater uses in the Surat and Bowen Basins. Stage 2c: Estimation of long-term groundwater extraction. Centre for Coal Seam Gas (University of Queensland). Brisbane, Australia.

Kelly, N., and Merrick, N. (2007). Groundwater Knowledge and Data Gaps in the Condamine Alliance Area. National Centre for Groundwater Managements, UTS.

Klohn Crippen Berger (2010). Central Condamine Alluvium Data Availability Report. Prepared for the Queensland Department of Environment and Resource Management.

Lane, W. B. (1979). Progress report on Condamine underground investigation to December 1978. Queensland Water Resources Commission. Brisbane, Australia.

Larsen, J. W. (2004). The effects of dissolved CO2 on coal structure and properties. *International Journal of Coal Geology* **57**(1), 63-70. https://doi.org/10.1016/j.coal.2003.08.001.

Laubach, S. E., Marrett, R. A., Olson, J. E., and Scott, A. R. (1998). Characteristics and origins of coal cleat: A review. *International Journal of Coal Geology* **35**(1), 175-207. https://doi.org/10.1016/S0166-5162(97)00012-8.

Lawton, E. C., Fragaszy, R. J., and Hetherington, M. D. (1992). Review of Wetting-Induced Collapse in Compacted Soil. *Journal of Geotechnical Engineering* **118**(9), 1376-1394. https://doi.org/10.1061/(ASCE)0733-9410(1992)118:9(1376).

Li, P., Vanapalli, S., and Li, T. (2016). Review of collapse triggering mechanism of collapsible soils due to wetting. *Journal of Rock Mechanics and Geotechnical Engineering* **8**(2), 256-274. https://doi.org/10.1016/j.jrmge.2015.12.002.

Li, Y., Gong, H., Zhu, L., Li, X., Wang, R., and Guo, G. (2017). Characterizing land displacement in complex hydrogeological and geological settings: a case study in the Beijing Plain, China. *Natural Hazards* **87**(1), 323-343. https://doi.org/10.1007/s11069-017-2771-0.

Liu, C.-H., Pan, Y.-W., Liao, J.-J., and Hung, W.-C. (2004). Estimating coefficients of volume compressibility from compression of strata and piezometric changes in a multiaquifer system in west Taiwan. *Engineering Geology* **75**(1), 33-47. https://doi.org/10.1016/j.enggeo.2004.04.007.

Liu, H.-H., and Rutqvist, J. (2010). A New Coal-Permeability Model: Internal Swelling Stress and Fracture–Matrix Interaction. *Transport in Porous Media* **82**(1), 157-171. https://doi.org/10.1007/s11242-009-9442-x.

Liu, J., Wang, J., Chen, Z., Wang, S., Elsworth, D., and Jiang, Y. (2011). Impact of transition from local swelling to macro swelling on the evolution of coal permeability. *International Journal of Coal Geology* **88**(1), 31-40. https://doi.org/10.1016/j.coal.2011.07.008.

Liu, S., and Harpalani, S. (2013). Permeability prediction of coalbed methane reservoirs during primary depletion. *International Journal of Coal Geology* **113**, 1-10. https://doi.org/10.1016/j.coal.2013.03.010.

Lumsden, A. C. (1966). Condamine valley groundwater investigations - hydrogeological report on eight 1:50,000 map sheets: unpublished report. Geological Survey of Queensland.

Masoudian, M. S. (2013). Chemo-hydro-mechanical aspects of CO_2 sequestration in deep coal seams. PhD Thesis, The University of Sydney. Sydney, Australia.

Masoudian, M. S. (2016). Multiphysics of carbon dioxide sequestration in coalbeds: A review with a focus on geomechanical characteristics of coal. *Journal of Rock Mechanics and Geotechnical Engineering* **8**(1), 93-112. https://doi.org/10.1016/j.jrmge.2015.08.002.

Masoudian, M. S., Airey, D. W., and El-Zein, A. (2013a). A chemo-poro-mechanical model for sequestration of carbon dioxide in coalbeds. *Géotechnique* **63**(3), 235-243. https://doi.org/10.1680/geot.SIP13.P.026.

Masoudian, M. S., Airey, D. W., and El-Zein, A. (2013b). Mechanical and flow behaviours and their interactions in coalbed geosequestration of CO_2. *Geomechanics and Geoengineering* **8**(4), 229-243.

https://doi.org/10.1080/17486025.2013.805252.

Masoudian, M. S., Airey, D. W., and El-Zein, A. (2014). Experimental investigations on the effect of CO2 on mechanics of coal. *International Journal of Coal Geology* **128-129**, 12-23. http://www.sciencedirect.com/science/article/pii/S0166516214000718.

Masoudian, M. S., Airey, D. W., and El-Zein, A. (2016a). The role of coal seam properties on coupled processes during CO_2 sequestration: A parametric study. *Greenhouse Gases: Science and Technology* **6**(4), 492-518. https://doi.org/10.1002/ghg.1575.

Masoudian, M. S., El-Zein, A., and Airey, D. W. (2016b). Modelling stress and strain in coal seams during CO_2 injection incorporating the rock–fluid interactions. *Computers and Geotechnics* **76**, 51-60. https://doi.org/10.1016/j.compgeo.2016.02.010.

Mbia, E. N., Fabricius, I. L., Krogsbøll, A., Frykman, P., and Dalhoff, F. (2014). Permeability, compressibility and porosity of Jurassic shale from the Norwegian–Danish Basin. *Petroleum Geoscience* **20**(3), 257-281. https://doi.org/10.1144/petgeo2013-035.

McMillan, T. C., Rau, G. C., Timms, W. A., and Andersen, M. S. (2019). Utilizing the impact of Earth and atmospheric tides on groundwater systems: A review reveals the future potential. *Reviews of Geophysics* **In Press**. https://doi.org/10.1029/2018RG000630.

Merritt, M. L. (2004). Estimating hydraulic properties of the Floridan aquifer system by analysis of earth-tide, ocean-tide, and barometric effects, Collier and Hendry Counties, Florida. U.S. Geological Survey.

OGIA (2016). Underground Water Impact Report for the Surat Cumulative Management Area. The Office of Groundwater Impact Assessment (OGIA). Queensland, Australia.

Or, D. (1996). Wetting-induced soil structural changes: The theory of liquid phase sintering. *Water Resources Research* **32**(10), 3041-3049. https://doi.org/10.1029/96WR02279.

Palmer, I., and Mansoori, J. (1996). How permeability depends on stress and pore pressure in coalbeds: A new model. In 'SPE Annual Technical Conference and Exhibition'. (Ed.^(Eds Editor.)(Society of Petroleum Engineers: Denver, Colorado.) https://doi.org/10.2118/36737-MS.

Pan, Z., and Connell, L. D. (2012). Modelling permeability for coal reservoirs: A review of analytical models and testing data. *International Journal of Coal Geology* **92**, 1-44. https://doi.org/10.1016/j.coal.2011.12.009.

Peng, Y., Liu, J., Pan, Z., Connell, L. D., Chen, Z., and Qu, H. (2017). Impact of coal matrix strains on the evolution of permeability. *Fuel* **189**, 270-283. https://doi.org/10.1016/j.fuel.2016.10.086.

Queensland Water Commission (2012). Underground water impact report for the Surat Cumulative

Management Area. Queensland Government. Queensland, Australia.

Rasmussen, T. C., and Crawford, L. A. (1997). Identifying and Removing Barometric Pressure Effects in Confined and Unconfined Aquifers. *Groundwater* **35**(3), 502-511. https://doi.org/10.1111/j.1745-6584.1997.tb00111.x.

Rau, G. C., Acworth, R. I., Halloran, L. J. S., Timms, W. A., and Cuthbert, M. O. (2018). Quantifying Compressible Groundwater Storage by Combining Cross-Hole Seismic Surveys and Head Response to Atmospheric Tides. *Journal of Geophysical Research: Earth Surface* **123**(8), 1910-1930. https://agupubs.onlinelibrary.wiley.com/doi/abs/10.1029/2018JF004660.

Reeves, J. A., Knight, R., Zebker, H. A., Kitanidis, P. K., and Schreüder, W. A. (2014). Estimating temporal changes in hydraulic head using InSAR data in the San Luis Valley, Colorado. *Water Resources Research* **50**(5), 4459-4473. https://doi.org/10.1002/2013WR014938.

Richards, L. A. (1931). Capillary conduction of liquids through porous mediums. *physics* **1**(5), 318-333.

Rojstaczer, S., and Agnew, D. C. (1989). The influence of formation material properties on the response of water levels in wells to Earth tides and atmospheric loading. *Journal of Geophysical Research: Solid Earth* **94**(B9), 12403-12411. https://doi.org/10.1029/JB094iB09p12403.

Saghafi, A., Faiz, M., and Roberts, D. (2007). CO2 storage and gas diffusivity properties of coals from Sydney Basin, Australia. *International Journal of Coal Geology* **70**(1), 240-254. https://doi.org/10.1016/j.coal.2006.03.006.

Shi, J.-Q., and Durucan, S. (2005). A model for changes in coalbed permeability during primary and enhanced methane recovery. *SPE Reservoir Evaluation & Engineering* **8**(04), 291-299. https://doi.org/10.2118/87230-PA.

Sinclair Knight Merz (1999). Conjunctive water use study: upper Condamine River: Interim report, Darling Downs Vision 2000. Department of Natural Resources. Brisbane, Australia.

Skempton, A. W. (1954). The Pore-Pressure Coefficients A and B. *Géotechnique* **4**(4), 143-147. https://doi.org/10.1680/geot.1954.4.4.143.

Smith, L. A., van der Kamp, G., and Jim Hendry, M. (2013). A new technique for obtaining high-resolution pore pressure records in thick claystone aquitards and its use to determine in situ compressibility. *Water Resources Research* **49**(2), 732-743. https://doi.org/10.1002/wrcr.20084.

Taigbenu, A. E. (1999). Unsaturated flow (Richards equation). In 'The Green Element Method'. (Ed. A. E. Taigbenu.) Vol. pp. 217-230. Springer US: Boston, MA. https://doi.org/10.1007/978-1-4757-6738-4_8.

Terzaghi, K., Peck, R. B., and Mesri, G. (1996). 'Soil mechanics in engineering practice'. John Wiley & Sons.

The University of Queensland (2017). 3D CSG Water Atlas. The University of Queensland. Brisbane, Australia. https://wateratlas.net/.

Tomás, R., Romero, R., Mulas, J., Marturià, J. J., Mallorquí, J. J., Lopez-Sanchez, J. M., Herrera, G., Gutiérrez, F., González, P. J., Fernández, J., Duque, S., Concha-Dimas, A., Cocksley, G., Castañeda, C., Carrasco, D., and Blanco, P. (2014). Radar interferometry techniques for the study of ground subsidence phenomena: a review of practical issues through cases in Spain. *Environmental Earth Sciences* **71**(1), 163-181. https://doi.org/10.1007/s12665-013-2422-z.

Van Camp, M., and Vauterin, P. (2005). Tsoft: graphical and interactive software for the analysis of time series and Earth tides. *Computers & Geosciences* **31**(5), 631-640. https://doi.org/10.1016/j.cageo.2004.11.015.

van der Kamp, G., and Gale, J. E. (1983). Theory of Earth tide and barometric effects in porous formations with compressible grains. *Water Resources Research* **19**(2), 538-544.

van der Kamp, G., and Maathuis, H. (1991). Annual fluctuations of groundwater levels as a result of loading by surface moisture. *Journal of Hydrology* **127**(1), 137-152. https://doi.org/10.1016/0022-1694(91)90112-U.

van der Kamp, G., and Schmidt, R. (2017). Moisture loading—the hidden information in groundwater observation well records. *Hydrogeology Journal* **25**(8), 2225-2233.

Van Genuchten, M. T. (1980). A closed-form equation for predicting the hydraulic conductivity of unsaturated soils 1. *Soil science society of America journal* **44**(5), 892-898.

Wang, H. (2000). 'Theory of Linear Poroelasticity with Applications to Geomechanics and Hydrogeology'. Princeton University Press.

Wang, K., Zang, J., Wang, G., and Zhou, A. (2014). Anisotropic permeability evolution of coal with effective stress variation and gas sorption: Model development and analysis. *International Journal of Coal Geology* **130**, 53-65. https://doi.org/10.1016/j.coal.2014.05.006.

Webb, S. W., and Ho, C. K. (2006). 'Gas Transport in Porous Media'. Springer.

Worden, R. H., and Morad, S. (2009). Clay Minerals in Sandstones: Controls on Formation, Distribution and Evolution. In 'Clay Mineral Cements in Sandstones'. Blackwell Science Ltd https://doi.org/10.1002/9781444304336.ch1.

Wu, G., Jia, S., Wu, B., and Yang, D. (2018). A discussion on analytical and numerical modelling of the land subsidence induced by coal seam gas extraction. *Environmental Earth Sciences* **77**(9), 353. https://doi.org/10.1007/s12665-018-7526-z.

Zang, J., Wang, K., and Zhao, Y. (2015). Evaluation of gas sorption-induced internal swelling in coal. *Fuel* **143**, 165-172. https://doi.org/10.1016/j.fuel.2014.11.007.

Zhang, C., Mitra, R., Oh, J., and Hebblewhite, B. (2016). Analysis of mining-induced valley closure movements. *Rock Mechanics and Rock Engineering* **49**(5), 1923-1941.

Zhu, W., Liu, L., Liu, J., Wei, C., and Peng, Y. (2018). Impact of gas adsorption-induced coal damage on the evolution of coal permeability. *International Journal of Rock Mechanics and Mining Sciences* **101**, 89-97. https://doi.org/10.1016/j.ijrmms.2017.11.007.